Elsevier Editorial System(tm) for Chemical Geology

Manuscript Draft

Manuscript Number: CHEMGE11255R1

Title: Atmospheric carbon sequestration in ultramafic mining residues and impacts on leachate water chemistry at the Dumont Nickel Project, Quebec, Canada

Article Type: Research paper

Keywords: Carbon mineralisation
Hydromagnesite
CO2 sequestration
Mining residues
Experimental field cell
Carbonation mechanisms
Leachate water geochemistry

Corresponding Author: Professor Georges Beaudoin,

Corresponding Author's Institution: Université laval

First Author: Antoine Gras, Ph.D

Order of Authors: Antoine Gras, Ph.D; Georges Beaudoin; John Molson; Benoît Plante

Abstract: Passive carbon mineralization in ultramafic mining residues, which allows the sequestration of CO2 through carbonate precipitation, is one of the options being considered to limit the accumulation of anthropogenic CO2 in the atmosphere. The Dumont Nickel Project (DNP) will generate approximately 1.7 Gt of utramafic mining residues over 33 years of production and the mine will release about 127,700 tonnes of CO2 each year. Using two experimental cells filled with ultramafic waste rock (EC-1) and milling residues (EC-2), the impacts of carbon mineralization on leachate water quality were studied and the quantity of sequestered carbon was estimated. Hydrotalcite supergroup minerals, aragonite, artinite, nesquehonite, dypingite and hydromagnesite precipitated through atmospheric weathering, while the inorganic carbon content of the weathered mining waste increased from 0.1 wt% to 4.0 wt% which indicate active CO2 sequestration. The leachate water, sampled at the bottom of the experimental cells, is characterized by an alkaline pH (~9.5), a high alkalinity (~90 to ~750 mg/L) and a high concentration of magnesium (~50 - ~750 mg/L), which is typical from weathering of ultramafic rocks in a system open to CO2.
Since 2012, the chemical composition of the leachate water has evolved seasonally. These seasonal variations are best explained by: (1) climatic variations over the year and, (2) increased carbonate precipitation between May and July. Increased carbonate precipitation decreased the alkalinity and magnesium concentrations in the leachate water and produced pore waters which were undersaturated with respect to carbonate minerals such as artinite and hydromagnesite. Carbonate precipitation thus self-limits carbon sequestration through a negative feed-back loop. The carbon sequestration potential of the DNP residues is also influenced

by the hydrogeological properties of the residues. In cell EC-2, a high liquid/solid ratio, which limits carbonate precipitation, was maintained by the hydrogeological properties. Since 2011, an estimate of 13 kg of atmospheric CO2 has been sequestered in the milling residues (EC-2), which corresponds to a mean rate of 1.4 (+/- 0.3) kgCO2/tonne/year. Using this mean rate, the 15 Mt of tailings produced each year, during the planned 33 years of mining operation, could potentially sequester 21,000 tonne of CO2 per year by passive carbon mineralization, about 16% of the 127,700 tonnes of CO2 annually emitted by the planned mining operation.

Research Data Related to this Submission

There are no linked research data sets for this submission. The following reason is given:
Data is in Supplementary Data appendices

*Revision Notes

Click here to download Revision Notes: Letter_Editor.pdf

UNIVERSITÉ LAVAL

Faculté des Sciences et de Génie
Département de Géologie
et de Génie Géologique

Québec, 28 April 2020

Dear Editor,

We are sorry for the long delay in submitting the revised version. The first author has moved to France and this has caused delays. I have taken over the role of corresponding author to complete the revisions. We thank the referees for their detailed comments which helped improve our paper significantly. We have made all required corrections except in a few minor cases where we disagree and explained our reasons. Our detailed response to the referees' comments are below.

Best regards,

Georges Beaudoin, géo.

Referee #1

Comments: 1. p. 1, line 34, and p. 3, lines 12-14. Over how many years will the anticipated 1.7 Gt of residues be produced? Over 33 years?

Yes, the anticipated 1.7Gt of mining residues should be produced over 33 years. The text has been modified in order to improve this section.

2.p. 2, lines 36-37. Consider separating these references according to which of the two processes (in situ versus ex situ) they relate to.

Difficult since some references refer to both (eg Olajire)

Georges Beaudoin, *Géo, Ph.D.*
Directeur du Centre E4m
Chaire de recherche industrielle CRSNG—
Agnico-Eagle en exploration minérale
Département de géologie et de génie géologique
1065, rue de la Médecine
Québec (Québec) G1V 0A6
CANADA

Téléphone : 418.656.3141
Cellulaire : 418.559.3140

courriel : beaudoin@ggl.ulaval.ca
www.ggl.ulaval.ca

3.p. 2, lines 45-47 and elsewhere in the manuscript. The notation for mineral formulae ought to be tidied up a bit. The rules are a sometimes a bit strange, but there's no need to use parentheses around the H2O in hydrated carbonates or hydrotalcite supergroup minerals. Also, a dot ought to be used rather than a full stop for the crystallographic H2O. Although the one interlayer CO3 per formula unit in pyroaurite polytypes is commonly given in parentheses (that's all good as-is), the CO3 group in the formulae of 1:1 Mg:CO3 carbonates (such as nesquehonite and lansfordite) is not given in parentheses.

Ok thanks for this correction.

4.p. 2, line 57. "by analyzing the carbon (C) isotope composition…" Is this stable and/or radiocarbon?

Stable, corrected

5.p. 3, lines 15-16. Does "high partial pressure of CO2" equate to pCO2 above atmospheric levels?

Yes, in this sentence high partial pressure of CO2" equate to pCO2 above atmospheric levels. A full description of these tests are available in Assima et al.

6.p. 4, line 17 or thereabouts, line 52 and line 57. I believe the Figure 3b cited here should be Figure 1.

Yes, thanks

7.p. 4, line 26. There's no need to give the single nesosilicate group in the olivine structure in parentheses. Missing '(' before the metal site in the serpentine formula.

Ok

8.p. 4, lines 38-40. It might be worth describing the approximate difference in grain size (or the precise ones if known) between tailings and waste rock for readers who are less familiar with these materials.

A sentence has been added to help the reader to understand the differences between cells EC1 and EC2 in the section describing each.

9.p. 4, line 59 and p. 5, line 9. I haven't come across the term "deshalming" previously. It's not desliming or something similar is it? I think it would be useful to add the definition for people who may not be familiar with the word.

Corrected to « desliming »

10. p. 5, line 49. A minor point: consider rephrasing this sentence to something like "after the method of Oskierski et al." and then providing a

Georges Beaudoin, *Géo, Ph.D.*
Professeur
Chaire de recherche industrielle CRSNG—
Agnico-Eagle en exploration minérale
Département de géologie et de génie géologique
1065, rue de la Médecine
Québec (Québec) G1V 0A6
CANADA

Téléphone : 418.656.3141
Cellulaire : 418.559.3140
Télécopieur : 418.656.7339

courriel : beaudoin@ggl.ulaval.ca
www.ggl.ulaval.ca

citation for Wateq4f. https://wwwbrr.cr.usgs.gov/projects/GWC_chemtherm/pubs/wq4fdoc.pdf

Revised accordingly.

11. p. 5, line 54. Consider using "white crusts of a mineral precipitate" rather than "white crusts".

Done.

12. p. 6, line 53. Were the standards "analysed three times" rather than "analysed after three analyses"?

Corrected to “after every set of 3 analyses”

13. p. 7, line 59. How is the uniformity coefficient defined?

The reader is refereed to Kandji et al.

14. p. 8, line 10. Is this the volumetric water content (as labeled in Figure 4)?

Corrected to volumetric water

15. p. 8, lines 12-16. Was the H2O liquid during the winter at such shallow depths?

We have checked that the temperature measured by the same probe was circa 0 to -1 C during these months such that H2O must have been in the liquid state.

16. p. 8, lines 24-26. Were DI blanks run for comparison with rain water and leachate water analyses? Not strictly necessary, but good to mention if so.

Analyses were carried in commercial laboratories following strict QA/QC protocols including blanks.

17. p. 8, general comment. It's very cool to see the seasonality in your leachate chemistry. The correlations are beautiful!

Thank you!

18. p. 8, line 54 to p. 9, line 9. Consider rephrasing this part to address pH separately from the values for concentration in mg/L.

Done.

19. p. 9, line 35. "since 2011". For clarity, consider rephrasing as something like "in the first 6 months of the experiment following set up in 2011".

Done.

Georges Beaudoin, *Géo, Ph.D.*
Professeur
Chaire de recherche industrielle CRSNG—Agnico-Eagle en exploration minérale
Département de géologie et de génie géologique
1065, rue de la Médecine
Québec (Québec) G1V 0A6
CANADA

Téléphone : 418.656.3141
Cellulaire : 418.559.3140
Télécopieur : 418.656.7339

courriel : beaudoin@ggl.ulaval.ca
www.ggl.ulaval.ca

20. p. 9, line 37. With declining calcium concentrations? And leachate water "generally remained over-saturated" since there are a few points below 0.

Added “generally”.

21. p. 9, lines 56-60. A general comment that doesn't need to be addressed: That's interesting that you see artinite. I've seen it (or amorphous phases of similar composition) in relatively water limited conditions in the field, as has Anna Harrison in the lab.

Thank you for the information.

22. p. 9, lines 56-60. Also very cool that you see brugnatellite. Do you see the pyroaurite species more commonly at depth? I'm curious because Turvey et al. (2018) IJGGC found a spatial relationship with hydrated Mg carbonates closer to the surface and hydrotalcites containing lower mass proportions of CO2 dominating at depth.

This was not noted.

23. p. 10, line 22. Habit rather than habitus.

Corrected.

24. p. 10, lines 25-37. Can you elaborate on what you mean by "cracked"? Can you be more specific about what you mean by "well-crystallized"? For instance, do these minerals form larger, euhedral crystals or do they have a larger crystallite size as determined from XRD data? Also, are you able to tell the difference between aragonite and artinite in Figure 8d? There's a lot of useful information in Figure 8. I think that annotating the subfigures to point out the features you're describing, and labelling minerals with species identifications, would be very helpful. With regard to Figure 8h, the scale here is too large to be able to point out prokaryotes and there doesn't appear to be a microbial mat preserved. (Were the samples preserved for biological microscopy using glutaraldehyde in the field?) The large string-like features look like fungal hyphae to me - those are commonly associated with ultramafic rocks in weathering environments and they can be imaged fairly well without preservation.

“Cracked” removed as not shown in figures. Well-crystallized seems self-explanatory- no changes, as figures show euhedral crystals. Artinite vs aragonite: we cannot be more specific as stated in text. Modified to “potential microbial mats or Fungal Hyphae”.

25. p. 11, lines 19-20. 0.4 wt.% Corg seems a bit high for the detection limit in light of the discussion in the next few sentences. Is this correct?

This is because the DL of Corg is much higher than that for Cinorg, see Gras et al. 2017.

26. p. 11, lines 29-36. Although you mention it toward the end of the manuscript (p. 20, lines 44-46), I think it's worth also mentioning that the trends you see in Figure 10 could also be related to sample heterogeneity rather

Georges Beaudoin, *Géo, Ph.D.*
Professeur
Chaire de recherche industrielle CRSNG—Agnico-Eagle en exploration minérale
Département de géologie et de génie géologique
1065, rue de la Médecine
Québec (Québec) G1V 0A6
CANADA

Téléphone : 418.656.3141
Cellulaire : 418.559.3140
Télécopieur : 418.656.7339

courriel : beaudoin@ggl.ulaval.ca
www.ggl.ulaval.ca

than seasonal dissolution and reprecipitation of carbonate minerals. I've seen similar data sets when taking many cores from heterogeneous sediments and tailings.

Sample heterogeneity added.

27. p. 12, line 56. Quantifying CO2 uptake is tough to do and no method is perfect. I think you've made a good contribution here and that you could replace "to attempt to quantify" with "to estimate the amount of…"

Thank you. Done.

28. p. 13, line 27. I would recommend using "geomicrobial" or "biological" rather than "organic" here.

Modified to biological.

29. p. 14, lines 22-32 and p. 19, lines 51-56. Do you see evidence for silica precipitation or Mg-leached silicate grains?

No. Despite looking for it.

30. p. 14, lines 51-54. Good to cite Barnes and O'Neil (1969) here since it's the original work that defined Types I and II waters.

O'Neil and Barnes 1971 added, instead.

31. p. 16, line 24. I like the discussion that follows about disequilibrium and the ways to recognize it. I think it could flow even better if you (1) mention here that it "could promote one of these three reactions over the others" and (2) mention very briefly how this would affect the overall carbonation reaction to tie this paragraph into the next one.

Added "over the others". 2nd part, however will lead to repetition.

32. p. 17, lines 9-13. That's quite cool. Do you see evidence for the same return to equilibrium in your stable isotope data from your previously published work? If so, it would be nice to tie that in here.

Thank you. We do not have new d13C to report.

33. p. 18, line 19. It looks like nesquehonite is oversaturated for most of the experiment from Figure 7. Are you referring to a specific time period? From May to July? It's tricky to read this easily from the plots in Figure 7. Perhaps pointing out the most important time periods using arrows or grey-shaded vertical bands would help relate this discussion to Figure 7 more intuitively.

The error was in the figure where wrong values are shown for the Y axis. Figure 7 modified with correct values.

Georges Beaudoin, *Géo, Ph.D.*
Professeur
Chaire de recherche industrielle CRSNG—
Agnico-Eagle en exploration minérale
Département de géologie et de génie géologique
1065, rue de la Médecine
Québec (Québec) G1V 0A6
CANADA

Téléphone : 418.656.3141
Cellulaire : 418.559.3140
Télécopieur : 418.656.7339

courriel : beaudoin@ggl.ulaval.ca
www.ggl.ulaval.ca

34. p. 18, lines 44-56. The typical decomposition sequence is lansfordite - nesquehonite - dypingite - hydromagnesite - magnesite, with all other phases being metastable with respect to magnesite. Can you elaborate on what you mean by hydrous carbonates evolving from lansfordite and nesquehonite (since these are the most hydrated species)?

Sequence of carbonate stability corrected as suggested by referee.

35. p. 19, lines 9-13. Possibly. It's tough to say what the role of bacteria might be since cell counts are commonly low in subaerial mine waste and tailings impoundments. What I suspect are fungi in Figure 8h would help to decompose organic material to potentially increase local concentrations of DIC. They would also help to leach the rocks on a small scale. There's a good picture of fungal hyphae on serpentinite in Power et al. (2009) Chem Geol for comparison (Figure 5).

Very similar indeed. Changed to fungi, caption of Fig 8h also updated. Reference to Power already included.

36. p. 19, lines 22-26. These results relating to hydrotalcite supergroup minerals have come out as Turvey et al. (2018) IJGGC.

Turvey et al. (2018) was not known at time of submission. We can add, but Turvey et al. 2015, 2017 already cited.

37. p. 20, lines 4-9. In addition to the impacts of crystallization pressure within pore spaces, could some of these fractures be artifacts of sample preparation (e.g., thin sectioning)?

NO because we embedded the samples in epoxy before fabrication of thin sections.

38. p. 20, line 51 to p. 21, line 20. This is really nice.

Thank you!

39. p. 21, line 59 and start of p. 22. Did you also estimate the amount of carbon sequestered in cell EC-1? If not, could you mention why (e.g., the grain size was too coarse for coring, it was too heterogeneous, etc.)?

This is explained at the start of section 5.3

40. p. 23, lines 6-9. This is a really valuable conclusion. I would recommend adding a little more to the very end of the manuscript. Describing possible ways of optimizing the hydrological properties to enhance carbon sequestration would kick it up a notch to really drive home the implications of your great study.

The various factors affecting carbonation are discussed at length in previous paragraphs. So we could rehash this in explaining control of water saturation, etc. We fear this will appear repetitive. But this is really an engineering optimization issue, somewhat outside the scope of the paper. If you request to add this we will add a paragraph on optimization.

Georges Beaudoin, *Géo, Ph.D.*
Professeur
Chaire de recherche industrielle CRSNG—
Agnico-Eagle en exploration minérale
Département de géologie et de génie géologique
1065, rue de la Médecine
Québec (Québec) G1V 0A6
CANADA

Téléphone : 418.656.3141
Cellulaire : 418.559.3140
Télécopieur : 418.656.7339

courriel : beaudoin@ggl.ulaval.ca
www.ggl.ulaval.ca

S.A. Wilson University of Alberta

Reviewer #2: The manuscript entitled "Atmospheric carbon sequestration in ultramafic mining residues and impacts on leachate water chemistry at the Dumont Nickel Project, Quebec, Canada" discusses results from a carbonation experiment run on waste rock and tailings of an ultramafic rock. The work is a follow-up on a previous work by the same authors, with three additional authors (Gras et al., 2017). While the previous paper introduced the experimental setup and focused on isotope composition of the carbonates formed, the present manuscript extends this work in a logical way by focusing on the composition of leachate water from the experimental cells over several years. The manuscript is in general well written and easy to read, and the topic fits the scope of the journal well. Carbonation of ultramafic rock is an active research topic presently, and research on carbonation of mine residues is particularly active. Thus, I expect that the paper will attract significant attention. However, I have some comments that should be taken into account, and recommend a moderate revision. In the following, I list a major issue that I believe is quite important to address, before I list some minor issues, including some spelling mistakes. Since the line numbers on the manuscript don't actually match the lines, I have used the line number nearest to the line I refer to.

Major issues I'm a bit concerned about the discussion of seasonal regimes in section 5.1.2. On page 16, line 32 it is stated that carbonate precipitation decreases magnesium and DIC concentrations in leachate water. This seems a bit strange. Clearly, during evaporation the concentrations increase until reaching saturation, and precipitation starts. I have a hard time understanding how this can lead to undersaturated leachate water. I would rather expect that the leachate water would then be close to saturation. Otherwise, the remaining water after evaporation would have to be diluted with less concentrated leachate water to produce the observed values. Similarly, when rainfall increases (page 17, line 6) the concentration of magnesium and DIC increases in response to less carbonate precipitation. This seems counterintuitive? Furthermore, (Page 17, line 9) it is stated that the carbon mineralization reactions return to equilibrium when rainfall increases. I would expect that the reactions are closer to equilibrium when water stays a long time in the experimental cell in dry periods than when lots of rain is entering continuously? Maybe all the fresh rainwater might lead to redissolution of some carbonates? The potential effect of such redissolution is not mentioned to any major extent in the manuscript, and would be interesting to see discussed in a bit more depth. Needless to say, I'm not sure I understand or believe the explanations the authors provide in this section, and I thus recommend that they improve their arguments here. This also has some impact on the conclusions.

We recognize the confusion created by this paragraph, which is in part repetitive. We have deleted it and added a sentence to the 2nd paragraph of the section:
Each year, the Mg concentrations and alkalinity values tend to be higher in the spring (May and June) and fall (September to November), and lowest in the summer (July and August). These trends are inverse with that of precipitations. It thus

Georges Beaudoin, *Géo, Ph.D.*
Professeur
Chaire de recherche industrielle CRSNG—Agnico-Eagle en exploration minérale
Département de géologie et de génie géologique
1065, rue de la Médecine
Québec (Québec) G1V 0A6
CANADA

Téléphone : 418.656.3141
Cellulaire : 418.559.3140
Télécopieur : 418.656.7339

courriel : beaudoin@ggl.ulaval.ca
www.ggl.ulaval.ca

seems that Mg concentrations and alkalinity values (related to DIC) might be controlled, at least in part, to dilution from rain and snowmelt water.

Minor issues :

Page 1, line 55: Either "... an estimated 13 ..." or "... an estimate of 13 ..."

Corrected to “an estimate of”.

Page 2, line 32: In situ carbonation is also considered in ultramafic rock, with the Oman Drilling Project probably being the largest project at the moment. As for references for the in situ part, I would suggest some publication related to the CarbFix project in Iceland for the mafic part and Kelemen et al. (2011) for the ultramafic part.

Added Matter et al. (2009) for the CarbFix, and Kelemen and Matter (2008).

Page 3, line 4: Although these are indeed advantages, it would also be good to mention some disadvantages, in order to be open about those.

Added a main disadvantage.

Page 4: All references to figure 3 are supposed to refer to figure 1.

Corrected.

Page 4, line 54: I assume that they intend to write "... rougher tails ..."

Corrected as suggested.

Page 4, line 56: Here, I assume that they intend to write "... run of mine ore ..."

Yes corrected.

Page 9, line 35: Nesquehonite does not look under-saturated on figure 7. Actually, the plotted data seems to be identical with the data for magnesite, which leads me to assume that the authors have plotted the wrong data set for nesquehonite.

Figure 7 modified as indicated in response to comments by S Wilson.

Page 9, line 56: As far as I know, there is no thermodynamic data for dypingite available. I think it would be good to state this clearly somewhere, as it otherwise seems a bit strange that nothing is written about dypingite in section 4.2.

Georges Beaudoin, *Géo, Ph.D.*
Professeur
Chaire de recherche industrielle CRSNG—
Agnico-Eagle en exploration minérale
Département de géologie et de génie géologique
1065, rue de la Médecine
Québec (Québec) G1V 0A6
CANADA

Téléphone : 418.656.3141
Cellulaire : 418.559.3140
Télécopieur : 418.656.7339

courriel : beaudoin@ggl.ulaval.ca
www.ggl.ulaval.ca

Not sure what to respond here. This section is the results description, and p. 9, L56 is the XRD results. Modelling is described later.

Page 11, line 29: Couldn't this also be caused by dissolution of carbonates during weathering? After all, according to Ulven et al. (2017) there is almost no carbonate left in the weathered part of the ultramafic rock.

The referee is mistaken, as this relates to the difficulty of measuring organic carbon using Walkey-Black.

Page 12, line 4: I assume that "precipitation" here refers to rainfall, but it would be good to distinguish more clearly between rain and carbonate precipitation, since it might be confusing when two different concepts are described by the same word.

Good point, changed to rain fall.

Page 12, line 46: I suggest rephrasing this sentence a bit. It seems the authors are stating that this occurred in 2013 only, which seems a bit strange. Rather, this is probably true for any year, but there is data for 2013 only. The difference is minor, but important.

Not sure what is meant here. This line mentions the residence time of water in cell EC-1. Then it discusses the flow rate in 2013, as measured, and compares EC-1 and EC-2.

Page 13, eq (5): The equation is unbalanced, while the two previous are balanced. I suggest having them all balanced. It's also unclear why the authors choose to end up with nesquehonite in the general reactions.

Reaction corrected, nesquehonite simply used as an example. Added Harrisson et al., CG, 2019

Page 14, line 56: There seems to be a conjunction missing after the comma.

Indeed, corrected.

Page 15, line 17: Could such abrupt increases at first rainfall be caused by formation of some easily dissolved minerals during dry periods, which would then rapidly dissolve at first rainfall?

We have no evidence for that. We can only discuss the change in concentration, and did not infer that dissolution involved only silicates from the waste materials.

Page 16, line 57: had -> have

Done.

Page 18, line 44: dypinte -> dypingite

Georges Beaudoin, *Géo, Ph.D.*
Professeur
Chaire de recherche industrielle CRSNG—
Agnico-Eagle en exploration minérale
Département de géologie et de génie géologique
1065, rue de la Médecine
Québec (Québec) G1V 0A6
CANADA

Téléphone : 418.656.3141
Cellulaire : 418.559.3140
Télécopieur : 418.656.7339

courriel : beaudoin@ggl.ulaval.ca
www.ggl.ulaval.ca

Done.

Page 18, line 46: nesquesonihte -> nesquehonite

Done.

Page 20, lines 4-8: I suggest rephrasing this sentence a bit. The authors seem to state that fracturing of the waste rock blocks actually occurred in the experiment. Since there isn't any data in the results supporting such a statement, I assume that the authors are intending to suggest the possibility based on the references.

Replaced “blocks” with “fragments” as this is documented here.

Page 20, lines 51-59: It would be interesting to know if the layer of tailing is flat, or whether water might pool in the middle. That would change the hydrological setting significantly, and might cause the observed difference in carbonate content.

Fig. 2e shows the surface is flat, but small irregularities pounded water. In the following text we discuss the effect of the decreased thickness of materials towards the edge of the cell.

Page 21, line 14: Again, I suggest distinguishing a bit clearer between precipitation of rain and carbonate.

Done.

Page 21, line 16: Ulven et al. (2017) argued that sheltering from rain prevented redissolution of the carbonates during rainfall. Could that be an alternative explanation here?

Sentence to this effect added.

Page 21, line 29: I suggest rephrasing this sentence, since I'm pretty sure the carbonate wasn't actually sequestered in the month of May 2015, but rather the years from 2011 to May 2015.

Modified accordingly.

Page 21, line 47: How can 21 kt be one quarter of 127.7 kt? To me it seems more like 16.4%. Furthermore, couldn't the tailing residues continue sequestering several years in optimal conditions, and lead to sequestration of more CO2 than estimated? If the rate is constant e.g. two years, then the first year 21 kt would be sequestered, and then 42 kt all following years as the pile of material is growing. One might have to consider optimal ways of spreading the tailing on the ground or getting CO2 to percolate into the pile using pipes or pumps or something, but it might be worth a try.

Indeed. Changed to 16%. Correct, we are describing annual rates.

Georges Beaudoin, *Géo, Ph.D.*
Professeur
Chaire de recherche industrielle CRSNG—
Agnico-Eagle en exploration minérale
Département de géologie et de génie géologique
1065, rue de la Médecine
Québec (Québec) G1V 0A6
CANADA

Téléphone : 418.656.3141
Cellulaire : 418.559.3140
Télécopieur : 418.656.7339

courriel : beaudoin@ggl.ulaval.ca
www.ggl.ulaval.ca

Page 22, line 46: alkanity -> alkalinity

Changed.

Figures 5, 6, 7: These multi-panel figures would be easier to read if there was some sort background grid, e.g. vertical lines showing the start of each year. As it is, I need to use a ruler if I want to compare data from the same time.

Will do if requested, but this will make a mess of grid lines….

Figures 3, 7: The tics on the horizontal top axes don't match those on the bottom axes. That's inconvenient. The same is valid for the right vertical axis in figure 7b).

Corrected

Georges Beaudoin, *Géo, Ph.D.*
Professeur
Chaire de recherche industrielle CRSNG—
Agnico-Eagle en exploration minérale
Département de géologie et de génie géologique
1065, rue de la Médecine
Québec (Québec) G1V 0A6
CANADA

Téléphone : 418.656.3141
Cellulaire : 418.559.3140
Télécopieur : 418.656.7339

courriel : beaudoin@ggl.ulaval.ca
www.ggl.ulaval.ca

Graphical Abstract

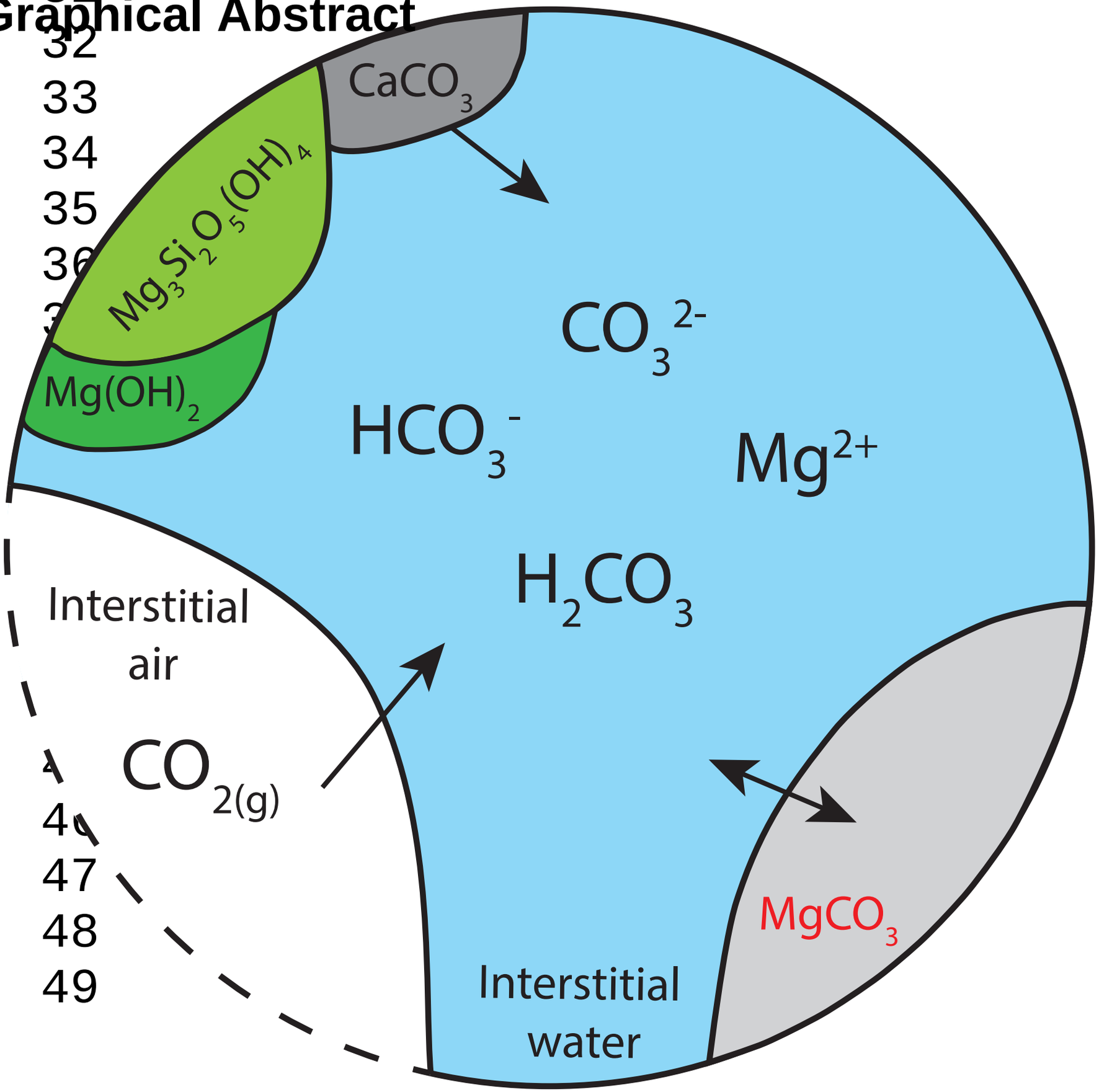

Highlights

- Passive carbon mineralization monitored in experimental ultramafic mine and milling waste
- Hydrotalcite supergroup minerals precipitated from atmospheric weathering, increasing C_{inorg} up to 4 wt.% Co2
- Leachate water chemistry indicate weathering in steady state system open to atmospheric CO_2.
- 1.4 kg CO_2/tonne/year are captured from the atmosphere by passive carbon mineralization reactions

Atmospheric carbon sequestration in ultramafic mining residues and impacts on leachate water chemistry at the Dumont Nickel Project, Quebec, Canada

A. Gras[1*], G. Beaudoin[1], J. Molson[1], B. Plante[2],

[1] Département de Géologie et de Génie Géologique, Université Laval,Québec, Canada

[2] Institut de Recherche en Mines et en Environnement, Université du Québec en Abitibi-Témiscamingue, Rouyn-Noranda, Canada

Abstract

Passive carbon mineralization in ultramafic mining residues, which allows the sequestration of CO_2 through carbonate precipitation, is one of the options being considered to limit the accumulation of anthropogenic CO_2 in the atmosphere. The Dumont Nickel Project (DNP) will generate approximately 1.7 Gt of utramafic mining residues over 33 years of production and the mine will release about 127,700 tonnes of CO_2 each year. Using two experimental cells filled with ultramafic waste rock (EC-1) and milling residues (EC-2), the impacts of carbon mineralization on leachate water quality were studied and the quantity of sequestered carbon was estimated. Hydrotalcite supergroup minerals, aragonite, artinite, nesquehonite, dypingite and hydromagnesite precipitated through atmospheric weathering, while the inorganic carbon content of the weathered mining waste increased from 0.1 wt% to 4.0 wt% which indicate active CO_2 sequestration. The leachate water, sampled at the bottom of the experimental cells, is characterized by an alkaline pH (~9.5), a high alkalinity (~90 to ~750 mg/L) and a high concentration of magnesium (~50 - ~750 mg/L), which is typical from weathering of ultramafic rocks in a system open to CO_2.

Since 2012, the chemical composition of the leachate water has evolved seasonally. These seasonal variations are best explained by: (1) climatic variations over the year and, (2) increased carbonate precipitation between May and July. Increased carbonate precipitation decreased the alkalinity and magnesium concentrations in the leachate water and produced pore waters which were undersaturated with respect to carbonate minerals such as artinite and hydromagnesite.

Formatted: Header distance from edge: 1.25 cm, Footer distance from edge: 1.25 cm

Formatted: English (Canada)

Formatted: Font: 11 pt

Formatted: Line spacing: 1.5 lines

Formatted: Font: 11 pt, English (Canada)

Formatted: Font: 11 pt

Formatted: Font: 11 pt, English (Canada)

Formatted: Font: 11 pt

Formatted: Font: 11 pt, English (Canada)

Formatted: Font: 11 pt

Formatted: Font: 11 pt, English (Canada)

Formatted: English (Canada)

Formatted: Font: 11 pt, English (Canada)

Carbonate precipitation thus self-limits carbon sequestration through a negative feed-back loop. The carbon sequestration potential of the DNP residues is also influenced by the hydrogeological properties of the residues. In cell EC-2, a high liquid/solid ratio, which limits carbonate precipitation, was maintained by the hydrogeological properties. Since 2011, an estimated of 13 kg of atmospheric CO_2 has been sequestered in the milling residues (EC-2), which corresponds to a mean rate of 1.4 (+/- 0.3) kgCO_2/tonne/year. Using this mean rate, the 15 Mt of tailings produced each year, during the planned 33 years of mining operation, could potentially sequester 21,000 tonne of CO_2 per year by passive carbon mineralization, about ~~one quarter~~16% of the 127,700 tonnes of CO_2 annually emitted by the planned mining operation.

1. Introduction

Anthropogenic CO_2 released into the atmosphere is considered a major driver of global climate change (IPCC, 2014). In order to limit accumulation of gaseous CO_2 in the atmosphere, several methods of carbon sequestration are envisaged including carbon mineralization (IPCC, 2005). As reviewed by Seifritz (1990), carbon mineralization technologies are derived from natural exothermic reactions, which occur spontaneously and trap CO_2 through carbonate precipitation (Berner and Kothavala, 2001; Gaillardet et al., 1999; Lackner et al., 1995). The general carbon mineralization reaction for silicate minerals such as serpentine is summarized in Reaction (1):

$$(Mg, Ca)_x Si_y O_{x+2y+z} H_{2z} + xCO_2 \rightarrow x(Mg, Ca)CO_3 + ySiO_2 + zH_2O + Heat \quad (1)$$

Carbon mineralization is attractive because no post-storage monitoring is necessary and carbon dioxide is sequestered over geological time scales. Two types of carbon mineralization are considered (Beaudoin et al., 2008; Gerdemann et al., 2007; Kelemen and Matter (2008); Matter et al. (2009); Olajire, 2013; Park and Fan, 2004; Pronost et al., 2011; Sanna et al., 2014; Sipilä et al., 2008; Teir et al., 2009):

(1) in-situ carbonation, wherein pure CO_2 is injected into subsurface mafic formations to form carbonate minerals, and

Formatted ...
Formatted: Indent: First line: 1.25 cm
Formatted: Font: 14 pt
Formatted: Font: 11 pt
Field Code Changed
Formatted ...
Formatted ...
Field Code Changed
Field Code Changed
Formatted ...
Field Code Changed
Formatted ...
Formatted ...
Formatted: Font: 11 pt
Formatted ...
Field Code Changed
Formatted: Font: 11 pt
Formatted: List Paragraph, Indent: Left: 2.77 cm

(2) ex-situ carbon mineralization, which uses mining or industrial residues as the carbon sink. ~~(2) ex-situ carbon mineralization, which uses mining or industrial residues as the carbon sink~~

Natural weathering of ultramafic mining residues captures atmospheric CO_2 through passive carbon mineralization. Carbonation rates of up to 1700 g C m^{-2} y^{-1}, for example, have been reported from historical and active mining sites. The main carbonate minerals precipitated in mining residues are ~~p~~Pyroaurite-3R [$Mg_6Fe_2^{3+}(CO_3)(OH)_{16}.4.(H_2O)$], nesquehonite [$Mg(CO_3).3.(H_2O)$], dypingite [$Mg_5(CO_3)_4(OH)_2.5.(H_2O)$], hydromagnesite [$Mg_5(CO_3)_4(OH)_2.4(H_2O)$], and aragonite [$CaCO_3$] (Beaudoin et al., 2008; Gras et al., 2017; Lechat et al., 2016; Oskierski et al., 2013; Power et al., 2013a, 2013b; Pronost et al., 2012; Rollo and Jamieson, 2006; Turvey et al., 2017; Wilson et al., 2011, 2006, 2014). Passive carbon mineralization has previously been studied by considering mineralogical evolution and leachate water geochemistry (Assima et al., 2014a, 2013; Beinlich and Austrheim, 2012; Harrison et al., 2017, 2013; Power et al., 2009; Rollo and Jamieson, 2006; Zarandi et al., 2017a, 2017b, 2016), and by analysing the stable carbon ~~(C)~~ isotope (C^{13} and C^{12} composition of dissolved inorganic carbon (DIC) and neo-formed carbonates (Beaudoin et al., 2017, 2008; Gras et al., 2017; Harrison et al., 2016, 2013, Oskierski et al., 2013b, 2016, Wilson et al., 2014, 2011, 2009). Ex-situ, passive carbon mineralization in mining residues has two main advantages: (1) the mine wastes can be re-used for environmental benefit, and (2) CO_2 can be directly sequestered from the atmosphere. Moreover, these processes can potentially lead to developing carbon-neutral mines (Harrison et al., 2013; Hitch and Dipple, 2012; Mills et al., 2010; Power et al., 2014). The main disadvantage is the slow rate of reaction, compared to ex-situ carbon mineralization.

The Dumont Nickel Project (DNP) of RNC Minerals (RNCM) is designed to produce 0.51 Gt of ultramafic waste rock and 1.18 Gt of milling (tailings) residues (Staples et al., 2013). The carbon sequestration capacity of these future residues at high partial pressure of CO_2, and the effect of mineralogy, water saturation, watering frequency, and temperature, have been well studied at the laboratory scale (Assima et al., 2014a, 2014b, 2013, 2012, Kandji et al., 2017b, 2015; Plante et al., 2014; Pronost et al., 2010; Zarandi et al., 2016, 2017a, 2017b). However, in order to develop useful engineered solutions for carbon sequestration, and to properly estimate the carbon sequestration capacity, more realistic field experiments are required (Olajire, 2013; Lechat et al., 2016; Gras et al., 2017).

Formatted: English (Canada)
Field Code Changed
Formatted: English (Canada), Check spelling and grammar
Formatted: English (Canada)
Field Code Changed
Formatted: Check spelling and grammar
Formatted: Superscript
Formatted: Superscript
Field Code Changed
Formatted: English (Canada), Check spelling and grammar
Formatted: English (Canada)
Field Code Changed
Formatted: Check spelling and grammar
Field Code Changed
Formatted: English (Canada), Check spelling and grammar
Formatted: English (Canada)

Using two experimental cells, Gras et al. (2017) demonstrated that between the three potential sources of CO_2, notably: (1) the atmosphere, (2) organic matter oxidation and (3) carbonate dissolution, atmospheric CO_2 was the main source of sequestered carbon during natural atmospheric weathering of the DNP residues. In addition, Gras et al. (2017) showed that dissolution of atmospheric CO_2 in interstitial water was the first step which limited the carbon mineralization capacity. However, additional factors can also limit the mineralization capacity. For example, natural weathering of ultramafic rocks will change the geochemistry of meteoric water which percolates through the mining residues (Rollo and Jamieson 2006; Beinlich et al., 2012; Oskierski et al., 2016) and natural terrain (Bruni et al., 2002; Cipolli et al., 2004; Marques et al., 2008; Paukert et al., 2012). Since changes in the water chemistry can affect carbonate precipitation, they may therefore also impact the carbon sequestration potential of mine residues (Appelo and Postma, 2005).

In this contribution, using two field experimental cells, EC-1 filled with mine waste, and EC-2 which contains milling residue from the DNP, we report on changes in (1) leachate water geochemistry, (2) waste mineralogy, and (3) carbon content. In addition, the effects of hydrogeological properties and leachate water geochemistry on carbonate mineral precipitation are investigated. Finally, the amount of atmospheric CO_2 trapped during atmospheric weathering of the DNP residues is estimated.

2. Geological setting

The DNP site is located near the town of Amos in north-western Québec (Figure 1~~3~~a). The deposit is hosted in a sill which had intruded into rock of the Superior province of the Canadian Shield. Two distinct units are identified in the sill: (1) a mafic zone of gabbro which is overlain by (2) an ultramafic zone formed by peridotite and dunite (Figure 1~~3~~b) (Duke, 1986; Eckstrand, 1975; Sciortino et al., 2015). The ultramafic zone, which contains a resource of 1.72 Mt of nickel ore, is approximately 6.8 km long with an average thickness of 450 m. In the Dumont sill, nickel enrichment of intercumulus minerals is a product of serpentinization (Duke, 1986; Sciortino et al., 2015) which is a hydrothermal process involving water and heat which alters silicate minerals, such as olivine [$(Mg,Fe,Ni)_2$~~(SiO_4)~~], to serpentine minerals [$(Mg,Fe,Ni)_3Si_2O_5(OH)_4$], as well as to brucite [$Mg(OH)_2$] and magnetite [$Fe^{2+}Fe_2^{3+}O_4$]. The dunite protolith was composed of Ni-rich

Field Code Changed
Formatted: English (Canada), Check spelling and grammar
Formatted: English (Canada)
Field Code Changed
Formatted: Check spelling and grammar
Formatted: Indent: First line: 1.25 cm
Formatted: Check spelling and grammar
Field Code Changed
Field Code Changed
Formatted: Check spelling and grammar

olivine with horizons rich in sulfide minerals. During serpentinization, the nickel was redistributed in intercumulus pentlandite [$(Fe,Ni)_9S_8$], awaruite [Ni_3Fe] and heazlewoodite [Ni_3S_2] (Sciortino et al., 2015). The main mineral assemblage in the dunite subzone consists of lizardite, magnetite, brucite, and chlorite, with variable amounts of pentlandite, awaruite, and heazlewoodite (Sciortino et al., 2015; Staples et al., 2013). The DNP is expected to generate approximately 1.7 Gt of ultramafic mining residue of two types: (1) ~1.18 Gt of tailing residues issued from the metallurgical processes, and (2) ~510 Mt of waste rocks (Staples et al., 2013).

3. Materials and Methods

3.1 Experimental cells:

Near the planned DNP mining site near Amos, Quebec, two experimental cells were built and instrumented in order to study weathering of the mine's ultramafic mining residues. Gras et al. (2017) provide detailed descriptions of the experimental cells. The first cell (EC-1) was filled using 104 tonnes of waste rock from blasting of a dunite outcrop (Figure ~~1b~~1b). The grain size of waste rock in EC-1 ranged from milimetric to pluricentrimetric blocs. The second cell (EC-2) contains approximately 2.6 tonnes of milling residues containing the slimes, fluff and rougher tails (non-magnetic) produced in a pilot plant. The run of mine ore, processed in the pilot plant, was taken from four boreholes located in the dunite subzone (Figure 1~~3~~b) (Staples et al., 2013). The pilot-plant process consisted of two cycles of grinding, ~~deshalming~~desliming, and flotation in a hydrocyclone followed by magnetic separation. During the first cycle, the run of mine ore was crushed and ground in wet media with the dispersant Calgon © (500 g/t) and potassium amyl xanthate (PAX) (150 g/t) to 80% passing minus 150 µm, then the non-magnetic portion from the first cycle was crushed and ground in wet media to 80% passing minus 74 µm for the second cycle of deshalming and flotation.

Within both experimental cells, gas sampling ports were installed in order to monitor CO_2 concentrations within the interstitial air (Gras et al., 2017). In addition, cell EC-2 contained a Decagon 5TM probe, 4 cm below the tailings surface, to monitor changes in volumetric water content and temperature. In November 2015, two additional Decagon 5TM probes were placed at 14 and 25 cm depths to measure changes in water content and temperature with depth. At the bottom of cells EC-1 and EC-2, a geomembrane and a drain were installed to collect the leachate water. Both drains were connected to tipping bucket rain gauges to log the flux of water at the output of the cells. A weather station recorded solar radiation, temperature, wind speed and direction, and a tipping bucket rain gauge measured rainfall.

Formatted: Check spelling and grammar

Field Code Changed

Formatted: Check spelling and grammar

Field Code Changed

Field Code Changed

3.2 Leachate water analyses:

Leachate water is produced from infiltration of rain and meltwater through the mining residues in experimental cells EC-1 and EC-2. The leachate was sampled twice a month between July 2011 and November 2013, and then monthly from May 2014 to November 2015. The leachate water pH was measured on site, while samples were collected in bottles which were sent to Maxxam Analytical (QC, Canada) and to SGS Canada (ON, Canada) to measure major and minor ions and metals (Al, Sb, As, Ba, Be, Bi, B, Cd, Ca, Cr, Co, Cu, Sn, Fe, Li, Mg, Mn, Mo, Hg, Ni, Pb, K, Se, Si soluble in HNO_3, SO_4, Na, Sr, Tl, Ti, U, V, Zn), and total alkalinity, until 2015. The geochemical model PhreeqC (Parkhurst et al., 1999) was used to calculate the saturation indices of major carbonate minerals in the leachate water. Since the temperature of the leachate was not measured, a temperature of 25°C was therefore used and after the method of Oskierski et al. (2016) the thermodynamic equilibrium calculations were carried out using the Wateq4f database (~~James W.~~ Ball a~~nd~~nd ~~D. Kirk~~ Nordstrom~~.~~, 1991~~Oskierski et al., 2016~~).

Field Code Changed

Formatted: English (Canada)

3.3 White crusts and core samples:

Within months of constructing the waste rock cell (EC-1), white crusts of a mineral precipitate started to coat the surface of the rock fragments during atmospheric weathering. The residues were sampled manually (Figure 2 a, b, c, d). White crusts of a mineral precipitate also indurated the tailings surface near the edges of cell EC-2 which were also sampled (Figure 2 e, f, g, h). Between 2012 and 2015, surface crusts were sampled 19 and 16 times in both EC-1 and EC-2, respectively. In order to document the weathering processes acting on the residues, 7 cores, ranging in length from 14 cm to 32 cm, were sampled from October 2013 to November 2015 in the center of EC-2 using a steel tube (Gras et al., 2017). Additionally, two cores, 5 cm and 3 cm in length, were sampled in October 2014 and May 2015. One core was sampled below a wooden access plank at the edges of the cells and the other at the edges of the cell EC-2 ~~-~~(Figures 2 e and f) (Supplementary information).

3.4 Mineralogical analysis

Crushed samples from cells EC-1 and EC-2 were analysed by XRD using a Siemens D5000 X-ray diffractometer (Cu-Kα radiation). XRD patterns were collected with a scanning step of 1°/min (0.02° step size) over a 5-40° scattering angle range. The Jade computer program was used to identify the mineral phases.

A JEOL 840-A scanning electron microscope (SEM) at Université Laval, Québec, equipped with an Avalon (PGT) energy-dispersive X-ray spectrometer (EDS), was used in order to describe mineral habits and texture, and for mineral identification of the neo-formed phases.

Polished thin sections of white crusts from EC-1 and EC-2 were analyzed using a CAMECA SX-100 Electron Probe Micro-Analyzer (EPMA) at Université Laval. The device is equipped with 5 wavelength-dispersive spectrometers. Chemical analyses were performed using a 15 kV accelerating voltage with a 20 nA beam current, and a 10 µm beam size. Simple oxides (GEO Standard Block of P and H Developments) and/or natural minerals (Mineral Standard Mount MINM 2553, Astimex Scientific; Jarosewich et al., 1980) were used to calibrate the instrument for chemical analyses.

3.5 Carbon content

The total carbon content was measured with an Electra CS 800 carbon and sulphur analyser at Université Laval (Gras et al., 2017). High and low carbon contents were calibrated using, respectively, AR 4018 (1.30 +/- 0.05 wt% C), and UB-N serpentine ANRT (0.106 +/- 0.08 wt% C). The standards (Ar 4018 and UB-N serpentine) were analysed after every set of three analyses to test reproducibility of the measurement over time, yielding a precision (1σ) of 0.2 wt% C and of 0.03 wt% C for the high and the low carbon contents, respectively.

The organic carbon content was measured using a modified Walkley Black method (Gras et al., 2017; Walkley and Black, 1934) . Equation (2) below, from De Vos et al (2007) was used to calculate the organic carbon content:

$$\%C_{org} = M \times \frac{(V_1 - V_2) \times 0.3}{W} \times 1.32 \qquad (2)$$

where M is the molarity of the reference Fe_2SO_4 solution, V_1 is the volume (mL) of Fe_2SO_4 needed in a blank titration, V_2 is the volume (mL) of Fe_2SO_4 consumed in the sample titration, W is the weight (g) of the sample and 1.32 is the correction factor (Chatterjee et al., 2009; Conyers et al., 2011; De Vos et al., 2007).

Formatted: Check spelling and grammar

Formatted: Check spelling and grammar

Formatted: Check spelling and grammar

Formatted: Check spelling and grammar

Formatted: English (Canada)

4. Results

4.1 Field observations:

The experimental cells are located near Amos, in north-western Quebec, in a continental climate characterized by large differences in temperature between cold winters and warm summers. The mean temperature and the mean solar radiation intensity between the years 2011 and 2016 varied respectively, from -18°C and 32 W/m^2 in winter to 17°C and 230 W/m^2 in summer (Table 1). During summer, the rainfall events slightly decreased but intense rainfall events occurred frequently (≥30 mm). The mean total annual precipitation (snow and rain) between 2011 and 2016 was 840 mm/yr. The recording of rainfall was sometimes disrupted by mechanical failure and was completed using data from Environment Canada.

At the bottom of the cells, the leachate flow rate was recorded between April and November using a typing bucket rain gauge. The logging was frequently disrupted due to weather. Figure 3 presents the flow rates recorded between May and August 2013, together with the rain events for the year. In 2013, following a precipitation event of 25 mm in one day, the maximum flow rate in EC-1 was ~2000 L/day whereas in EC-2 it was ~1400 L/day (Figure 3). The mean discharge recorded between 2011 and 2015 ranged from 217 L/day to 546 L/day for EC-1 and from 111 L/day to 241 L/day for EC-2 (Figure 3)

In cell EC-1, the grain size of the waste rock is heterogeneous and ranges from silt to pluri-centimetric blocks whereas material from EC-2 is characterized by a D10 of 2.2 µm, a D80 of 119 µm and a uniformity coefficient (Cu=D10/D60) of 22 (Kandji et al., 2017) (Figure 2 a and e). The mean porosity in cell EC-2 is 44% and the dry bulk density is 1242 kg/m^3 +/- 55 kg/m^3. Other hydrogeological parameters for EC-1 and EC-2, presented in Gras et al. (2017), were estimated from the literature (Aubertin et al., 1996; Lechat et al., 2016; Molson et al., 2008, 2005, Peregoedova et al., 2014, 2012).

Figure 4 presents the evolution of the volumetric water content with depth in EC-2, with total precipitation for the year 2016. During the winter, the water content just below the surface (~ 4 cm deep) was constant near 10% whereas at 14 cm and 25 cm depths the water content reached 30% and 40 %, respectively. In spring, the water content increased by 10 % throughout the cell and fluctuated with rain events (Figure 4). Between 2011 and 2015, the average water content was ~25 % at 4 cm depth in cell EC-2.

Formatted: Check spelling and grammar

Formatted: English (Canada)

4.2 Chemical evolution of the leachate water:

Rainwater chemical analyses yielded a pH of 5.5 and contained trace amounts of Al (0.03 mg/L), Pb (0.001 mg/L) and Zn (0.03 mg/L). Between December and April, the interstitial waters were frozen, thus chemical analyses on leachate water were performed only from May to November. The leachate analyses from both cells revealed the same pattern of evolution, with a transient phase after construction during the summer of 2011, followed by a regime characterized by seasonal cycles (Figures 5 and 6).

In EC-1 during the first summer (2011), the magnesium concentration, alkalinity, and pH increased from 6.5 to 110 mg/L (Mg), from 240 to 510 mg/L $CaCO_3$ (Alk) and from 8.17 to 8.81 (pH), respectively (Figure 5 a). During the same period, calcium and silica concentrations decreased from 85 to 36 mg/L and from 7.8 to 3.3 mg/L, respectively (Figure 5 b). Since 2012, the magnesium and silica concentrations, as well as the alkalinity and pH, varied in seasonal cycles from 125 to ~~750~~ 180 mg/L (Mg), from 1.2 to 6.2 mg/L (Si), from 125 to 70~~5~~0 mg/L $CaCO_3$ (Alk) and from 8.1 to 9.7 (pH), respectively. During these seasonal cycles, the magnesium concentration, pH and alkalinity decreased while silica concentrations increased from May to August. From August to November the trends were reversed (Figure 5 a,b). The calcium concentration generally decreases from year to year but had the same seasonal variations as silica and ranged from 3.4 to 20 mg/L (Ca).

In EC-2~~, with the exception of pH,~~ the concentrations of chemical elements were lower than in EC-1 (Figure 6). Between July and November 2011, the magnesium concentration was highly variable, with a minimum and maximum value of 70 and 120 mg/L, respectively. Meanwhile, the alkalinity and pH increased from 45 to 180 mg/L $CaCO_3$ (Alk) and from 7.64 to 9.45 (pH), respectively (Figure 6 a), whereas calcium and silica concentrations decreased from 85 to 36 mg/L (Ca) and from 7.8 to 3.3 mg/L (Si), respectively (Figure 6 b). Between 2012 and 2015, as in EC-1, the magnesium, silica and calcium concentrations, as well as alkalinity and pH, varied seasonally between 50 and 140 mg/L (Mg), 0.9 to 7.2 mg/L (Ca), 0.67 to 2.7 mg/L (Si), 91 to 509 mg/L $CaCO_3$ (Alk)~~ and~~, with a rise in pH from 8.93 to 10~~ (pH)~~, respectively. While seasonal variations were the same as in EC-1, the intensity of seasonal variations in magnesium concentrations and alkalinity has decreased over the years in cell EC-2 (Figures 6 a,b).

In both experimental cells, potassium and sodium concentrations decreased from year to year since 2011. Additionally, similar to silica, the potassium and sodium concentrations increased each year between May and July then decreased until November (Figures 5 and 6). The potassium

and sodium concentrations ranged from 4 to 2.3 mg/L (K) and from 13 to 2 mg/L (Na), respectively in EC-1, and from 15 to 0.2 mg/L (K) and from 26 to 0.9 mg/L (Na) in EC-2 (Supplementary information). The concentrations of other chemical components were near or below their detection limits (Supplementary information). Finally, in both cells the amplitude of the seasonal cycles seemed to decrease from year to year (Figures 5 and 6).

Thermodynamic equilibrium calculations revealed that carbonate saturation indices first increased in 2011 and then evolved seasonally following pH and alkalinity. The calculations suggest that magnesite, calcite and aragonite were over-saturated in leachate water, whereas nesquehonite remained under-saturated in the first 6 months of the experiment following set up in 2011~~since 2011~~ (Figure 7). The saturation indices of aragonite and calcite decreased over the years with calcium concentrations, but the leachate water remained generally over-saturated with respect to these minerals. Between May and July, saturation indices for hydromagnesite and artinite decreased with the leachate becoming under-saturated whereas during the next three months, saturation indices increased, with the leachate becoming over-saturated in November (Figure 7). The thermodynamic equilibrium calculations also suggest that the partial pressure of CO_2 in the leachate water was often below the atmospheric partial pressure, also fluctuating with seasonal variations. However, the temperature of the leachate water was not measured which reduces precision on the pCO_2 calculations.

4.3 Mineralogical analysis:

XRD analyses of weathered mining residues from both cells revealed the presence of nesquehonite, dypingite, hydromagnesite, aragonite, artinite, and several minerals from the hydrotalcite supergroup, including brugnatellite [$Mg_6Fe^{3+}(CO_3)(OH)_{13}.4(H_2O)$], pyroaurite 3R, and pyroaurite 2H [$Mg_6Fe_2^{3+}(CO_3)(OH)_{16}.4(H_2O)$]. However, owing to the low modal abundance of the carbonate minerals, XRD data did not allow an accurate identification of the hydrotalcite supergroup minerals. Of the 19 samples analysed from EC-1, 10 contained hydromagnesite whereas only one EC-2 sample contained hydromagnesite. Surface samples from EC-2 most often contained dypingite. Well-crystalized, primary calcite [$CaCO_3$] was also found in rock fragments from EC-1 (Gras et al., 2017). Finally, in the first 3 centimeters of the core samples at the center of cell EC-2, a decrease in intensity or an absence of brucite peaks was observed in the XRD patterns of the weathered samples.

The SEM observations of weathered samples from EC-1 and EC-2 revealed the texture and habit of the precipitated carbonates (Figure 8). The weathered surfaces of samples from the waste rock cell (EC-1) were entirely (Figure 8 a) to partially (Figure 8 b) covered by carbonate minerals with a lamellar texture similar to the habit~~us~~ of hydromagnesite (Figure 8 c). On the surface of several samples, at the grain surfaces, depressions were filled with carbonate minerals ~~which appeared cracked~~, whereas on the top of the grains some well-crystallized lamellar minerals were observed. Well-crystallized carbonate minerals with the typical texture of aragonite or artinite have also been observed on samples from EC-1 (Figure 8 d). At the surface of EC-2, carbonate minerals cement small grains of tailings (Figure 8 e). Flaky carbonate minerals covered by well-crystalized needle-like minerals were observed on the same serpentine grains (Figure 8 f). Additionally, several crystal sizes of nesquehonite were observed on the same samples which indicate repeated precipitation phases (Figure 8 g). Finally, some samples from EC-2 ~~were characterized by intergrowths of~~ contain potential microbial mats of fungal hyphae intertwined with carbonate minerals (Figure 8 h).

Using samples from cells EC-1 and EC-2, thin sections were impregnated with epoxy under vacuum, in order to preserve the carbonate-matrix interface. The carbonate crusts from EC-2 samples were too thin for EPMA analysis. Back Scattered Electron (BSE) imaging of the thin sections from EC-1 revealed different patterns of carbonate coating. The carbonate minerals were observed as: (1) thin layers on the serpentine substrate separated from lamellar minerals by a fracture (Figure 9 a), (2) within fractures cemented by carbonate with mining residue fragments (Figure 9 b) or (3) in complex fractures filled by carbonates and with brucite (Figure 9 c). The minerals at the carbonate-matrix interface had oxygen, magnesium and silica concentrations ranging respectively from 61.9 to 13.8 wt% (O), from 47.1 to 6.7 wt % (Mg) and from the detection limits to 21 wt% (Si). Nickel, calcium and aluminum never exceeded 2.3 wt % whereas the iron was commonly lower than 2 wt% , reading 8 wt% in one grain.

4.4 Evolution of the carbon content:

The unweathered mining residues within the experimental cell EC-1 were characterized by a total carbon content of 0.13 wt%, whereas the white crusts, which do not contain primary calcite, had a total carbon content ranging from 0.3 wt% to 4.4 wt%C_{tot} (Gras et al., 2017). In cell EC-1, no evidence of organic carbon was observed, and therefore the total carbon content is equivalent to the inorganic carbon content. In contrast, in cell EC-2, spruce needles and leaf fragments were found at the surface (Figure 2 f) thus the organic carbon content was measured in order to compute the

inorganic carbon content. In several samples the organic carbon content was near the detection limit (0.4 wt% C_{org}) (Conyers et al., 2011). Therefore, in samples with a carbon content below 0.4 %C_{org}, the total carbon was considered to be inorganic carbon (Gras et al., 2017). In EC-2, the unweathered residues had a total carbon content of 0.08 wt%. The crusts sampled at the edge of the cell were characterized by an inorganic carbon content ranging from 0.1 wt%C_{inorg} to 4.0 wt%C_{inorg} (Gras et al., 2017). The samples from the first few centimeters of core samples, at the center of cell EC-2, yielded inorganic carbon contents lower than the carbon content of the unweathered mining residues (Figure 10). This is likely a consequence of measurement errors related to the Walkey-Black method or sample heterogeneity. Moreover, the inorganic carbon content changed according to the month of sampling. Below the first centimeter of depth, the inorganic carbon content decreased quickly from 1 cm to 3 cm depth. Between 2014 and 2015, the inorganic carbon content ranged from 0.15 wt% to 0.43 wt% and was higher in July than in May or October/November. From below 3 cm depth to the bottom of cell EC-2, the inorganic carbon content was constant near 0.2 wt% (Gras et al., 2017) (Figure 10). Figure 11 presents the inorganic carbon content measured at the surface of EC-2 since 2011, and a cross-section of cell EC-2 with the spatial distribution of the inorganic carbon content measured in May 2015. The contours were drawn using linear interpolation between the core samples. The mining residues under the wood plank, at the edges of cell EC-2, (Figure 2 g) had an average inorganic carbon content of 1.08 wt% whereas at the edges of the cell in May 2015, the inorganic carbon content decreased from 0.5 wt % at the surface, to 0.3 wt% at a depth of 10 cm.

5. DISCUSSION

Since construction of the experimental cells during the summer of 2011, the mining residues underwent atmospheric weathering. Previous work demonstrated that passive carbon mineralization had indeed induced atmospheric carbon sequestration in the DNP residues (Gras et al., 2017). The main parameters controlling the extent of mineral carbonation include characteristics inherent to the residues such as the mineral composition, surface area, porosity and permeability. Other parameters depend on the environment, such as ~~precipitation~~ rain fall frequency, temperature, and relative humidity (Assima et al., 2014c, 2013, 2012; Awoh et al., 2014; Bea et al., 2012; Harrison et al., 2015; Kandji et al., 2017a, 2017b; Pronost et al., 2011; Wilson et al., 2014; Zarandi et al., 2017b, 2016). Both experimental cells (EC-1 and EC-2) were filled with ultramafic mining residues from the same nickel deposit. Mining residues in EC-1 and EC-2 therefore had a similar initial mineralogy (Figure 3a-b) where the main minerals were chrysotile, lizardite, brucite, chlorite and magnetite, whereas calcite was found in minor amounts in the waste rock residues (Pronost et

Field Code Changed

Field Code Changed

Formatted: English (Canada), Check spelling and grammar

Formatted: English (Canada)

al., 2010; 2012; Staples et al., 2013; Gras et al. 2017). The brucite content in the tailings residues of cell EC-2, was approximately 10.2 wt% (Assima et al., 2013). During 4 years of monitored weathering, the residues were submitted to the same conditions of precipitation, temperature and relative humidity variations. However, the hydrogeological characteristics of the mining residues (porosity, water content, tortuosity, permeability), which are specific to each cell, control the flows of gas and water. Cell EC-1 has hydrogeological properties analogous to a heterogeneous gravel-silt, whereas in cell EC-2 the porous medium is similar to that of a silty-clay (Figure 2). On the other hand, the cells contained respectively, approximately 104 tonnes (EC-1) and 5 tonnes (EC-2) of residues and the surface area exposed to rainwater was greater for cell EC-1 (~35 m^2) than for EC-2 (~19 m^2). As a result, the cell thicknesses are about 2 meters and 35 centimeters, respectively, for EC-1 and EC-2. The liquid-solid ratio and thus also the water content were higher in EC-2 (Figure 4) than in EC-1 (Gras et al., 2017). The flow rates measured at the bottom of the cells thus depended on the hydrogeological properties of each cell. After a rain event, an abrupt increase of the flow rate was recorded in both cells (Figure 4). Counter-intuitively to what the hydrogeological properties would suggest, in cell EC-1 the flow rate decreased slowly in the recession curve (Figure 3) whereas in EC-2 the flow rate decreased more quickly after a rain event. This is best explained by the small amount of mining residues within EC-2. Despite a porous medium similar to a silty-clay, the smaller thickness in EC-2 (35 cm) resulted in a short residence time for water. In EC-1, the residence time of water was longer but did not exceed a few days (Figure 3). In 2013, the flow rate measured at the bottom of EC-1 was higher than in EC-2 which was most likely due to the difference in the surface area exposed to rain. Physical property differences between the two cells may influence the carbon mineralization reactions and, therefore, the carbon sequestration capacity. In the following sections, the observed impacts of atmospheric weathering on leachate water geochemistry will be used to discuss the evolution of carbon mineralization over time and to attempt to quantifyestimate the amount of the atmospheric CO_2 sequestered in the cells.

5.1 Impacts of atmospheric weathering on leachate geochemistry.

In cells EC-1 and EC-2, rainwater in equilibrium with atmospheric CO_2 infiltrates the mining residues and dissolves the magnesium (Mg^{2+}) from minerals such as brucite or serpentine. The $Mg^{2+}_{(aq)}$ released into leachate water reacts with interstitial water carbonate (CO_3^{2-}) and bicarbonate (HCO_3^-) ions to form carbonate minerals (Sanna et al., 2014; Harrison et al., 2019), following reactions 3-5 below:

$$CO_{2(g)} + H_2O_{(l)} = H_2CO_{3(aq)} = H^+_{(aq)} + HCO^-_{3(aq)} \quad (3)$$

Formatted: Font: 11 pt, Not Bold

$$Mg_3Si_2O_5(OH)_4 + 6H^+ = 3Mg^{2+} + 2SiO_2 + 5H_2O \quad (4)$$

$$3Mg^{2+} + HCO_3^{2-} + 3H_2O = MgCO_3.3H_2O \quad (5)$$

Dissolution reactions (3 and 4) and carbonate precipitation (5) are controlled by temperature, pH and solution chemistry, and may also be affected by ~~organic~~ biological processes (McCutcheon et al., 2016; Power et al., 2013a, 2016, 2010, 2009). In the experimental cells, reactions 3, 4 and 5 occur simultaneously such that the leachate waters collected at the bottom of both cells reflect the equilibrium between these reactions at the times of sampling. From 2011 to 2015, and despite differences in physical properties between the two cells, two regimes can be recognized for leachate water chemistry (Figures 5 and 6). First, a transitional regime in 2011 during which the pH, alkalinity and magnesium concentrations increase in the leachate water whereas silica, calcium, potassium and sodium concentrations decrease. In the second regime, starting in 2012, the pH, alkalinity, Mg, Si, Ca, Na and K concentrations in leachate water show seasonal variations, while the other metal concentrations are stable or below detection (Supporting information). The greater amount of mining residues and the larger surface area of EC-1 to collect rain, as well as its hydrogeological parameters which are more favourable to water infiltration compared to that of cell EC-2, could explain the higher concentrations observed in cell EC-1 (Figures 5 and 6). However, the concentrations normalized to the volume of mining residues demonstrate that the release rates of different components in EC-1 were lower than in EC-2 (Kandji et al., 2017). The contrast in release rates between both cells may be explained by (1) the finer grain-size and thus a higher specific surface in cell EC-2, and (2) the high liquid-solid ratio in EC-2 (Plante et al., 2014, Kandji et al., 2017). Despite these differences, the same processes appear to control the evolution of the leachate water chemistry in both cells (Figures 5 and 6).

5.1.1 Transitional regime

In July 2011, atmospheric weathering of the mining residues began with acidic meteoric water (pH ~ 5.5) infiltrating the mining residues and dissolving serpentine minerals, brucite and minor amounts of diopside, albite, biotite and calcite (Staples et al., 2013; Pronost et al., 2012, Kandji et al., 2017). The increase of Mg concentration in leachate water was congruent with the dissolution of serpentine minerals, brucite and minor silicate minerals. Dissolution of brucite is further suggested by a decrease of intensity or absence of the XRD peaks of brucite in weathered EC-2 samples. Concurrent to dissolution, H^+ was consumed through weathering, which caused pH and alkalinity increases in leachate water (Figures 5 and 6) (Kandji et al., 2017b; Lechat et al.,

Field Code Changed

Field Code Changed

Formatted: English (Canada), Check spelling and grammar

2016; Ulven et al., 2017). Concentrations of Si, Ca, Na or K in leachate water indicate active dissolution of serpentine minerals and silicate minerals such as diopside, albite or biotite. On the other hand, a decrease of Si and other metal concentrations between July and November 2011 suggests a lower dissolution rate of serpentine and silicate minerals during this period, which is consistent with the pH increase and a decrease of the abundance of these minerals (Figures 5 and 6). Additionally, the increasing pH may cause incongruent dissolution of serpentine minerals, and a preferential release of Mg over Si (Pokrovsky and Schott, 2000), which supports the observed decrease of Si concentrations from July to November 2011. Brucite was therefore the main but not the only source of Mg in interstitial water of the experimental cells, which is consistent with kinetic tests completed in the laboratory (Kandji et al., 2017). During this transitional regime, the saturation indices of all carbonates increase, and several become over-saturated such as magnesite, nesquehonite aragonite and calcite (Figure 7).

5.1.2 Seasonal regime

Since 2012, leachate water from cells EC-1 and EC-2 has been characterized by high concentrations of Mg, ranging from 50 to 180 mg/L, and a pH ranging from 8.1 to 10 in which HCO_3^- is the dominant carbonate species (Appelo and Postma 2005). The leachate water from both cells is therefore similar to a Mg-HCO_3^- - type, or type I water, characteristic of open-system interaction between CO_2-bearing meteoric water and ultramafic rocks (Bruni et al., 2002; Cipolli et al., 2004; Marques et al., 2008; O'Neil and Barnes, 1971; Oskierski et al., 2016; Paukert et al., 2012; Rollo and Jamieson, 2006). Nevertheless, dissolution of CO_2 in interstitial water is the first limiting step of carbon mineralization in the experimental cells, (Gras et al., 2017), and the leachate water geochemistry indicates that reactions occur in an open system with atmospheric CO_2. The pH, alkalinity, and the Si, Mg, Ca, K, and Na concentrations from leachate waters in both cells evolved seasonally while concentrations from other chemical components were stable or below detection (Figures 6 and 7) (Supplementary information). These seasonal variations of leachate geochemistry can be explained by: (1) changes in the hydrologic regime (Nordstrom, 2011, 2009), and (2) changes of the equilibrium conditions between the carbon mineralization reactions (Wilson et al., 2010).

Changes in hydrological regimes at mine waste sites over time can have important impacts on water quality (Nordstrom, 2011). During dry periods, for example, the concentration of dissolved metals increases slowly in the leachate water. In contrast, the first strong rainstorm following a dry period (first flush), or an intense rain event, may cause an abrupt increase of

Formatted: English (Canada)

Field Code Changed

Formatted: English (Canada), Check spelling and grammar

Field Code Changed

Formatted: English (Canada)

Field Code Changed

Field Code Changed

Field Code Changed

concentrations followed by a decrease (Nordstrom, 2011, 2009). The climate near Amos (Quebec), is characterized by large changes in environmental conditions over the year (Table 1). During winter, precipitation is lowest, and the water content in both cells is minimal, near the field capacity and the permanent wilting point. Despite these conditions, carbon mineralization should be effective and carbonates such as landsfordite, could precipitate (Beinlich and Austrheim, 2012; Ulven et al., 2017; Zarandi et al., 2016). Spring snowmelt induces a first flush of water after the relative dry winter period, which was observed in May 2016 as an increase in water content at all depths in cell EC-2. Such a first flush in spring or intense rain events throughout the year may have impacted the leachate water geochemistry and could explain abrupt changes. Each year, the Mg concentrations and alkalinity values tend to be higher in the spring (May and June) and fall (September to November), and lowest in the summer (July and August). These trends are inverse with that of precipitations. It thus seems that Mg concentrations and alkalinity values (related to DIC) might be controlled, at least in part, to dilution from rain and snowmelt water. ~~However, no general co-evolution between leachate geochemistry and snow melting or rain events has been observed.~~

Field Code Changed

Field Code Changed

Every year, between May and July, the temperature and solar radiation increased, while from August to October a decrease was observed. The relative humidity in the atmosphere and total precipitation were slightly lower from May to July than between August to October. Additionally, during the summer, rain events were slightly less frequent (Figures 5 and 6) (Table 1). Decreasing rainfall events between May and July caused a deficit of water in the cells, over a period during which temperature and solar radiation were conducive to evaporation. During this period, a decrease in water content at 4 cm depth in EC-2 was observed in 2013 and 2014. Similarly, between the end of July and November of each year, increases in precipitation caused ingress of water within the cells and in 2016, the water content at 4 cm depth increased in cell EC-2 (Figure 4 and Table 1).

Potassium and sodium ions react little during transport in the experimental cells and are thus considered conservative in this study. Furthermore, these elements were not affected by changes in equilibrium of the carbon mineralization reactions. During dry seasons (May to July), when evaporation was highest, K, Na, Si and Ca concentrations increased. In contrast, when precipitation then increased (August to November), concentrations of K, Na, Si, Ca, decreased. Changes in the hydrological regimes over the year then impacted leachate water quality in the DNP residues. However, the decrease of magnesium concentrations during this seasonal regime, is not directly correlated with changes in precipitation and evaporation conditions, and is not yet fully understood.

Changes in evaporation conditions and in watering may alter the equilibrium between the three principal reactions of carbon mineralization presented earlier: (3) dissolution of CO_2 in water, (4) dissolution of reactive minerals, and (5) carbonate precipitation (Assima et al., 2012; Kandji et al., 2017b; Wilson et al., 2014; Zarandi et al., 2017b). Dissolution of CO_2 in interstitial waters contributes to the dissolved inorganic carbon which produces bicarbonate (HCO_3^-) and carbonate (CO_3^{2-}) ions. Reaction 4 releases magnesium ions in the interstitial water, while reaction (5) consumes magnesium ions and bicarbonate ions. Changes in climatic conditions and precipitation could promote one of these three reactions over the others and induce disequilibrium which in turn would modify the leachate water geochemistry (Beinlich and Austrheim, 2012; Wilson et al., 2010).

~~Between May and July, maximum evaporation promoted carbonate mineral precipitation in cells EC 1 and EC 2. Gras et al. (2017) documented the impacts of evaporation on isotopic compositions of neo-formed carbonate minerals. This carbonate precipitation decreases magnesium and dissolved inorganic carbon concentrations in leachate water. Increasing carbonate precipitation over other carbon mineralization reactions, observed between May and July, might have led to the observed decrease of magnesium concentrations in leachate waters from cells EC 1 and EC 2 (Figures 5 and 6). Additionally, from May to July, slightly reduced rainfall increased the leachate water residence time in the experimental cells, thus the leachate would have remained longer in a CO_2 - poor environment where dissolution of CO_2 in pore water was limited (Gras et al., 2017, Lechat et al., 2016; Oskierski et al., 2016). Bicarbonate ions consumed by carbonate mineral precipitation could therefore not be replaced by dissolution of CO_2 from the atmosphere. The decrease of DIC concentration in leachate waters from EC 1 and EC 2 is induced by consumption of bicarbonate ions during carbonate precipitation. This is also consistent with the decrease of pCO_2 calculated using PhreeqC (Supplementry information). The main contributors to alkalinity in leachate water from cells EC 1 and EC 2 were bicarbonate and carbonate (CO_3^{2-}). Consumption of bicarbonate ions and a decrease of alkalinity might, at least in part, have led to a decrease of pH from May to July. Moreover, the increase of orthosilicic acid in the water related to the increase of silica concentration, might had led to the annual drop in pH. During carbon mineralization in the laboratory and in natural environments, decreases in magnesium concentration and DIC caused by carbonate precipitation have been previously described (Bruni et al., 2002; Cipolli et al., 2004; Harrison et al., 2013; Lechat, 2016; Paukert et al., 2012; Wilson et al., 2010). Similarly, when precipitation increased from July until November, fresh water percolated through the residue, the residence time of water decreased, and the meteorological conditions were less favourable for evaporation. Decreasing carbonate precipitation and the return to equilibrium between the carbon~~

Formatted: English (Canada), Check spelling and grammar
Field Code Changed
Formatted: English (Canada)
Field Code Changed
Field Code Changed
Formatted: English (Canada), Check spelling and grammar
Formatted: English (Canada)

~~mineralization reactions then led to an increase of magnesium and DIC concentrations, and to increased alkalinity (Figures 5 and 6). Displacement of the equilibrium between the three carbon mineralization reactions, leading to an increase in carbonate precipitation, therefore contributed to the seasonal regimes in the experiment cell leachate waters.~~

From year to year, the intensity of the seasonal cycles in Mg concentrations and alkalinity seems to decrease, particularly in cell EC-2, while the pH slightly increases (Figures 5 and 6). This long-term evolution could be related to a decrease of carbonate precipitation over the years. Indeed, Gras et al. (2017) demonstrated that, since 2012, the decrease in $CO_{2(g)}$ consumption capacity of cells EC-1 and EC-2 was associated with the decrease in brucite content near the surface and due to surface passivation (Assima et al., 2012; Harrison et al., 2015; Zarandi et al., 2016). Near the surface, a decrease of magnesium in the leachate waters, related to the smaller proportion of brucite, may limit the precipitation of carbonates (which would otherwise be promoted by evaporation) and might explain the long-term geochemical evolution (Figures 5 and 6). Furthermore, a decrease of porosity near the surface, caused by carbonate precipitation, may also alter the carbon mineralization reactions which would also impact the leachate water geochemistry from year to year (Acero et al., 2007; Beinlich and Austrheim, 2012). Further investigations are needed to confirm and understand the long-term evolution of leachate water geochemistry.

Field Code Changed

Field Code Changed

In summary, results have shown that leachate water geochemistry from the experimental cells EC-1 and EC-2 was influenced by (1) the local weather (temperature, relative humidity, and precipitation) and (2) evolution of the equilibrium between the governing carbon mineralization reactions, leading to an increase of carbonate precipitation.

5.2 Carbonate precipitation

The evolution of leachate geochemistry presented in the previous section influences the carbonate precipitation reactions. Thermodynamic equilibrium calculations reveal that, despite the differences between cells EC-1 and EC-2, the saturation indices of the carbonate minerals have been similar since 2011. However, the saturation indices evolve following seasonal changes of pH, alkalinity and Mg concentrations (Figure 7). The saturation indices of all carbonate minerals first decreased between May and July, then increased until November. Despite these variations, calcite, aragonite and magnesite were over-saturated, since 2011, in leachate water from both cells. Notwithstanding the oversaturation, Ca concentrations were not affected by the increase of carbonate precipitation between May and July. The leachate waters from EC-1 and EC-2 were

characterized by high Mg concentrations which can inhibit calcium carbonate precipitation (Hopkinson et al., 2008). Inhibition of calcium carbonate precipitation can explain why Ca concentrations did not change over seasonal cycles and is further consistent with the low modal proportion of neo-formed calcium carbonates observed in this study and by Gras et al., (2017). Saturation indices of artinite and hydromagnesite reflected either over- or under-saturated conditions, whereas nesquehonite was under-saturated (Figure 7). It is important to note that evaporation of leachate water, which may significantly increase the carbonate saturation indices, was not considered here. Oskierski et al. (2016), for example, demonstrated that evaporation of 20% of the leachate water from the Woodsreef mine induced oversaturation for hydromagnesite. At the surface of the cells, where evaporation was highest, the carbonate minerals were therefore most likely over-saturated. Nervertheless, changes in leachate water geochemistry, between May and July, decreased the carbonate mineral saturation indices and thus these carbonate minerals became under-saturated deeper within the cells. The increase in carbonate precipitation between May and July, which altered the leachate water geochemistry, therefore created a feed-back loop limiting the carbon sequestration potential of the cells.

In experimental cells EC-1 and EC-2, the neo-formed carbonate minerals trap atmospheric CO_2 (Gras et al., 2017). In surface samples from both cells, artinite, nesquehonite, dypingite, and hydromagnesite were observed, with rare aragonite. The amount of bound carbon depends on the specific mineral. Nesquehonite has a ratio of CO_2 to Mg of 1, whereas the ratio is 4/5 for hydromagnesite and dypingite. The stability of magnesium carbonate minerals increases from lansfordite and artinite to nesquehonite, then dypingite, hydromagnesite, and stable magnesite, ~~through to higher stability minerals of nesquesonihte, dypingite and hydromagnesite~~ (Canterford et al., 1984; Hopkinson et al., 2008; Langmuir, 1965). At temperatures above 25°C, hydrous-carbonates can evolve from landsfordite to nesquehonite (Beinlich and Austrheim, 2012; Hopkinson et al., 2008), whereas nesquehonite can be converted to dypingite and hydromagnesite during associated wetting/drying cycles and increasing temperature (Hopkinson et al., 2008; Oskierski et al., 2016; Power et al., 2009; Wilson et al., 2009; Zarandi et al., 2017b). Hydromagnesite was more common in samples from EC-1, whereas in EC-2 the main carbonate was dypingite. In cell EC-1, the blocks of waste rock which were more conducive to wetting/drying cycles and evaporation, were coated with carbonate minerals. Conversion from the less stable phases (artinite, nesquehonite) to hydromagnesite was favoured in cell EC-1 which can explain the higher proportion of hydromagnesite in EC-1. In contrast, the finer grain size of the tailings in cell EC-2 maintains a higher water content (Figure 4), which may slow the rate of dehydration of

Field Code Changed

Field Code Changed

Field Code Changed

Field Code Changed

Formatted: English (Canada), Check spelling and grammar

Formatted: English (Canada)

nesquhenotite to hydromagnesite. ~~Microorganisms~~ Fungi at the surface of cell EC-2 (Figures 8 h) could also promote precipitation of dypingite (McCutcheon et al., 2016; Power et al., 2010, 2009). The grain size of the mining residue may therefore influence the type of carbonate minerals precipitated, whereas evaporation and wetting-drying cycles control the conversion. Clearly, the hydrogeological conditions can therefore also influence the quantity of carbon trapped in the residues. In deeper EC-2 samples, however, only hydrotalcite supergroup minerals formed (Supplementary information). As described in previous studies, in both cells EC-1 and EC-2, for example, hydrotalcite supergroup minerals had formed during atmospheric weathering (Gras et al., 2017; Oskierski et al., 2016; Turvey, 2015; Turvey et al., 2017). These minerals precipitated rapidly after exposure to the atmosphere through weathering of brucite under CO_2 - limited conditions (McCutcheon et al., 2016; Mumpton and Thompson, 1966; Turvey et al., 2017).

In cell EC-1, carbonate coatings may also have contributed to surface passivation (Figures 2 c, d and 8 a,b) (Assima et al., 2012; Zarandi et al., 2017b), whereas in cell EC-2, the carbonates cemented the tailing grains, causing a decrease in porosity and permeability (Acero et al., 2007) (Figures 2 h and 8 e). Therefore, precipitation of carbonates within the cells may decrease atmospheric CO_2 consumption. In order to characterize the carbonate matrix interface, EPMA analysis was used on waste rock samples from EC-1. In order to identify the minerals at the carbonate-matrix interface, chemical analyses and theoretical mineral compositions have been plotted on ternary diagrams (Figure 9). Most often, the carbonate-matrix interface is sharp, and the chemical composition changed from serpentine to carbonates or brucite (Figure 9 c). However, on several samples the chemical compositions of minerals at the carbonate-matrix interface range from the pole of serpentine to a magnesium pole depleted in silica which corresponds either to brucite or carbonates (Figure 9 a,b). Because the EPMA beam size (10 µm) is in some places larger than the target minerals, superposition of serpentine or epoxy and carbonates may have altered the signal to the measured composition. Nevertheless, the range of composition from the pole of serpentine to the magnesian pole is consistent with the incongruent dissolution of serpentine in high pH water, in which Si will be preferentially released over Mg (Pokrovsky and Schott, 2000; Ruiz-Agudo et al., 2012).

The EPMA analyses did not allow precisely identifying the carbonate minerals in the mining residues. In addition, the BSE images revealed that carbonate minerals at the surface were fragile (Figure 9 a) and filled the fractures at the expense of brucite (Figures 9 b and c). Frost cycles and dehydration of the carbonate minerals increased the fracturing of waste rock ~~blocks~~ fragments and thus the carbonate coating may have been peeled off (Beinlich and Austrheim, 2012; Ulven et al.,

Field Code Changed

Formatted: English (Canada), Check spelling and grammar

Field Code Changed

Formatted: English (Canada)

Field Code Changed

Field Code Changed

Field Code Changed

Field Code Changed

Formatted: English (Canada), Check spelling and grammar

2017; Zarandi et al., 2017b, 2016). Carbonate precipitation therefore contributes to (1) exposure of fresh serpentine to weathering, which maintains atmospheric CO_2 sequestration, and (2) increased surface passivation, which may decrease atmospheric CO_2 consumption. Carbonate precipitation dynamics in the DNP residues, which changed leachate water geochemistry, thus decreased porosity and permeability, promoted fracturation of the mining residues and caused surface passivation, creating a feed-back loop limiting the carbon sequestration potential.

5.3 Quantification of atmospheric CO_2 sequestration

Carbon sampling of cell EC-1 was limited to surface samples, and therefore it was not possible to accurately quantify the carbon sequestered. However, extensive sampling at the center and at the edges of cell EC-2 allowed tracking the evolution of carbon sequestration over time and thus allowed estimating the quantity of captured CO_2.

At the center of cell EC-2, the inorganic carbon content increased slowly from year to year (Gras et al., 2017) but changed seasonally. Most notably, the carbon content was higher in summer than in autumn or spring (Figure 10). Dissolution of less stable neo-formed carbonate minerals during rain events (Ulven et al., 2017) or changes in water geochemistry (Figures 5 and 6) may have led to these seasonal variations of the carbon content. However, the cores were randomly sampled at the center of the cell, irrespective of surface mineralization, and carbon mineralization at the surface of the cell was not continuous or homogeneous as shown by an evaporitic crust and cones (Figures 2, and 11). In addition, the carbonate crusts were thin and fragile and might have been disturbed over time (Figure 2 h). The small seasonal variations might therefore be an artifact induced by the sampling process. Additional analyses are necessary to better understand the annual evolution of the carbon content in experimental cell EC-2.

The inorganic carbon content in cell EC-2 also varied laterally. At the center of the cell, for example, the carbon content was lower and the carbonation front shallower than at the edges of the cell (Figure 11). The water content, at the center of cell EC-2 was near 25 % at 4 cm depth since 2011, but below this depth the water saturation reaches 25 to 40 % (Figure 4). Since the mean porosity of the tailings in cell EC-2 was 44%, the residues were therefore almost fully saturated below 4 cm depth. Towards the edges the residue thickness decreases, and the impact of evaporation became gradually more important such that mean water content became lower. Previous studies have shown that high and low water saturations tend to reduce the carbon mineralization reaction rates (Assima et al., 2013, 2012; Awoh et al., 2014; Harrison et al., 2015).

Formatted: English (Canada)

Field Code Changed

Field Code Changed

In cell EC-2, the watering frequency corresponds to actual rainfall events and thus was the same at the center and the edges of the cell. Carbon mineralization was thus more efficient near the edges of the cell because of the lower water saturation compared to the center of the cell. Similarly, under the wood plank (Figure 2 g), the residues are partially protected from ~~precipitation~~ rain fall and the water content was lower, thus carbon mineralization was likely more efficient yielding a higher carbon content (Figures 2 e and 11). In contrast, the capture of carbon near the center of cell EC-2 was inhibited by the higher water content in the mining residues. Altenatively, sheltering from rain by the wood plank may have prevented carbonate dissolution, as argued by Ulven et al. (2017)

The quantity of CO_2 sequestered within the experimental cell EC-2 was estimated using the measured inorganic carbon content. The carbon of the core samples was weighted by the mass of a layer using the thickness of the core sample. For the three upper layers, two-thirds of the volume was ascribed to the central core, and one-third to the core from the edge of the cell (Figure 11). With this approach, ~~in~~ up to May 2015, an estimated 13 kg of atmospheric CO_2 was sequestered by the mining residues in cell EC-2, which corresponds to a mean rate of 1.4 (+/- 0.3) $kgCO_2$/tonne/year. This rate is about twice as high as the rate calculated by Bea et al., (2012) using numerical simulations for tailing pounds near Mount Keith (Australia). The DNP residues, however, are characterized by a higher brucite content (10.2 vol%) (Assima et al., 2012) compared to the tailings of the Mount Keith mine (2.5 vol%). Brucite is a key mineral which reacts quickly during carbon mineralization and controls its extent (Assima et al., 2013; Pronost et al., 2012; Harrison 2013, 2015, 2016, 2017; Kandji et al., 2015). It is therefore likely the higher brucite content in the DNP residues may have induced the higher sequestration rate. The DNP mine will generate, each year, approximately 15 Mt of tailings and release about 127,700 tonnes of CO_2 (Staples et al., 2013; Kandji et al., 2017b). Using the sequestration rate of the experimental cell EC-2, the tailing residues will sequester about 21 kt of atmospheric CO_2 each year, which represents around ~~one quarter~~16% of the CO_2 emitted. This rate of sequestration is lower than the rate calculated from laboratory kinetic tests (8.5 $kgCO_2$/tonne) (Kandji et al., 2017). The contrast between laboratory and natural conditions may be explained by differences in precipitation/watering and climatic conditions (Temperature, RH). Additionaly, the experimental cell EC-2 was frequently flooded after intense rain events and during the summer's drought cracks were observed. These extreme water contents limited the carbonation of the residues and may explain the difference between the laboratory and experimental cell tests. In cell EC-1, the hydrogeological properties, which control the fluid flow and influence the mineral carbonation, are different than in EC-2. In addition, the hydrogeological properties are very heterogeneous (Aubertin

Field Code Changed

et al., 1996). Therefore, the results from EC-2 cannot be easily extrapolated, and the estimated amounts of CO_2 capture might be quite different from the real amounts sequestered (Awoh et al., 2014; Lechat et al., 2016).

Formatted: English (Canada)

Field Code Changed

6. CONCLUSION

Two experimental cells were used to study impacts of atmospheric weathering on passive carbon mineralization in mining residues from the Dumont Nickel Project. The mining residues filling the experimental cells had a similar mineralogy and were submitted to the same weather conditions (temperature, RH, precipitation). However, the hydrogeological properties, which influence the supply of CO_2 and the water content of the cells, were different. Despite these hydrogeological differences, the same processes control the evolution of leachate water geochemistry. High magnesium concentrations and a moderate to alkaline pH characterize the leachate water from both cells, which is consistent with weathering of ultramafic rocks in a system open to CO_2. Seasonal variations of leachate water geochemistry are caused by (1) seasonal and longer-term changes in rainfall and weather conditions, and (2) a displacement of the equilibrium between the carbon mineralization reactions. Between May and July each year, leachate water flows in a CO_2 - depleted environment where supply of atmospheric CO_2 to water is limited (Gras et al., 2017). During this period, evaporation is at its maximum, therefore precipitation of carbonate minerals increases causing a decrease in magnesium concentration and alkalinity. Seasonal variations in leachate water geochemistry also impact the saturation indices of carbonate minerals. Between May and July, hydromagnesite and artinite become under-saturated which limits carbon sequestration. Furthermore, carbonate precipitation, self-limits carbon sequestration through a negative feed-back loop.

Over the years, magnesium concentrations and alkalinity decrease which is related to a decrease of CO_2 consumption (Gras et al., 2017). In experimental cells EC-1 and EC-2, carbonate precipitation is mainly driven by evaporation. Dehydration of nesquehonite to hydromagnesite is promoted by the larger grain size in EC-1 and dypingite is more common in EC-2. Since the hydrogeological properties of EC-2 are similar to a silty-clay porous medium, a high liquid/solid ratio is maintained, and residues are nearly saturated at shallow depths which limits carbonate precipitation. Approximately 13 kg (+/- 1) of atmospheric CO_2 were sequestered in cell EC-2 between 2011 and 2015, which corresponds to a mean rate of 1.4 (+/-0.3) $kgCO_2$/tonne/year. However, the carbon sequestration capacity was inhibited by the high water content.

This study underlines the critical impact of hydrogeological properties and leachate water geochemistry on atmospheric CO_2 sequestration capacity of ultramafic mine wastes. Changes in these properties during passive carbon mineralization must be addressed in order to optimise atmospheric CO_2 sequestration in large-scale mining waste deposits.

Acknowledgements

We thank RN an anonymous reviewer for their comments which helped improve the paper significantly.

~~**Figure 1** : a) Site location and b) geological context of the proposed DNP mine site and Dumont sill.~~

~~**Figure 2** : Textures in the experimental cells EC-1 and EC-2. a) General view of waste-rock cell EC-1 with pluri-centimetric blocks at the surface, b) white crusts coating surfaces and fractures in samples from EC-1, c) surface of a pluri-centimetric block in EC-1 coated with white crusts, d) white crust observed with binocular magnifier, with several phases of precipitation visible, e) general view of the tailings cell EC-2, f) evaporitic structure (cones) observed at the edges of cell EC-2, g) residues cemented and covered with white crust below the wood support beam at the edges of cell EC-2, h) indurated flat crust, sampled at the edge of cell EC-2.~~

~~**Figure 3** : Evolution of water flux at the bottom of the experimental cells in 2013.~~

~~**Figure 4** : Water content evolution with depth in EC-2 and rainfall in 2016.~~

~~**Figure 5** : Evolution of chemical composition of leachate in EC-1 since 2011.~~

~~**Figure 6** : Evolution of chemical composition of leachate from EC-2 since 2011.~~

~~**Figure 7** : Evolution of saturation indices of the main carbonate minerals.~~

~~**Figure 8** : Scanning electron micrographs of surface samples from EC-1 and EC-2. a) Surface of a white crust sampled in cell EC-1; depressions are filled with fissured carbonates whereas on the top well-crystalized carbonates are visible, b) serpentine grain, from cell EC-1, partially covered with flaky carbonate minerals, c) white crust, from cell EC-1, with well-crystalized hydromagnesite, d) needle of well-crystalized aragonite observed on sample surface from EC-1, e) surface of a flat crust, from EC-2. Carbonate minerals have coated the surface and cemented the tailings grains. f) Serpentine grain, from flat crust in EC-2, partially covered with flaky carbonates overcome by well-crystalized nesquehonite, g) different sizes of nesquehonite crystals observed on a surface sample from EC-2, h) intergrowth of microbial mats and carbonate minerals observed at the surface of cell EC-2.~~

~~**Figure 9** : Back-scattered electron micrographs of polished thin sections from cell EC-1 and EPMA chemical compositions reported on ternary diagrams.~~

~~**Figure 10** : Inorganic* carbon content at the center of cell EC-2~~

~~**Figure 11** : Cross-section of cell EC-2 in May 2015 and contoured inorganic carbon content.~~

Formatted: Font: Bold

Formatted: Left

Formatted: Font: 12 pt

Formatted: Line spacing: 1.5 lines

References

Acero, P., Ayora, C., Carrera, J., 2007. Coupled thermal, hydraulic and geochemical evolution of pyritic tailings in unsaturated column experiments. Geochim. Cosmochim. Acta 71, 5325–5338. doi:10.1016/j.gca.2007.09.007

Appelo, C.A.J., Postma, D., 2005. Geochemistry, groundwater andpollution. Rotterdam, Netherlands, AA Balkema. SegundaEdici{ó}n.

Assima, G.P., Larachi, F., Beaudoin, G., Molson, J., 2012. CO2 sequestration in chrysotile mining residues-implication of watering and passivation under environmental conditions. Ind. Eng. Chem. Res. 51, 8726–8734. doi:10.1021/ie202693q

Assima, G.P., Larachi, F., Molson, J., Beaudoin, G., 2014a. Comparative study of five Québec ultramafic mining residues for use in direct ambient carbon dioxide mineral sequestration. Chem. Eng. J. 245, 56–64. doi:10.1016/j.cej.2014.02.010

Assima, G.P., Larachi, F., Molson, J., Beaudoin, G., 2014b. Impact of temperature and oxygen availability on the dynamics of ambient CO2 mineral sequestration by nickel mining residues. Chem. Eng. J. 240, 394–403. doi:10.1016/j.cej.2013.12.010

Assima, G.P., Larachi, F., Molson, J., Beaudoin, G., 2014c. New tools for stimulating dissolution and carbonation of ultramafic mining residues. Can. J. Chem. Eng. 92, 2029–2038. doi:10.1002/cjce.22066

Assima, G.P., Larachi, F.F., Beaudoin, G., Molson, J., 2013. Dynamics of carbon dioxide uptake in chrysotile mining residues - Effect of mineralogy and liquid saturation. Int. J. Greenh. Gas Control 12, 124–135. doi:10.1016/j.ijggc.2012.10.001

Aubertin, M., Bussiere, B., Chapuis, R.P., 1996. Hydraulic conductivity of homogenized tailings from hard rock mines. Can. Geotech. J. 33, 470–482. doi:10.1139/t96-068

Awoh, A.S., Plante, B., Bussière, B., Mbonimpa, M., 2014. Measurement and prediction of the CO2 effective diffusion coefficient in unsaturated media. Geo Regina.

Bea, S., Wilson, S., Mayer, K.U., Dipple, G.M., Power, I.M., Gamazo, P., 2012. Reactive Transport Modeling of Natural Carbon Sequestration in Ultramafic Mine Tailings. Vadose Zo. J. 11, 0. doi:10.2136/vzj2011.0053

Beaudoin, G., Hébert, R., Constantin, M., Duchesne, J., Cecchi, E., Huot, F., Vigneau, S., Fiola, R.,

Formatted: English (Canada)

2008. Spontaneous carbonation of serpentine in milling and mining waste, southern Qué}bec and Italy. Proc. Accel. Carbonation Environ. Mater. Eng. 73À}82.

Beaudoin, G., Nowamooz, A., Assima, G.P., Lechat, K., Gras, A., Entezari, A., Awoh, A.-S., Horswill, M., Turcotte, S., Larachi, F., others, 2017. Passive Mineral Carbonation of Mg-rich Mine Wastes by Atmospheric CO2. Energy Procedia 114, 6083–6086.

Beinlich, A., Austrheim, H., 2012. In situ sequestration of atmospheric CO 2 at low temperature and surface cracking of serpentinized peridotite in mine shafts. Chem. Geol. 332–333, 32–44. doi:10.1016/j.chemgeo.2012.09.015

Berner, R.A., Kothavala, Z., 2001. Geocarb III: A revised model of atmospheric CO2 over phanerozoic time. Am. J. Sci. 301, 182–204. doi:10.2475/ajs.294.1.56

Bruni, J., Canepa, M., Chiodini, G., Cioni, R., Cipolli, F., Longinelli, A., Marini, L., Ottonello, G., Vetuschi Zuccolini, M., 2002. Irreversible water-rock mass transfer accompanying the generation of the neutral, Mg-HCO3 and high-pH, Ca-OC spring waters of the Genova province, Italy. Appl. Geochemistry 17, 455–474. doi:10.1016/S0883-2927(01)00113-5

Canterford, J.H., Tsambourakis, G., Lambert, B., 1984. Some observations on the properties of dypingite, Mg5 (CO3) 4 (OH) 2{·} 5H2O, and related minerals. Mineral. Mag. 48, 437–442.

Chatterjee, A., Lal, R., Wielopolski, L., Martin, M.Z., Ebinger, M.H., 2009. Evaluation of Different Soil Carbon Determination Methods. CRC. Crit. Rev. Plant Sci. 28, 164–178. doi:10.1080/07352680902776556

Cipolli, F., Gambardella, B., Marini, L., Ottonello, G., Zuccolini, M.V., 2004. Geochemistry of high-pH waters from serpentinites of the Gruppo di Voltri (Genova, Italy) and reaction path modeling of CO2 sequestration in serpentinite aquifers. Appl. Geochemistry 19, 787–802. doi:10.1016/j.apgeochem.2003.10.007

Conyers, M.K., Poile, G.J., Oates, A.A., Waters, D., Chan, K.Y., 2011. Comparison of three carbon determination methods on naturally occurring substrates and the implication for the quantification of "soil carbon." Soil Res. 49, 27–33. doi:10.1071/SR10103

De Vos, B., Lettens, S., Muys, B., Deckers, J.A., 2007. Walkley-Black analysis of forest soil organic carbon: Recovery, limitations and uncertainty. Soil Use Manag. 23, 221–229. doi:10.1111/j.1475-2743.2007.00084.x

Duke, J.M., 1986. Petrology and economic geology of the Dumont sill: an Archean intrusion of komatiitic affinity in northwestern Quebec. Ottawa.

Eckstrand, O.R., 1975. The dumont serpentinite: A model for control of nickel-if erous opaque mineral assemblages by alteration reactions in ultramafic rocks. Econ. Geol. 70, 183–201. doi:10.2113/gsecongeo.70.1.183

Gaillardet, J., Dupré, B., Louvat, P., Allegre, C.J., 1999. Global silicate weathering and CO 2 consumption rates deduced from the chemistry of large rivers. Chem. Geol. 159, 3–30.

Gerdemann, S.J., O'Connor, W.K., Dahlin, D.C., Penner, L.R., Rush, H., 2007. Ex situ aqueous

mineral carbonation. Environ. Sci. Technol. 41, 2587–2593. doi:10.1021/es0619253

Gras, A., Beaudoin, G., Molson, J., Plante, B., Bussière, B., Lemieux, J.M., Dupont, P.P., 2017. Isotopic evidence of passive mineral carbonation in mine wastes from the Dumont Nickel Project (Abitibi, Quebec). Int. J. Greenh. Gas Control 60, 10–23. doi:10.1016/j.ijggc.2017.03.002

Harrison, A.L., Dipple, G.M., Power, I.M., Mayer, K.U., 2016. The impact of evolving mineral-water-gas interfacial areas on mineral-fluid reaction rates in unsaturated porous media. Chem. Geol. 421, 65–80. doi:10.1016/j.chemgeo.2015.12.005

Harrison, A.L., Dipple, G.M., Power, I.M., Mayer, K.U., 2015. Influence of surface passivation and water content on mineral reactions in unsaturated porous media: Implications for brucite carbonation and CO2 sequestration. Geochim. Cosmochim. Acta 148, 477–495. doi:10.1016/j.gca.2014.10.020

Harrison, A.L., Dipple, G.M., Song, W., Power, I.M., Mayer, K.U., Beinlich, A., Sinton, D., 2017. Changes in mineral reactivity driven by pore fluid mobility in partially wetted porous media. Chem. Geol. 463, 1–11. doi:10.1016/j.chemgeo.2017.05.003

Harrison, A.L., Power, I.M., Dipple, G.M., 2013. Accelerated carbonation of brucite in mine tailings for carbon sequestration. Environ. Sci. Technol. 47, 126–134. doi:10.1021/es3012854

Harrison, A.L., Mavromatis, V., Oelkers, E.H., Bénézeth, P., 2019. Solubility of the hydrated Mg-carbonates nesquehonite and dypingite from 5 to 35 °C: Implications for CO2 storage and the relative stability of Mg-carbonates. Chemical Geology, 504: 123-135.

Hitch, M., Dipple, G.M., 2012. Economic feasibility and sensitivity analysis of integrating industrial-scale mineral carbonation into mining operations. Miner. Eng. 39, 268–275. doi:10.1016/j.mineng.2012.07.007

Hopkinson, L., Rutt, K.., Cressey, G., 2008. The transformation of nesquehonite to hydromagnesite in the system CaO-MgO-H2O-CO2: an experimental spectroscopic study. J. Geol. 116, 387–400. doi:10.1086/588834

IPCC, 2014. Climate Change 2014: Synthesis Report. Contribution of Working Groups I, II and III to the Fifth Assessment Report of the Intergovernmental Panel on Climate Change, Core Writing Team, R.K. Pachauri and L.A. Meyer. doi:10.1017/CBO9781107415324

IPCC, 2005. IPCC special report on carbon dioxide capture and storage. Prepared by working group III of the Intergovernmental Panel on Climate Change, in: IPCC Special Report on Carbon Dioxide Capture and Storage. p. 442. doi:10.1002/anie.201000431

Kandji, Plante, B., Bussière, B., Awoh, A.S., Ibrahim Saïb, B.A., Dupont, P.P., 2015. Prediction of drainage water quality from mining waste with carbon sequestration potential. Proc. (IMWA/ICARD), Santiago, Chili, 21-24 avril 2015.

Kandji, Plante, B., Bussière, B., Beaudoin, G., Dupont, P.P., 2017a. Kinetic testing to evaluate the mineral carbonation and metal leaching potential of ultramafic tailings: Case study of the Dumont Nickel Project, Amos, Québec. Appl. Geochemistry 84, 262–276.

doi:10.1016/j.apgeochem.2017.07.005

Kandji, Plante, B., Bussière, B., Beaudoin, G., Dupont, P.P., Bussiere, B., Beaudoin, G., Dupont, P.P., Bussière, B., Beaudoin, G., Dupont, P.P., 2017b. Geochemical behavior of ultramafic waste rocks with carbon sequestration potential: a case study of the Dumont Nickel Project, Amos, Québec. Environ. Sci. Pollut. Res. 24, 11734–11751. doi:10.1007/s11356-017-8735-9

Kelemen, P.B., Matter, J.r., 2008. In situ carbonation of peridotite for CO2 storage. Proceedings of the National Academy of Sciences, 105(45 %U http://www.pnas.org/content/105/45/17295.abstract): 17295-17300.

Lackner, K.S., Wendt, C.H., Butt, D.P., Joyce, E.L., Sharp, D.H., 1995. Carbon dioxide disposal in carbonate minerals. Energy 20, 1153–1170. doi:10.1016/0360-5442(95)00071-N

Langmuir, D., 1965. Stability of Carbonates in the System. J. Geol. 73, 730–754.

Lechat, K., Lemieux, J.M., Molson, J., Beaudoin, G., Hébert, R., 2016. Field evidence of CO2 sequestration by mineral carbonation in ultramafic milling wastes, Thetford Mines, Canada. Int. J. Greenh. Gas Control 47, 110–121. doi:10.1016/j.ijggc.2016.01.036

Lechat, K.D., 2016. Séquestration géologique du CO2 par carbonatation minérale dans les résidus miniers Séquestration géologique du CO2 par carbonatation minérale dans les résidus miniers. Université Laval.

Matter, J.M. et al., 2009. Permanent Carbon Dioxide Storage into Basalt: The CarbFix Pilot Project, Iceland. Energy Procedia, 1(1): 3641-3646.

Marques, J.M., Carreira, P.M., Carvalho, M.R., Matias, M.J., Goff, F.E., Basto, M.J., Graça, R.C., Aires-Barros, L., Rocha, L., 2008. Origins of high pH mineral waters from ultramafic rocks, Central Portugal. Appl. Geochemistry 23, 3278–3289. doi:10.1016/j.apgeochem.2008.06.029

McCutcheon, J., Wilson, S.A., Southam, G., 2016. Microbially Accelerated Carbonate Mineral Precipitation as a Strategy for in Situ Carbon Sequestration and Rehabilitation of Asbestos Mine Sites. Environ. Sci. Technol. 50, 1419–1427. doi:10.1021/acs.est.5b04293

Mills, S.J., Wilson, S.A., Dipple, G.M., Raudsepp, M., 2010. The decomposition of konyaite: importance in CO2 fixation in mine tailings. Mineral. Mag. 74, 903–917. doi:10.1180/minmag.2010.074.5.903

Molson, J., Aubertin, M., Bussière, B., Benzaazoua, M., 2008. Geochemical transport modelling of drainage from experimental mine tailings cells covered by capillary barriers. Appl. Geochemistry 23, 1–24. doi:10.1016/j.apgeochem.2007.08.004

Molson, J.W., Fala, O., Aubertin, M., Bussière, B., 2005. Numerical simulations of pyrite oxidation and acid mine drainage in unsaturated waste rock piles. J. Contam. Hydrol. 78, 343–371. doi:10.1016/j.jconhyd.2005.06.005

Mumpton, F. a., Thompson, C.S., 1966. The Stability of Brucite in the Weathering Zone of the New Idria Serpentinite. Clays Clay Miner. 14, 249–257. doi:10.1346/CCMN.1966.0140122

Nordstrom, D.K., 2011. Hydrogeochemical processes governing the origin, transport and fate of major and trace elements from mine wastes and mineralized rock to surface waters. Appl. Geochemistry 26, 1777–1791. doi:10.1016/j.apgeochem.2011.06.002

Nordstrom, D.K., 2009. Acid rock drainage and climate change. J. Geochemical Explor. 100, 97–104. doi:10.1016/j.gexplo.2008.08.002

Olajire, A.A., 2013. A review of mineral carbonation technology in sequestration of CO2. J. Pet. Sci. Eng. 109, 364–392. doi:10.1016/j.petrol.2013.03.013

O'Neil, J. R.; Barnes, I. C^{13} and O^{18} compositions in some freshwater carbonates associated with ultramafic rocks and serpentinites: Western United States. Geochim. Cosmochim. Acta 1971, 35, 687–697.

Oskierski, H.C., Dlugogorski, B.Z., Oliver, T.K., Jacobsen, G., 2016. Chemical and isotopic signatures of waters associated with the carbonation of ultramafic mine tailings, Woodsreef Asbestos Mine, Australia. Chem. Geol. 436, 11–23. doi:10.1016/j.chemgeo.2016.04.014

Oskierski, Dlugogorski, B.Z., Jacobsen, G., 2013a. Sequestration of atmospheric CO2 in chrysotile mine tailings of the Woodsreef Asbestos Mine, Australia: Quantitative mineralogy, isotopic fingerprinting and carbonation rates. Chem. Geol. 358, 156–169. doi:10.1016/j.chemgeo.2013.09.001

Oskierski, Dlugogorski, B.Z., Jacobsen, G., Oskierski, Dlugogorski, B.Z., Jacobsen, G., 2013b. Sequestration of atmospheric CO2 in a weathering-derived, serpentinite-hosted magnesite deposit: 14C tracing of carbon sources and age constraints for a refined genetic model. Geochim. Cosmochim. Acta 122, 226–246. doi:10.1016/j.gca.2013.08.029

Park, A.H.A., Fan, L.S., 2004. CO2 mineral sequestration: Physically activated dissolution of serpentine and pH swing process. Chem. Eng. Sci. 59, 5241–5247. doi:10.1016/j.ces.2004.09.008

Parkhurst, D.L., Appelo, C.A.J., others, 1999. User's guide to PHREEQC (Version 2): A computer program for speciation, batch-reaction, one-dimensional transport, and inverse geochemical calculations.

Paukert, A.N., Matter, J.M., Kelemen, P.B., Shock, E.L., Havig, J.R., 2012. Reaction path modeling of enhanced in situ CO 2 mineralization for carbon sequestration in the peridotite of the Samail Ophiolite, Sultanate of Oman. Chem. Geol. 330–331, 86–100. doi:10.1016/j.chemgeo.2012.08.013

Peregoedova, A., Aubertin, M., Bussière, B., 2014. Evaluation of the water retention curve of mine waste rock using laboratory tests and predictive models. Geo Regina.

Peregoedova, A., Aubertin, M., Polytechnique, É., 2012. Laboratory measurement and prediction of the saturated hydraulic conductivity of mine waste rock.

Plante, B., Kandji, E.H.B., Bussière, B., Awoh, A.S., Ibrahim-Saib, B.A., Beaudoin, G., Gras, A., Molson, J., Dupont, P.P., 2014. Geochemical behavior of carbon-sequestrating mine wastes: Dumont project Royal Nickel Corporation. Proc. Tailings and mine waste. Proc. Tailings mine

waste 2014.

Pokrovsky, O.S., Schott, J., 2000. Kinetics and mechanism of forsterite dissolution at 25 degrees C and pH from 1 to 12. Geochim. Cosmochim. Acta 64, 3313–3325. doi:10.1016/s0016-7037(00)00434-8

Power, I.M., Dipple, G.M., Southam, G., 2010. Bioleaching of ultramafic tailings by Acidithiobacillus spp. for CO 2 sequestration. Environ. Sci. Technol. 44, 456–462. doi:10.1021/es900986n

Power, I.M., Harrison, A.L., Dipple, G.M., 2016. Accelerating Mineral Carbonation Using Carbonic Anhydrase. Environ. Sci. Technol. 50, 2610–2618. doi:10.1021/acs.est.5b04779

Power, I.M., Wilson, S.A., Thom, J.M., Dipple, G.M., Gabites, J.E., Southam, G., 2009. The hydromagnesite playas of Atlin, British Columbia, Canada: A biogeochemical model for CO2 sequestration. Chem. Geol. 260, 302–316. doi:10.1016/j.chemgeo.2009.01.012

Power, Harrison, A.L., Dipple, G.M., Southam, G., 2013a. Carbon sequestration via carbonic anhydrase facilitated magnesium carbonate precipitation. Int. J. Greenh. Gas Control 16, 145–155. doi:10.1016/j.ijggc.2013.03.011

Power, McCutcheon, J., Harrison, A., Wilson, S., Dipple, G., Kelly, S., Southam, C., Southam, G., 2014. Strategizing Carbon-Neutral Mines: A Case for Pilot Projects. Minerals 4, 399–436. doi:10.3390/min4020399

Power, Wilson, S.A., Dipple, G.M., 2013b. Serpentinite carbonation for CO2 sequestration. Elements 9, 115–121. doi:10.2113/gselements.9.2.115

Pronost, J., Beaudoin, G., Lemieux, J.M., Hébert, R., Constantin, M., Marcouiller, S., Klein, M., Duchesne, J., Molson, J.W., Larachi, F., Maldague, X., 2012. CO2-depleted warm air venting from chrysotile milling waste (Thetford Mines, Canada): Evidence for in-situ carbon capture from the atmosphere. Geology 40, 275–278. doi:10.1130/G32583.1

Pronost, J., Beaudoin, G., Tremblay, J., Larachi, F., Duchesne, J., Hébert, R., Constantin, M., 2011. Carbon sequestration kinetic and storage capacity of ultramafic mining waste. Environ. Sci. Technol. 45, 9413–9420. doi:10.1021/es203063a

Pronost, J., Ph, D., Beaudoin, G., Ph, D., Constantin, M., Ph, D., Duchesne, J., Ph, D., Hébert, R., Ph, D., 2010. Evaluation of the mineral carbonation potential of mining residues produced by Royal Nickel pilot plant , Amos.

Rollo, H.A., Jamieson, H.E., 2006. Interaction of diamond mine waste and surface water in the Canadian Arctic. Appl. Geochemistry 21, 1522–1538. doi:10.1016/j.apgeochem.2006.05.008

Ruiz-Agudo, E., Putnis, C. V., Rodriguez-Navarro, C., Putnis, A., 2012. Mechanism of leached layer formation during chemical weathering of silicate minerals. Geology 40, 947–950. doi:10.1130/G33339.1

Sanna, A., Uibu, M., Caramanna, G., Kuusik, R., Maroto-Valer, M.M., 2014. A review of mineral carbonation technologies to sequester CO2. Chem. Soc. Rev. 43, 8049–8080.

doi:10.1039/C4CS00035H

Sciortino, M., Mungall, J.E., Muinonen, J., 2015. Generation of High-Ni sulfide and alloy phases during serpentinization of dunite in the dumont sill, Quebec. Econ. Geol. 110, 733–761. doi:10.2113/econgeo.110.3.733

Seifritz, W., 1990. CO_2 disposal by means of silicates, Nature. doi:10.1038/345486b0

Sipilä, J., Teir, S., Zevenhoven, R., 2008. Carbon dioxide sequestration by mineral carbonation Literature review update 2005 – 2007. Rep. VT 52. doi:10.1080/00908310600628263

Staples, L.P., Bowen, J.M., Bernier, S.B., Warren, D.A., Scott, C.C., Duncan, J.F., Murphy, B.A., Bertrand, V.J., Scott, K.C., Latulippe, S., 2013. Technical Report on the Dumont Ni Project, Launay and Trécesson Townships, Quebec, Canada - 2013 432.

Teir, S., Eloneva, S., Fogelholm, C.J., Zevenhoven, R., 2009. Fixation of carbon dioxide by producing hydromagnesite from serpentinite. Appl. Energy 86, 214–218. doi:10.1016/j.apenergy.2008.03.013

Turvey, C., 2015. Hydrotalcites As a Secondary Carbon Sink in Serpentinites. Fifth Int. Conf. Accel. ed Carbonation Environ. Mater. Eng. New York, 21–24 June 2015. 3208.

Turvey, C.C., Wilson, S.A., Hamilton, J.L., Southam, G., 2017. Field-based accounting of CO2 sequestration in ultramafic mine wastes using portable X-ray diffraction. Am. Mineral. 102, 1302–1310. doi://doi.org/10.2138/am-2017-5953

Ulven, O.I., Beinlich, A., Hövelmann, J., Austrheim, H., Jamtveit, B., 2017. Subarctic physicochemical weathering of serpentinized peridotite. Earth Planet. Sci. Lett. 468, 11–26. doi:10.1016/j.epsl.2017.03.030

Walkley, A., Black, I.A., 1934. An examination of the Degtjareff method for determining soil organic matter, and proposed modification of the chromic acid titration method. Soil Sci. 37, 29–38. doi:10.1097/00010694-193401000-00003

Wilson, S.A., Barker, S.L.L., Dipple, G.M., Atudorei, V., 2010. Isotopic disequilibrium during uptake of atmospheric CO2 into mine process waters: Implications for CO2 sequestration. Environ. Sci. Technol. 44, 9522–9529. doi:10.1021/es1021125

Wilson, S.A., Dipple, G.M., Power, I.M., Barker, S.L.L., Fallon, S.J., Southam, G., 2011. Subarctic weathering of mineral wastes provides a sink for atmospheric CO 2. Environ. Sci. Technol. 45, 7727–7736. doi:10.1021/es202112y

Wilson, S.A., Dipple, G.M., Power, I.M., Thom, J.M., Anderson, R.G., Raudsepp, M., Gabites, J.E., Southam, G., 2009. Carbon dioxide fixation within mine wastes of ultramafic-hosted ore deposits: Examples from the Clinton Creek and Cassiar Chrysotile deposits, Canada. Econ. Geol. 104, 95–112. doi:10.2113/gsecongeo.104.1.95

Wilson, S.A., Harrison, A.L., Dipple, G.M., Power, I.M., Barker, S.L.L., Ulrich Mayer, K., Fallon, S.J., Raudsepp, M., Southam, G., 2014. Offsetting of CO2 emissions by air capture in mine tailings at the Mount Keith Nickel Mine, Western Australia: Rates, controls and prospects for

carbon neutral mining. Int. J. Greenh. Gas Control 25, 121–140. doi:10.1016/j.ijggc.2014.04.002

Wilson, S.A., Raudsepp, M., Dipple, G.M., 2006. Verifying and quantifying carbon fixation in minerals from serpertine-rich mine tailings using the Rietveld method with X-ray powder diffraction data. Am. Mineral. 91, 1331–1341. doi:10.2138/am.2006.2058

Zarandi, A., Larachi, F., Beaudoin, G., Plante, B., Sciortino, M., 2017a. Ambient mineral carbonation of different lithologies of mafic to ultramafic mining wastes/tailings--A comparative study. Int. J. Greenh. Gas Control 63, 392–400.

Zarandi, A., Larachi, F., Beaudoin, G., Plante, B., Sciortino, M., 2017b. Nesquehonite as a carbon sink in ambient mineral carbonation of ultramafic mining wastes. Chem. Eng. J. 314, 160–168. doi:10.1016/j.cej.2017.01.003

Zarandi, A., Larachi, F., Beaudoin, G., Plante, B., Sciortino, M., 2016. Multivariate study of the dynamics of CO2 reaction with brucite-rich ultramafic mine tailings. Int. J. Greenh. Gas Control 52, 110–119. doi:10.1016/j.ijggc.2016.06.022

Figure captions

Figure 1 : a) Site location and b) geological context of the proposed DNP mine site and Dumont sill.

Figure 2 : Textures in the experimental cells EC-1 and EC-2. a) General view of waste-rock cell EC-1 with pluri-centimetric blocks at the surface, b) white crusts coating surfaces and fractures in samples from EC-1, c) surface of a pluri-centimetric block in EC-1 coated with white crusts, d) white crust observed with binocular magnifier, with several phases of precipitation visible, e) general view of the tailings cell EC-2, f) evaporitic structure (cones) observed at the edges of cell EC-2, g) residues cemented and covered with white crust below the wood support beam at the edges of cell EC-2, h) indurated flat crust, sampled at the edge of cell EC-2.

Figure 3 : Evolution of water flux at the bottom of the experimental cells in 2013.

Figure 4 : Water content evolution with depth in EC-2 and rainfall in 2016.

Figure 5 : Evolution of chemical composition of leachate in EC-1 since 2011.

Formatted: Font: 12 pt

Formatted: Line spacing: 1.5 lines

Figure 6 : Evolution of chemical composition of leachate from EC-2 since 2011.

Figure 7 : Evolution of saturation indices of the main carbonate minerals.

Figure 8 : Scanning electron micrographs of surface samples from EC-1 and EC-2. a) Surface of a white crust sampled in cell EC-1; depressions are filled with fissured carbonates whereas on the top well-crystalized carbonates are visible, b) serpentine grain, from cell EC-1, partially covered with flaky carbonate minerals, c) white crust, from cell EC-1, with well-crystalized hydromagnesite, d) needle of well-crystalized aragonite observed on sample surface from EC-1, e) surface of a flat crust, from EC-2. Carbonate minerals have coated the surface and cemented the tailings grains. f) Serpentine grain, from flat crust in EC-2, partially covered with flaky carbonates overcome by well-crystalized nesquehonite, g) different sizes of nesquehonite crystals observed on a surface sample from EC-2, h) intergrowth of fungi and carbonate minerals observed at the surface of cell EC-2.

Figure 9 : Back-scattered electron micrographs of polished thin sections from cell EC-1 and EPMA chemical compositions reported on ternary diagrams.

Figure 10 : Inorganic* carbon content at the center of cell EC-2

Figure 11 : Cross-section of cell EC-2 in May 2015 and contoured inorganic carbon content.

Formatted: Font: 12 pt, English (Canada)

Atmospheric carbon sequestration in ultramafic mining residues and impacts on leachate water chemistry at the Dumont Nickel Project, Quebec, Canada

A. Gras[1*], G. Beaudoin[1], J. Molson[1], B. Plante[2],

[1] Département de Géologie et de Génie Géologique, Université Laval,Québec, Canada

[2] Institut de Recherche en Mines et en Environnement, Université du Québec en Abitibi-Témiscamingue, Rouyn-Noranda, Canada

Abstract

Passive carbon mineralization in ultramafic mining residues, which allows the sequestration of CO_2 through carbonate precipitation, is one of the options being considered to limit the accumulation of anthropogenic CO_2 in the atmosphere. The Dumont Nickel Project (DNP) will generate approximately 1.7 Gt of utramafic mining residues over 33 years of production and the mine will release about 127,700 tonnes of CO_2 each year. Using two experimental cells filled with ultramafic waste rock (EC-1) and milling residues (EC-2), the impacts of carbon mineralization on leachate water quality were studied and the quantity of sequestered carbon was estimated. Hydrotalcite supergroup minerals, aragonite, artinite, nesquehonite, dypingite and hydromagnesite precipitated through atmospheric weathering, while the inorganic carbon content of the weathered mining waste increased from 0.1 wt% to 4.0 wt% which indicate active CO_2 sequestration. The leachate water, sampled at the bottom of the experimental cells, is characterized by an alkaline pH (~9.5), a high alkalinity (~90 to ~750 mg/L) and a high concentration of magnesium (~50 - ~750 mg/L), which is typical from weathering of ultramafic rocks in a system open to CO_2.

Since 2012, the chemical composition of the leachate water has evolved seasonally. These seasonal variations are best explained by: (1) climatic variations over the year and, (2) increased carbonate precipitation between May and July. Increased carbonate precipitation decreased the alkalinity and magnesium concentrations in the leachate water and produced pore waters which were undersaturated with respect to carbonate minerals such as artinite and hydromagnesite.

Carbonate precipitation thus self-limits carbon sequestration through a negative feed-back loop. The carbon sequestration potential of the DNP residues is also influenced by the hydrogeological properties of the residues. In cell EC-2, a high liquid/solid ratio, which limits carbonate precipitation, was maintained by the hydrogeological properties. Since 2011, an estimate of 13 kg of atmospheric CO_2 has been sequestered in the milling residues (EC-2), which corresponds to a mean rate of 1.4 (+/- 0.3) $kgCO_2$/tonne/year. Using this mean rate, the 15 Mt of tailings produced each year, during the planned 33 years of mining operation, could potentially sequester 21,000 tonne of CO_2 per year by passive carbon mineralization, about 16% of the 127,700 tonnes of CO_2 annually emitted by the planned mining operation.

1. Introduction

Anthropogenic CO_2 released into the atmosphere is considered a major driver of global climate change (IPCC, 2014). In order to limit accumulation of gaseous CO_2 in the atmosphere, several methods of carbon sequestration are envisaged including carbon mineralization (IPCC, 2005). As reviewed by Seifritz (1990), carbon mineralization technologies are derived from natural exothermic reactions, which occur spontaneously and trap CO_2 through carbonate precipitation (Berner and Kothavala, 2001; Gaillardet et al., 1999; Lackner et al., 1995). The general carbon mineralization reaction for silicate minerals such as serpentine is summarized in Reaction (1):

$$\mathbf{(Mg,Ca)_xSi_yO_{x+2y+z}H_{2z} + xCO_2 \rightarrow x(Mg,Ca)CO_3 + ySiO_2 + zH_2O + Heat} \quad \mathbf{(1)}$$

Carbon mineralization is attractive because no post-storage monitoring is necessary and carbon dioxide is sequestered over geological time scales. Two types of carbon mineralization are considered (Beaudoin et al., 2008; Gerdemann et al., 2007; Kelemen and Matter (2008); Matter et al. (2009); Olajire, 2013; Park and Fan, 2004; Pronost et al., 2011; Sanna et al., 2014; Sipilä et al., 2008; Teir et al., 2009) :

(1) in-situ carbonation, wherein pure CO_2 is injected into subsurface mafic formations to form carbonate minerals, and

(2) ex-situ carbon mineralization, which uses mining or industrial residues as the carbon sink.

Natural weathering of ultramafic mining residues captures atmospheric CO_2 through passive carbon mineralization. Carbonation rates of up to 1700 g C m^{-2} y^{-1}, for example, have been reported from historical and active mining sites. The main carbonate minerals precipitated in mining

residues are pyroaurite-3R [$Mg_6Fe_2^{3+}(CO_3)(OH)_{16}.4.H_2O$], nesquehonite [$MgCO_3.3.H_2O$], dypingite [$Mg_5(CO_3)_4(OH)_2.5.H_2O$], hydromagnesite [$Mg_5(CO_3)_4(OH)_2.4(H_2O)$], and aragonite [$CaCO_3$] (Beaudoin et al., 2008; Gras et al., 2017; Lechat et al., 2016; Oskierski et al., 2013; Power et al., 2013a, 2013b; Pronost et al., 2012; Rollo and Jamieson, 2006; Turvey et al., 2017; Wilson et al., 2011, 2006, 2014). Passive carbon mineralization has previously been studied by considering mineralogical evolution and leachate water geochemistry (Assima et al., 2014a, 2013; Beinlich and Austrheim, 2012; Harrison et al., 2017, 2013; Power et al., 2009; Rollo and Jamieson, 2006; Zarandi et al., 2017a, 2017b, 2016), and by analysing the stable carbon isotope (C^{13} and C^{12} composition of dissolved inorganic carbon (DIC) and neo-formed carbonates (Beaudoin et al., 2017, 2008; Gras et al., 2017; Harrison et al., 2016, 2013, Oskierski et al., 2013b, 2016, Wilson et al., 2014, 2011, 2009). Ex-situ, passive carbon mineralization in mining residues has two main advantages: (1) the mine wastes can be re-used for environmental benefit, and (2) CO_2 can be directly sequestered from the atmosphere. Moreover, these processes can potentially lead to developing carbon-neutral mines (Harrison et al., 2013; Hitch and Dipple, 2012; Mills et al., 2010; Power et al., 2014). The main disadvantage is the slow rate of reaction, compared to ex-situ carbon mineralization.

The Dumont Nickel Project (DNP) of RNC Minerals (RNCM) is designed to produce 0.51 Gt of ultramafic waste rock and 1.18 Gt of milling (tailings) residues (Staples et al., 2013). The carbon sequestration capacity of these future residues at high partial pressure of CO_2, and the effect of mineralogy, water saturation, watering frequency, and temperature, have been well studied at the laboratory scale (Assima et al., 2014a, 2014b, 2013, 2012, Kandji et al., 2017b, 2015; Plante et al., 2014; Pronost et al., 2010; Zarandi et al., 2016, 2017a, 2017b). However, in order to develop useful engineered solutions for carbon sequestration, and to properly estimate the carbon sequestration capacity, more realistic field experiments are required (Olajire, 2013; Lechat et al., 2016; Gras et al., 2017).

Using two experimental cells, Gras et al. (2017) demonstrated that between the three potential sources of CO_2, notably: (1) the atmosphere, (2) organic matter oxidation and (3) carbonate dissolution, atmospheric CO_2 was the main source of sequestered carbon during natural atmospheric weathering of the DNP residues. In addition, Gras et al. (2017) showed that dissolution of atmospheric CO_2 in interstitial water was the first step which limited the carbon mineralization capacity. However, additional factors can also limit the mineralization capacity. For example, natural weathering of ultramafic rocks will change the geochemistry of meteoric water which percolates through the mining residues (Rollo and Jamieson 2006; Beinlich et al., 2012; Oskierski et

al., 2016) and natural terrain (Bruni et al., 2002; Cipolli et al., 2004; Marques et al., 2008; Paukert et al., 2012). Since changes in the water chemistry can affect carbonate precipitation, they may therefore also impact the carbon sequestration potential of mine residues (Appelo and Postma, 2005).

In this contribution, using two field experimental cells, EC-1 filled with mine waste, and EC-2 which contains milling residue from the DNP, we report on changes in (1) leachate water geochemistry, (2) waste mineralogy, and (3) carbon content. In addition, the effects of hydrogeological properties and leachate water geochemistry on carbonate mineral precipitation are investigated. Finally, the amount of atmospheric CO_2 trapped during atmospheric weathering of the DNP residues is estimated.

2. Geological setting

The DNP site is located near the town of Amos in north-western Québec (Figure 1a). The deposit is hosted in a sill which had intruded into rock of the Superior province of the Canadian Shield. Two distinct units are identified in the sill: (1) a mafic zone of gabbro which is overlain by (2) an ultramafic zone formed by peridotite and dunite (Figure 1b) (Duke, 1986; Eckstrand, 1975; Sciortino et al., 2015). The ultramafic zone, which contains a resource of 1.72 Mt of nickel ore, is approximately 6.8 km long with an average thickness of 450 m. In the Dumont sill, nickel enrichment of intercumulus minerals is a product of serpentinization (Duke, 1986; Sciortino et al., 2015) which is a hydrothermal process involving water and heat which alters silicate minerals, such as olivine [$(Mg,Fe,Ni)_2SiO_4$], to serpentine minerals [$(Mg,Fe,Ni)_3Si_2O_5(OH)_4$], as well as to brucite [$Mg(OH)_2$] and magnetite [$Fe^{2+}Fe_2^{3+}O_4$]. The dunite protolith was composed of Ni-rich olivine with horizons rich in sulfide minerals. During serpentinization, the nickel was redistributed in intercumulus pentlandite [$(Fe,Ni)_9S_8$], awaruite [Ni_3Fe] and heazlewoodite [Ni_3S_2] (Sciortino et al., 2015). The main mineral assemblage in the dunite subzone consists of lizardite, magnetite, brucite, and chlorite, with variable amounts of pentlandite, awaruite, and heazlewoodite (Sciortino et al., 2015; Staples et al., 2013). The DNP is expected to generate approximately 1.7 Gt of ultramafic mining residue of two types: (1) ~1.18 Gt of tailing residues issued from the metallurgical processes, and (2) ~510 Mt of waste rocks (Staples et al., 2013).

3. Materials and Methods

3.1 Experimental cells:

Near the planned DNP mining site near Amos, Quebec, two experimental cells were built and instrumented in order to study weathering of the mine's ultramafic mining residues. Gras et al. (2017) provide detailed descriptions of the experimental cells. The first cell (EC-1) was filled using 104 tonnes of waste rock from blasting of a dunite outcrop (Figure 1b). The grain size of waste rock in EC-1 ranged from milimetric to pluricentrimetric blocs. The second cell (EC-2) contains approximately 2.6 tonnes of milling residues containing the slimes, fluff and rougher tails (non-magnetic) produced in a pilot plant. The run of mine ore, processed in the pilot plant, was taken from four boreholes located in the dunite subzone (Figure 1b) (Staples et al., 2013). The pilot-plant process consisted of two cycles of grinding, desliming, and flotation in a hydrocyclone followed by magnetic separation. During the first cycle, the run of mine ore was crushed and ground in wet media with the dispersant Calgon © (500 g/t) and potassium amyl xanthate (PAX) (150 g/t) to 80% passing minus 150 μm, then the non-magnetic portion from the first cycle was crushed and ground in wet media to 80% passing minus 74 μm for the second cycle of deshalming and flotation.

Within both experimental cells, gas sampling ports were installed in order to monitor CO_2 concentrations within the interstitial air (Gras et al., 2017). In addition, cell EC-2 contained a Decagon 5TM probe, 4 cm below the tailings surface, to monitor changes in volumetric water content and temperature. In November 2015, two additional Decagon 5TM probes were placed at 14 and 25 cm depths to measure changes in water content and temperature with depth. At the bottom of cells EC-1 and EC-2, a geomembrane and a drain were installed to collect the leachate water. Both drains were connected to tipping bucket rain gauges to log the flux of water at the output of the cells. A weather station recorded solar radiation, temperature, wind speed and direction, and a tipping bucket rain gauge measured rainfall.

3.2 Leachate water analyses:

Leachate water is produced from infiltration of rain and meltwater through the mining residues in experimental cells EC-1 and EC-2. The leachate was sampled twice a month between July 2011 and November 2013, and then monthly from May 2014 to November 2015. The leachate water pH was measured on site, while samples were collected in bottles which were sent to Maxxam Analytical (QC, Canada) and to SGS Canada (ON, Canada) to measure major and minor ions and metals (Al, Sb, As, Ba, Be, Bi, B, Cd, Ca, Cr, Co, Cu, Sn, Fe, Li, Mg, Mn, Mo, Hg, Ni, Pb,

K, Se, Si soluble in HNO_3, SO_4, Na, Sr, Tl, Ti, U, V, Zn), and total alkalinity, until 2015. The geochemical model PhreeqC (Parkhurst et al., 1999) was used to calculate the saturation indices of major carbonate minerals in the leachate water. Since the temperature of the leachate was not measured, a temperature of 25°C was therefore used and after the method of Oskierski et al. (2016) the thermodynamic equilibrium calculations were carried out using the Wateq4f database (Ball and Nordstrom, 1991).

3.3 White crusts and core samples:

Within months of constructing the waste rock cell (EC-1), white crusts of a mineral precipitate started to coat the surface of the rock fragments during atmospheric weathering. The residues were sampled manually (Figure 2 a, b, c, d). White crusts of a mineral precipitate also indurated the tailings surface near the edges of cell EC-2 which were also sampled (Figure 2 e, f, g, h). Between 2012 and 2015, surface crusts were sampled 19 and 16 times in both EC-1 and EC-2, respectively. In order to document the weathering processes acting on the residues, 7 cores, ranging in length from 14 cm to 32 cm, were sampled from October 2013 to November 2015 in the center of EC-2 using a steel tube (Gras et al., 2017). Additionally, two cores, 5 cm and 3 cm in length, were sampled in October 2014 and May 2015. One core was sampled below a wooden access plank at the edges of the cells and the other at the edges of the cell EC-2 (Figures 2 e and f) (Supplementary information).

3.4 Mineralogical analysis

Crushed samples from cells EC-1 and EC-2 were analysed by XRD using a Siemens D5000 X-ray diffractometer (Cu-Kα radiation). XRD patterns were collected with a scanning step of 1°/min (0.02° step size) over a 5-40° scattering angle range. The Jade computer program was used to identify the mineral phases.

A JEOL 840-A scanning electron microscope (SEM) at Université Laval, Québec, equipped with an Avalon (PGT) energy-dispersive X-ray spectrometer (EDS), was used in order to describe mineral habits and texture, and for mineral identification of the neo-formed phases.

Polished thin sections of white crusts from EC-1 and EC-2 were analyzed using a CAMECA SX-100 Electron Probe Micro-Analyzer (EPMA) at Université Laval. The device is equipped with 5 wavelength-dispersive spectrometers. Chemical analyses were performed using a 15 kV accelerating voltage with a 20 nA beam current, and a 10 μm beam size. Simple oxides

(GEO Standard Block of P and H Developments) and/or natural minerals (Mineral Standard Mount MINM 2553, Astimex Scientific; Jarosewich et al., 1980) were used to calibrate the instrument for chemical analyses.

3.5 Carbon content

The total carbon content was measured with an Eltra CS 800 carbon and sulphur analyser at Université Laval (Gras et al., 2017). High and low carbon contents were calibrated using, respectively, AR 4018 (1.30 +/- 0.05 wt% C), and UB-N serpentine ANRT (0.106 +/- 0.08 wt% C). The standards (Ar 4018 and UB-N serpentine) were analysed after every set of three analyses to test reproducibility of the measurement over time, yielding a precision (1σ) of 0.2 wt% C and of 0.03 wt% C for the high and the low carbon contents, respectively.

The organic carbon content was measured using a modified Walkley Black method (Gras et al., 2017; Walkley and Black, 1934) . Equation (2) below, from De Vos et al (2007) was used to calculate the organic carbon content:

$$\%C_{org} = M \times \frac{(V_1 - V_2) \times 0.3}{W} \times 1.32 \qquad (2)$$

where M is the molarity of the reference Fe_2SO_4 solution, V_1 is the volume (mL) of Fe_2SO_4 needed in a blank titration, V_2 is the volume (mL) of Fe_2SO_4 consumed in the sample titration, W is the weight (g) of the sample and 1.32 is the correction factor (Chatterjee et al., 2009; Conyers et al., 2011; De Vos et al., 2007).

4. Results

4.1 Field observations:

The experimental cells are located near Amos, in north-western Quebec, in a continental climate characterized by large differences in temperature between cold winters and warm summers. The mean temperature and the mean solar radiation intensity between the years 2011 and 2016 varied respectively, from -18°C and 32 W/m^2 in winter to 17°C and 230 W/m^2 in summer (Table 1). During summer, the rainfall events slightly decreased but intense rainfall events occurred frequently (≥30 mm). The mean total annual precipitation (snow and rain) between 2011 and 2016 was 840 mm/yr. The recording of rainfall was sometimes disrupted by mechanical failure and was completed using data from Environment Canada.

At the bottom of the cells, the leachate flow rate was recorded between April and November using a typing bucket rain gauge. The logging was frequently disrupted due to weather. Figure 3 presents the flow rates recorded between May and August 2013, together with the rain events for the year. In 2013, following a precipitation event of 25 mm in one day, the maximum flow rate in EC-1 was ~2000 L/day whereas in EC-2 it was ~1400 L/day (Figure 3). The mean discharge recorded between 2011 and 2015 ranged from 217 L/day to 546 L/day for EC-1 and from 111 L/day to 241 L/day for EC-2 (Figure 3)

In cell EC-1, the grain size of the waste rock is heterogeneous and ranges from silt to pluri-centimetric blocks whereas material from EC-2 is characterized by a D10 of 2.2 μm, a D80 of 119 μm and a uniformity coefficient (Cu=D10/D60) of 22 (Kandji et al., 2017) (Figure 2 a and e). The mean porosity in cell EC-2 is 44% and the dry bulk density is 1242 kg/m^3 +/- 55 kg/m^3. Other hydrogeological parameters for EC-1 and EC-2, presented in Gras et al. (2017), were estimated from the literature (Aubertin et al., 1996; Lechat et al., 2016; Molson et al., 2008, 2005, Peregoedova et al., 2014, 2012).

Figure 4 presents the evolution of the volumetric water content with depth in EC-2, with total precipitation for the year 2016. During the winter, the water content just below the surface (~ 4 cm deep) was constant near 10% whereas at 14 cm and 25 cm depths the water content reached 30% and 40 %, respectively. In spring, the water content increased by 10 % throughout the cell and fluctuated with rain events (Figure 4). Between 2011 and 2015, the average water content was ~25 % at 4 cm depth in cell EC-2.

4.2 Chemical evolution of the leachate water:

Rainwater chemical analyses yielded a pH of 5.5 and contained trace amounts of Al (0.03 mg/L), Pb (0.001 mg/L) and Zn (0.03 mg/L). Between December and April, the interstitial waters were frozen, thus chemical analyses on leachate water were performed only from May to November. The leachate analyses from both cells revealed the same pattern of evolution, with a transient phase after construction during the summer of 2011, followed by a regime characterized by seasonal cycles (Figures 5 and 6).

In EC-1 during the first summer (2011), the magnesium concentration, alkalinity, and pH increased from 6.5 to 110 mg/L (Mg), from 240 to 510 mg/L $CaCO_3$ (Alk) and from 8.17 to 8.81 (pH), respectively (Figure 5 a). During the same period, calcium and silica concentrations decreased from 85 to 36 mg/L and from 7.8 to 3.3 mg/L, respectively (Figure 5 b). Since 2012, the magnesium

and silica concentrations, as well as the alkalinity and pH, varied in seasonal cycles from 125 to 180 mg/L (Mg), from 1.2 to 6.2 mg/L (Si), from 125 to 700 mg/L $CaCO_3$ (Alk) and from 8.1 to 9.7 (pH), respectively. During these seasonal cycles, the magnesium concentration, pH and alkalinity decreased while silica concentrations increased from May to August. From August to November the trends were reversed (Figure 5 a,b). The calcium concentration generally decreases from year to year but had the same seasonal variations as silica and ranged from 3.4 to 20 mg/L (Ca).

In EC-2, the concentrations of chemical elements were lower than in EC-1 (Figure 6). Between July and November 2011, the magnesium concentration was highly variable, with a minimum and maximum value of 70 and 120 mg/L, respectively. Meanwhile, the alkalinity and pH increased from 45 to 180 mg/L $CaCO_3$ (Alk) and from 7.64 to 9.45 (pH), respectively (Figure 6 a), whereas calcium and silica concentrations decreased from 85 to 36 mg/L (Ca) and from 7.8 to 3.3 mg/L (Si), respectively (Figure 6 b). Between 2012 and 2015, as in EC-1, the magnesium, silica and calcium concentrations, as well as alkalinity and pH, varied seasonally between 50 and 140 mg/L (Mg), 0.9 to 7.2 mg/L (Ca), 0.67 to 2.7 mg/L (Si), 91 to 509 mg/L $CaCO_3$ (Alk), with a rise in pH from 8.93 to 10, respectively. While seasonal variations were the same as in EC-1, the intensity of seasonal variations in magnesium concentrations and alkalinity has decreased over the years in cell EC-2 (Figures 6 a,b).

In both experimental cells, potassium and sodium concentrations decreased from year to year since 2011. Additionally, similar to silica, the potassium and sodium concentrations increased each year between May and July then decreased until November (Figures 5 and 6). The potassium and sodium concentrations ranged from 4 to 2.3 mg/L (K) and from 13 to 2 mg/L (Na), respectively in EC-1, and from 15 to 0.2 mg/L (K) and from 26 to 0.9 mg/L (Na) in EC-2 (Supplementary information). The concentrations of other chemical components were near or below their detection limits (Supplementary information). Finally, in both cells the amplitude of the seasonal cycles seemed to decrease from year to year (Figures 5 and 6).

Thermodynamic equilibrium calculations revealed that carbonate saturation indices first increased in 2011 and then evolved seasonally following pH and alkalinity. The calculations suggest that magnesite, calcite and aragonite were over-saturated in leachate water, whereas nesquehonite remained under-saturated in the first 6 months of the experiment following set up in 2011 (Figure 7). The saturation indices of aragonite and calcite decreased over the years with calcium concentrations, but the leachate water remained generally over-saturated with respect to these minerals. Between May and July, saturation indices for hydromagnesite and artinite decreased

with the leachate becoming under-saturated whereas during the next three months, saturation indices increased, with the leachate becoming over-saturated in November (Figure 7). The thermodynamic equilibrium calculations also suggest that the partial pressure of CO_2 in the leachate water was often below the atmospheric partial pressure, also fluctuating with seasonal variations. However, the temperature of the leachate water was not measured which reduces precision on the pCO_2 calculations.

4.3 Mineralogical analysis:

XRD analyses of weathered mining residues from both cells revealed the presence of nesquehonite, dypingite, hydromagnesite, aragonite, artinite, and several minerals from the hydrotalcite supergroup, including brugnatellite [$Mg_6Fe^{3+}(CO_3)(OH)_{13}.4(H_2O)$], pyroaurite 3R, and pyroaurite 2H [$Mg_6Fe_2^{3+}(CO_3)(OH)_{16}.4(H_2O)$]. However, owing to the low modal abundance of the carbonate minerals, XRD data did not allow an accurate identification of the hydrotalcite supergroup minerals. Of the 19 samples analysed from EC-1, 10 contained hydromagnesite whereas only one EC-2 sample contained hydromagnesite. Surface samples from EC-2 most often contained dypingite. Well-crystalized, primary calcite [$CaCO_3$] was also found in rock fragments from EC-1 (Gras et al., 2017). Finally, in the first 3 centimeters of the core samples at the center of cell EC-2, a decrease in intensity or an absence of brucite peaks was observed in the XRD patterns of the weathered samples.

The SEM observations of weathered samples from EC-1 and EC-2 revealed the texture and habit of the precipitated carbonates (Figure 8). The weathered surfaces of samples from the waste rock cell (EC-1) were entirely (Figure 8 a) to partially (Figure 8 b) covered by carbonate minerals with a lamellar texture similar to the habit of hydromagnesite (Figure 8 c). On the surface of several samples, at the grain surfaces, depressions were filled with carbonate minerals, whereas on the top of the grains some well-crystallized lamellar minerals were observed. Well-crystallized carbonate minerals with the typical texture of aragonite or artinite have also been observed on samples from EC-1 (Figure 8 d). At the surface of EC-2, carbonate minerals cement small grains of tailings (Figure 8 e). Flaky carbonate minerals covered by well-crystalized needle-like minerals were observed on the same serpentine grains (Figure 8 f). Additionally, several crystal sizes of nesquehonite were observed on the same samples which indicate repeated precipitation phases (Figure 8 g). Finally, some samples from EC-2 contain potential microbial mats of fungal hyphae intertwined with carbonate minerals (Figure 8 h).

Using samples from cells EC-1 and EC-2, thin sections were impregnated with epoxy under vacuum, in order to preserve the carbonate-matrix interface. The carbonate crusts from EC-2 samples were too thin for EPMA analysis. Back Scattered Electron (BSE) imaging of the thin sections from EC-1 revealed different patterns of carbonate coating. The carbonate minerals were observed as: (1) thin layers on the serpentine substrate separated from lamellar minerals by a fracture (Figure 9 a), (2) within fractures cemented by carbonate with mining residue fragments (Figure 9 b) or (3) in complex fractures filled by carbonates and with brucite (Figure 9 c). The minerals at the carbonate-matrix interface had oxygen, magnesium and silica concentrations ranging respectively from 61.9 to 13.8 wt% (O), from 47.1 to 6.7 wt % (Mg) and from the detection limits to 21 wt% (Si). Nickel, calcium and aluminum never exceeded 2.3 wt % whereas the iron was commonly lower than 2 wt% , reading 8 wt% in one grain.

4.4 Evolution of the carbon content:

The unweathered mining residues within the experimental cell EC-1 were characterized by a total carbon content of 0.13 wt%, whereas the white crusts, which do not contain primary calcite, had a total carbon content ranging from 0.3 wt% to 4.4 wt%C_{tot} (Gras et al., 2017). In cell EC-1, no evidence of organic carbon was observed, and therefore the total carbon content is equivalent to the inorganic carbon content. In contrast, in cell EC-2, spruce needles and leaf fragments were found at the surface (Figure 2 f) thus the organic carbon content was measured in order to compute the inorganic carbon content. In several samples the organic carbon content was near the detection limit (0.4 wt% C_{org}) (Conyers et al., 2011). Therefore, in samples with a carbon content below 0.4 %C_{org}, the total carbon was considered to be inorganic carbon (Gras et al., 2017). In EC-2, the unweathered residues had a total carbon content of 0.08 wt%. The crusts sampled at the edge of the cell were characterized by an inorganic carbon content ranging from 0.1 wt%C_{inorg} to 4.0 wt%C_{inorg} (Gras et al., 2017). The samples from the first few centimeters of core samples, at the center of cell EC-2, yielded inorganic carbon contents lower than the carbon content of the unweathered mining residues (Figure 10). This is likely a consequence of measurement errors related to the Walkey-Black method or sample heterogeneity. Moreover, the inorganic carbon content changed according to the month of sampling. Below the first centimeter of depth, the inorganic carbon content decreased quickly from 1 cm to 3 cm depth. Between 2014 and 2015, the inorganic carbon content ranged from 0.15 wt% to 0.43 wt% and was higher in July than in May or October/November. From below 3 cm depth to the bottom of cell EC-2, the inorganic carbon content was constant near 0.2 wt% (Gras et al., 2017) (Figure 10). Figure 11 presents the inorganic carbon content measured at the surface of EC-2 since 2011, and a cross-section of cell EC-2 with the spatial distribution of

the inorganic carbon content measured in May 2015. The contours were drawn using linear interpolation between the core samples. The mining residues under the wood plank, at the edges of cell EC-2, (Figure 2 g) had an average inorganic carbon content of 1.08 wt% whereas at the edges of the cell in May 2015, the inorganic carbon content decreased from 0.5 wt % at the surface, to 0.3 wt% at a depth of 10 cm.

5. DISCUSSION

Since construction of the experimental cells during the summer of 2011, the mining residues underwent atmospheric weathering. Previous work demonstrated that passive carbon mineralization had indeed induced atmospheric carbon sequestration in the DNP residues (Gras et al., 2017). The main parameters controlling the extent of mineral carbonation include characteristics inherent to the residues such as the mineral composition, surface area, porosity and permeability. Other parameters depend on the environment, such as rain fall frequency, temperature, and relative humidity (Assima et al., 2014c, 2013, 2012; Awoh et al., 2014; Bea et al., 2012; Harrison et al., 2015; Kandji et al., 2017a, 2017b; Pronost et al., 2011; Wilson et al., 2014; Zarandi et al., 2017b, 2016). Both experimental cells (EC-1 and EC-2) were filled with ultramafic mining residues from the same nickel deposit. Mining residues in EC-1 and EC-2 therefore had a similar initial mineralogy (Figure 3a-b) where the main minerals were chrysotile, lizardite, brucite, chlorite and magnetite, whereas calcite was found in minor amounts in the waste rock residues (Pronost et al., 2010; 2012; Staples et al., 2013; Gras et al. 2017). The brucite content in the tailing residues of cell EC-2, was approximately 10.2 wt% (Assima et al., 2013). During 4 years of monitored weathering, the residues were submitted to the same conditions of precipitation, temperature and relative humidity variations. However, the hydrogeological characteristics of the mining residues (porosity, water content, tortuosity, permeability), which are specific to each cell, control the flows of gas and water. Cell EC-1 has hydrogeological properties analogous to a heterogeneous gravel-silt, whereas in cell EC-2 the porous medium is similar to that of a silty-clay (Figure 2). On the other hand, the cells contained respectively, approximately 104 tonnes (EC-1) and 5 tonnes (EC-2) of residues and the surface area exposed to rainwater was greater for cell EC-1 (~35 m^2) than for EC-2 (~19 m^2). As a result, the cell thicknesses are about 2 meters and 35 centimeters, respectively, for EC-1 and EC-2. The liquid-solid ratio and thus also the water content were higher in EC-2 (Figure 4) than in EC-1 (Gras et al., 2017). The flow rates measured at the bottom of the cells thus depended on the hydrogeological properties of each cell. After a rain event, an abrupt increase of the flow rate was recorded in both cells (Figure 4). Counter-intuitively to what the hydrogeological properties would suggest, in cell EC-1 the flow rate decreased slowly in the recession curve (Figure 3) whereas in

EC-2 the flow rate decreased more quickly after a rain event. This is best explained by the small amount of mining residues within EC-2. Despite a porous medium similar to a silty-clay, the smaller thickness in EC-2 (35 cm) resulted in a short residence time for water. In EC-1, the residence time of water was longer but did not exceed a few days (Figure 3). In 2013, the flow rate measured at the bottom of EC-1 was higher than in EC-2 which was most likely due to the difference in the surface area exposed to rain. Physical property differences between the two cells may influence the carbon mineralization reactions and, therefore, the carbon sequestration capacity. In the following sections, the observed impacts of atmospheric weathering on leachate water geochemistry will be used to discuss the evolution of carbon mineralization over time and to estimate the amount of atmospheric CO_2 sequestered in the cells.

5.1 Impacts of atmospheric weathering on leachate geochemistry.

In cells EC-1 and EC-2, rainwater in equilibrium with atmospheric CO_2 infiltrates the mining residues and dissolves the magnesium (Mg^{2+}) from minerals such as brucite or serpentine. The $Mg^{2+}_{(aq)}$ released into leachate water reacts with interstitial water carbonate (CO_3^{2-}) and bicarbonate (HCO_3^-) ions to form carbonate minerals (Sanna et al., 2014; Harrison et al., 2019), following reactions 3-5 below:

$$CO_{2(g)} + H_2O_{(l)} = H_2CO_{3(aq)} = H^+_{(aq)} + HCO^-_{3(aq)} \quad (3)$$

$$Mg_3Si_2O_5(OH)_4 + 6H^+ = 3Mg^{2+} + 2SiO_2 + 5H_2O \quad (4)$$

$$Mg^{2+} + CO_3^{2-} + 3H_2O = MgCO_3.3H_2O \quad (5)$$

Dissolution reactions (3 and 4) and carbonate precipitation (5) are controlled by temperature, pH and solution chemistry, and may also be affected by biological processes (McCutcheon et al., 2016; Power et al., 2013a, 2016, 2010, 2009). In the experimental cells, reactions 3, 4 and 5 occur simultaneously such that the leachate waters collected at the bottom of both cells reflect the equilibrium between these reactions at the times of sampling. From 2011 to 2015, and despite differences in physical properties between the two cells, two regimes can be recognized for leachate water chemistry (Figures 5 and 6). First, a transitional regime in 2011 during which the pH, alkalinity and magnesium concentrations increase in the leachate water whereas silica, calcium, potassium and sodium concentrations decrease. In the second regime, starting in 2012, the pH, alkalinity, Mg, Si, Ca, Na and K concentrations in leachate water show seasonal variations, while the other metal concentrations are stable or below detection (Supporting information). The greater

amount of mining residues and the larger surface area of EC-1 to collect rain, as well as its hydrogeological parameters which are more favourable to water infiltration compared to that of cell EC-2, could explain the higher concentrations observed in cell EC-1 (Figures 5 and 6). However, the concentrations normalized to the volume of mining residues demonstrate that the release rates of different components in EC-1 were lower than in EC-2 (Kandji et al., 2017). The contrast in release rates between both cells may be explained by (1) the finer grain-size and thus a higher specific surface in cell EC-2, and (2) the high liquid-solid ratio in EC-2 (Plante et al., 2014, Kandji et al., 2017). Despite these differences, the same processes appear to control the evolution of the leachate water chemistry in both cells (Figures 5 and 6).

5.1.1 Transitional regime

In July 2011, atmospheric weathering of the mining residues began with acidic meteoric water (pH ~ 5.5) infiltrating the mining residues and dissolving serpentine minerals, brucite and minor amounts of diopside, albite, biotite and calcite (Staples et al., 2013; Pronost et al., 2012, Kandji et al., 2017). The increase of Mg concentration in leachate water was congruent with the dissolution of serpentine minerals, brucite and minor silicate minerals. Dissolution of brucite is further suggested by a decrease of intensity or absence of the XRD peaks of brucite in weathered EC-2 samples. Concurrent to dissolution, H^+ was consumed through weathering, which caused pH and alkalinity increases in leachate water (Figures 5 and 6) (Kandji et al., 2017b; Lechat et al., 2016; Ulven et al., 2017). Concentrations of Si, Ca, Na or K in leachate water indicate active dissolution of serpentine minerals and silicate minerals such as diopside, albite or biotite. On the other hand, a decrease of Si and other metal concentrations between July and November 2011 suggests a lower dissolution rate of serpentine and silicate minerals during this period, which is consistent with the pH increase and a decrease of the abundance of these minerals (Figures 5 and 6). Additionally, the increasing pH may cause incongruent dissolution of serpentine minerals, and a preferential release of Mg over Si (Pokrovsky and Schott, 2000), which supports the observed decrease of Si concentrations from July to November 2011. Brucite was therefore the main but not the only source of Mg in interstitial water of the experimental cells, which is consistent with kinetic tests completed in the laboratory (Kandji et al., 2017). During this transitional regime, the saturation indices of all carbonates increase, and several become over-saturated such as magnesite, nesquehonite aragonite and calcite (Figure 7).

5.1.2 Seasonal regime

Since 2012, leachate water from cells EC-1 and EC-2 has been characterized by high concentrations of Mg, ranging from 50 to 180 mg/L, and a pH ranging from 8.1 to 10 in which HCO_3^- is the dominant carbonate species (Appelo and Postma 2005). The leachate water from both cells is therefore similar to a Mg-HCO_3^- - type, or type I water, characteristic of open-system interaction between CO_2-bearing meteoric water and ultramafic rocks (Bruni et al., 2002; Cipolli et al., 2004; Marques et al., 2008; O'Neil and Barnes, 1971; Oskierski et al., 2016; Paukert et al., 2012; Rollo and Jamieson, 2006). Nevertheless, dissolution of CO_2 in interstitial water is the first limiting step of carbon mineralization in the experimental cells (Gras et al., 2017), and the leachate water geochemistry indicates that reactions occur in an open system with atmospheric CO_2. The pH, alkalinity, and the Si, Mg, Ca, K, and Na concentrations from leachate waters in both cells evolved seasonally while concentrations from other chemical components were stable or below detection (Figures 6 and 7) (Supplementary information). These seasonal variations of leachate geochemistry can be explained by: (1) changes in the hydrologic regime (Nordstrom, 2011, 2009), and (2) changes of the equilibrium conditions between the carbon mineralization reactions (Wilson et al., 2010).

Changes in hydrological regimes at mine waste sites over time can have important impacts on water quality (Nordstrom, 2011). During dry periods, for example, the concentration of dissolved metals increases slowly in the leachate water. In contrast, the first strong rainstorm following a dry period (first flush), or an intense rain event, may cause an abrupt increase of concentrations followed by a decrease (Nordstrom, 2011, 2009). The climate near Amos (Quebec), is characterized by large changes in environmental conditions over the year (Table 1). During winter, precipitation is lowest, and the water content in both cells is minimal, near the field capacity and the permanent wilting point. Despite these conditions, carbon mineralization should be effective and carbonates such as landsfordite, could precipitate (Beinlich and Austrheim, 2012; Ulven et al., 2017; Zarandi et al., 2016). Spring snowmelt induces a first flush of water after the relative dry winter period, which was observed in May 2016 as an increase in water content at all depths in cell EC-2. Such a first flush in spring or intense rain events throughout the year may have impacted the leachate water geochemistry and could explain abrupt changes. Each year, the Mg concentrations and alkalinity values tend to be higher in the spring (May and June) and fall (September to November), and lowest in the summer (July and August). These trends are inverse with that of precipitations. It thus seems that Mg concentrations and alkalinity values (related to DIC) might be controlled, at least in part, to dilution from rain and snowmelt water.

Every year, between May and July, the temperature and solar radiation increased, while from August to October a decrease was observed. The relative humidity in the atmosphere and total precipitation were slightly lower from May to July than between August to October. Additionally, during the summer, rain events were slightly less frequent (Figures 5 and 6) (Table 1). Decreasing rainfall events between May and July caused a deficit of water in the cells, over a period during which temperature and solar radiation were conducive to evaporation. During this period, a decrease in water content at 4 cm depth in EC-2 was observed in 2013 and 2014. Similarly, between the end of July and November of each year, increases in precipitation caused ingress of water within the cells and in 2016, the water content at 4 cm depth increased in cell EC-2 (Figure 4 and Table 1).

Potassium and sodium ions react little during transport in the experimental cells and are thus considered conservative in this study. Furthermore, these elements were not affected by changes in equilibrium of the carbon mineralization reactions. During dry seasons (May to July), when evaporation was highest, K, Na, Si and Ca concentrations increased. In contrast, when precipitation then increased (August to November), concentrations of K, Na, Si, Ca, decreased. Changes in the hydrological regimes over the year then impacted leachate water quality in the DNP residues. However, the decrease of magnesium concentrations during this seasonal regime, is not directly correlated with changes in precipitation and evaporation conditions, and is not yet fully understood.

Changes in evaporation conditions and in watering may alter the equilibrium between the three principal reactions of carbon mineralization presented earlier: (3) dissolution of CO_2 in water, (4) dissolution of reactive minerals, and (5) carbonate precipitation (Assima et al., 2012; Kandji et al., 2017b; Wilson et al., 2014; Zarandi et al., 2017b). Dissolution of CO_2 in interstitial waters contributes to the dissolved inorganic carbon which produces bicarbonate (HCO_3^-) and carbonate (CO_3^{2-}) ions. Reaction 4 releases magnesium ions in the interstitial water, while reaction (5) consumes magnesium ions and bicarbonate ions. Changes in climatic conditions and precipitation could promote one of these three reactions over the others and induce disequilibrium which in turn would modify the leachate water geochemistry (Beinlich and Austrheim, 2012; Wilson et al., 2010).

From year to year, the intensity of the seasonal cycles in Mg concentrations and alkalinity seems to decrease, particularly in cell EC-2, while the pH slightly increases (Figures 5 and 6). This long-term evolution could be related to a decrease of carbonate precipitation over the years. Indeed, Gras et al. (2017) demonstrated that, since 2012, the decrease in $CO_{2(g)}$ consumption capacity of cells EC-1 and EC-2 was associated with the decrease in brucite content near the surface and due to

surface passivation (Assima et al., 2012; Harrison et al., 2015; Zarandi et al., 2016). Near the surface, a decrease of magnesium in the leachate waters, related to the smaller proportion of brucite, may limit the precipitation of carbonates (which would otherwise be promoted by evaporation) and might explain the long-term geochemical evolution (Figures 5 and 6). Furthermore, a decrease of porosity near the surface, caused by carbonate precipitation, may also alter the carbon mineralization reactions which would also impact the leachate water geochemistry from year to year (Acero et al., 2007; Beinlich and Austrheim, 2012). Further investigations are needed to confirm and understand the long-term evolution of leachate water geochemistry.

In summary, results have shown that leachate water geochemistry from the experimental cells EC-1 and EC-2 was influenced by (1) the local weather (temperature, relative humidity, and precipitation) and (2) evolution of the equilibrium between the governing carbon mineralization reactions, leading to an increase of carbonate precipitation.

5.2 Carbonate precipitation

The evolution of leachate geochemistry presented in the previous section influences the carbonate precipitation reactions. Thermodynamic equilibrium calculations reveal that, despite the differences between cells EC-1 and EC-2, the saturation indices of the carbonate minerals have been similar since 2011. However, the saturation indices evolve following seasonal changes of pH, alkalinity and Mg concentrations (Figure 7). The saturation indices of all carbonate minerals first decreased between May and July, then increased until November. Despite these variations, calcite, aragonite and magnesite were over-saturated, since 2011, in leachate water from both cells. Notwithstanding the oversaturation, Ca concentrations were not affected by the increase of carbonate precipitation between May and July. The leachate waters from EC-1 and EC-2 were characterized by high Mg concentrations which can inhibit calcium carbonate precipitation (Hopkinson et al., 2008). Inhibition of calcium carbonate precipitation can explain why Ca concentrations did not change over seasonal cycles and is further consistent with the low modal proportion of neo-formed calcium carbonates observed in this study and by Gras et al., (2017). Saturation indices of artinite and hydromagnesite reflected either over- or under-saturated conditions, whereas nesquehonite was undersaturated (Figure 7). It is important to note that evaporation of leachate water, which may significantly increase the carbonate saturation indices, was not considered here. Oskierski et al. (2016), for example, demonstrated that evaporation of 20% of the leachate water from the Woodsreef mine induced oversaturation for hydromagnesite. At the surface of the cells, where evaporation was highest, the carbonate minerals were therefore most

likely over-saturated. Nevertheless, changes in leachate water geochemistry, between May and July, decreased the carbonate mineral saturation indices and thus these carbonate minerals became under-saturated deeper within the cells. The increase in carbonate precipitation between May and July, which altered the leachate water geochemistry, therefore created a feed-back loop limiting the carbon sequestration potential of the cells.

In experimental cells EC-1 and EC-2, the neo-formed carbonate minerals trap atmospheric CO_2 (Gras et al., 2017). In surface samples from both cells, artinite, nesquehonite, dypingite, and hydromagnesite were observed, with rare aragonite. The amount of bound carbon depends on the specific mineral. Nesquehonite has a ratio of CO_2 to Mg of 1, whereas the ratio is 4/5 for hydromagnesite and dypingite. The stability of magnesium carbonate minerals increases from lansfordite and artinite to nesquehonite, then dypingite, hydromagnesite, and stable magnesite, (Canterford et al., 1984; Hopkinson et al., 2008; Langmuir, 1965). At temperatures above 25°C, hydrous-carbonates can evolve from landsfordite to nesquehonite (Beinlich and Austrheim, 2012; Hopkinson et al., 2008), whereas nesquehonite can be converted to dypingite and hydromagnesite during associated wetting/drying cycles and increasing temperature (Hopkinson et al., 2008; Oskierski et al., 2016; Power et al., 2009; Wilson et al., 2009; Zarandi et al., 2017b). Hydromagnesite was more common in samples from EC-1, whereas in EC-2 the main carbonate was dypingite. In cell EC-1, the blocks of waste rock which were more conducive to wetting/drying cycles and evaporation, were coated with carbonate minerals. Conversion from the less stable phases (artinite, nesquehonite) to hydromagnesite was favoured in cell EC-1 which can explain the higher proportion of hydromagnesite in EC-1. In contrast, the finer grain size of the tailings in cell EC-2 maintains a higher water content (Figure 4), which may slow the rate of dehydration of nesquhenotite to hydromagnesite. Fungi at the surface of cell EC-2 (Figures 8 h) could also promote precipitation of dypingite (McCutcheon et al., 2016; Power et al., 2010, 2009). The grain size of the mining residue may therefore influence the type of carbonate minerals precipitated, whereas evaporation and wetting-drying cycles control the conversion. Clearly, the hydrogeological conditions can therefore also influence the quantity of carbon trapped in the residues. In deeper EC-2 samples, however, only hydrotalcite supergroup minerals formed (Supplementary information). As described in previous studies, in both cells EC-1 and EC-2, for example, hydrotalcite supergroup minerals had formed during atmospheric weathering (Gras et al., 2017; Oskierski et al., 2016; Turvey, 2015; Turvey et al., 2017). These minerals precipitated rapidly after exposure to the atmosphere through weathering of brucite under CO_2 - limited conditions (McCutcheon et al., 2016; Mumpton and Thompson, 1966; Turvey et al., 2017).

In cell EC-1, carbonate coatings may also have contributed to surface passivation (Figures 2 c, d and 8 a,b) (Assima et al., 2012; Zarandi et al., 2017b), whereas in cell EC-2, the carbonates cemented the tailing grains, causing a decrease in porosity and permeability (Acero et al., 2007) (Figures 2 h and 8 e). Therefore, precipitation of carbonates within the cells may decrease atmospheric CO_2 consumption. In order to characterize the carbonate matrix interface, EPMA analysis was used on waste rock samples from EC-1. In order to identify the minerals at the carbonate-matrix interface, chemical analyses and theoretical mineral compositions have been plotted on ternary diagrams (Figure 9). Most often, the carbonate-matrix interface is sharp and the chemical composition changed from serpentine to carbonates or brucite (Figure 9 c). However, on several samples the chemical compositions of minerals at the carbonate-matrix interface range from the pole of serpentine to a magnesium pole depleted in silica which corresponds either to brucite or carbonates (Figure 9 a,b). Because the EPMA beam size (10 μm) is in some places larger than the target minerals, superposition of serpentine or epoxy and carbonates may have altered the signal to the measured composition. Nevertheless, the range of composition from the pole of serpentine to the magnesian pole is consistent with the incongruent dissolution of serpentine in high pH water, in which Si will be preferentially released over Mg (Pokrovsky and Schott, 2000; Ruiz-Agudo et al., 2012).

The EPMA analyses did not allow precisely identifying the carbonate minerals in the mining residues. In addition, the BSE images revealed that carbonate minerals at the surface were fragile (Figure 9 a) and filled the fractures at the expense of brucite (Figures 9 b and c). Frost cycles and dehydration of the carbonate minerals increased the fracturing of waste rock fragments and thus the carbonate coating may have been peeled off (Beinlich and Austrheim, 2012; Ulven et al., 2017; Zarandi et al., 2017b, 2016). Carbonate precipitation therefore contributes to (1) exposure of fresh serpentine to weathering, which maintains atmospheric CO_2 sequestration, and (2) increased surface passivation, which may decrease atmospheric CO_2 consumption. Carbonate precipitation dynamics in the DNP residues, which changed leachate water geochemistry, thus decreased porosity and permeability, promoted fracturation of the mining residues and caused surface passivation, creating a feed-back loop limiting the carbon sequestration potential.

5.3 Quantification of atmospheric CO_2 sequestration

Carbon sampling of cell EC-1 was limited to surface samples, and therefore it was not possible to accurately quantify the carbon sequestered. However, extensive sampling at the center

and at the edges of cell EC-2 allowed tracking the evolution of carbon sequestration over time and thus allowed estimating the quantity of captured CO_2.

At the center of cell EC-2, the inorganic carbon content increased slowly from year to year (Gras et al., 2017) but changed seasonally. Most notably, the carbon content was higher in summer than in autumn or spring (Figure 10). Dissolution of less stable neo-formed carbonate minerals during rain events (Ulven et al., 2017) or changes in water geochemistry (Figures 5 and 6) may have led to these seasonal variations of the carbon content. However, the cores were randomly sampled at the center of the cell, irrespective of surface mineralization, and carbon mineralization at the surface of the cell was not continuous or homogeneous as shown by an evaporitic crust and cones (Figures 2, and 11). In addition, the carbonate crusts were thin and fragile and might have been disturbed over time (Figure 2 h). The small seasonal variations might therefore be an artifact induced by the sampling process. Additional analyses are necessary to better understand the annual evolution of the carbon content in experimental cell EC-2.

The inorganic carbon content in cell EC-2 also varied laterally. At the center of the cell, for example, the carbon content was lower and the carbonation front shallower than at the edges of the cell (Figure 11). The water content, at the center of cell EC-2 was near 25 % at 4 cm depth since 2011, but below this depth the water saturation reaches 25 to 40 % (Figure 4). Since the mean porosity of the tailings in cell EC-2 was 44%, the residues were therefore almost fully saturated below 4 cm depth. Towards the edges the residue thickness decreases, and the impact of evaporation became gradually more important such that mean water content became lower. Previous studies have shown that high and low water saturations tend to reduce the carbon mineralization reaction rates (Assima et al., 2013, 2012; Awoh et al., 2014; Harrison et al., 2015). In cell EC-2, the watering frequency corresponds to actual rainfall events and thus was the same at the center and the edges of the cell. Carbon mineralization was thus more efficient near the edges of the cell because of the lower water saturation compared to the center of the cell. Similarly, under the wood plank (Figure 2 g), the residues are partially protected from rain fall and the water content was lower, thus carbon mineralization was likely more efficient yielding a higher carbon content (Figures 2 e and 11). In contrast, the capture of carbon near the center of cell EC-2 was inhibited by the higher water content in the mining residues. Altenatively, sheltering from rain by the wood plank may have prevented carbonate dissolution, as argued by Ulven et al. (2017)

The quantity of CO_2 sequestered within the experimental cell EC-2 was estimated using the measured inorganic carbon content. The carbon of the core samples was weighted by the mass of a

layer using the thickness of the core sample. For the three upper layers, two-thirds of the volume was ascribed to the central core, and one-third to the core from the edge of the cell (Figure 11). With this approach, up to May 2015, an estimated 13 kg of atmospheric CO_2 was sequestered by the mining residues in cell EC-2, which corresponds to a mean rate of 1.4 (+/-0.3) $kgCO_2$/tonne/year. This rate is about twice as high as the rate calculated by Bea et al., (2012) using numerical simulations for tailing pounds near Mount Keith (Australia). The DNP residues, however, are characterized by a higher brucite content (10.2 vol%) (Assima et al., 2012) compared to the tailings of the Mount Keith mine (2.5 vol%). Brucite is a key mineral which reacts quickly during carbon mineralization and controls its extent (Assima et al., 2013; Pronost et al., 2012; Harrison 2013, 2015, 2016, 2017; Kandji et al., 2015). It is therefore likely the higher brucite content in the DNP residues may have induced the higher sequestration rate. The DNP mine will generate, each year, approximately 15 Mt of tailings and release about 127,700 tonnes of CO_2 (Staples et al., 2013; Kandji et al., 2017b). Using the sequestration rate of the experimental cell EC-2, the tailing residues will sequester about 21 kt of atmospheric CO_2 each year, which represents around 16% of the CO_2 emitted. This rate of sequestration is lower than the rate calculated from laboratory kinetic tests (8.5 $kgCO_2$/tonne) (Kandji et al., 2017). The contrast between laboratory and natural conditions may be explained by differences in precipitation/watering and climatic conditions (Temperature, RH). Additionaly, the experimental cell EC-2 was frequently flooded after intense rain events and during the summer's drought cracks were observed. These extreme water contents limited the carbonation of the residues and may explain the difference between the laboratory and experimental cell tests. In cell EC-1, the hydrogeological properties, which control the fluid flow and influence the mineral carbonation, are different than in EC-2. In addition, the hydrogeological properties are very heterogeneous (Aubertin et al., 1996). Therefore, the results from EC-2 cannot be easily extrapolated, and the estimated amounts of CO_2 capture might be quite different from the real amounts sequestered (Awoh et al., 2014; Lechat et al., 2016).

6. CONCLUSION

Two experimental cells were used to study impacts of atmospheric weathering on passive carbon mineralization in mining residues from the Dumont Nickel Project. The mining residues filling the experimental cells had a similar mineralogy and were submitted to the same weather conditions (temperature, RH, precipitation). However, the hydrogeological properties, which influence the supply of CO_2 and the water content of the cells, were different. Despite these hydrogeological differences, the same processes control the evolution of leachate water geochemistry. High magnesium concentrations and a moderate to alkaline pH characterize the

leachate water from both cells, which is consistent with weathering of ultramafic rocks in a system open to CO_2. Seasonal variations of leachate water geochemistry are caused by (1) seasonal and longer-term changes in rainfall and weather conditions, and (2) a displacement of the equilibrium between the carbon mineralization reactions. Between May and July each year, leachate water flows in a CO_2 - depleted environment where supply of atmospheric CO_2 to water is limited (Gras et al., 2017). During this period, evaporation is at its maximum, therefore precipitation of carbonate minerals increases causing a decrease in magnesium concentration and alkalinity. Seasonal variations in leachate water geochemistry also impact the saturation indices of carbonate minerals. Between May and July, hydromagnesite and artinite become under-saturated which limits carbon sequestration. Furthermore, carbonate precipitation, self-limits carbon sequestration through a negative feed-back loop.

Over the years, magnesium concentrations and alkalinity decrease which is related to a decrease of CO_2 consumption (Gras et al., 2017). In experimental cells EC-1 and EC-2, carbonate precipitation is mainly driven by evaporation. Dehydration of nesquehonite to hydromagnesite is promoted by the larger grain size in EC-1 and dypingite is more common in EC-2. Since the hydrogeological properties of EC-2 are similar to a silty-clay porous medium, a high liquid/solid ratio is maintained, and residues are nearly saturated at shallow depths which limits carbonate precipitation. Approximately 13 kg (+/- 1) of atmospheric CO_2 were sequestered in cell EC-2 between 2011 and 2015, which corresponds to a mean rate of 1.4 (+/-0.3) $kgCO_2$/tonne/year. However, the carbon sequestration capacity was inhibited by the high water content.

This study underlines the critical impact of hydrogeological properties and leachate water geochemistry on atmospheric CO_2 sequestration capacity of ultramafic mine wastes. Changes in these properties during passive carbon mineralization must be addressed in order to optimise atmospheric CO_2 sequestration in large-scale mining waste deposits.

Acknowledgements

We thank RNC Minerals and the Natural Science and Engineering Research Council of Canada for funding the research. We thank Stanislas Ketelers and Frederic Dufresne (RNC Minerals) for their help in the field. We thank S. A. Wilson and an anonymous reviewer for their comments which helped improve the paper significantly.

References

Acero, P., Ayora, C., Carrera, J., 2007. Coupled thermal, hydraulic and geochemical evolution of pyritic tailings in unsaturated column experiments. Geochim. Cosmochim. Acta 71, 5325–5338. doi:10.1016/j.gca.2007.09.007

Appelo, C.A.J., Postma, D., 2005. Geochemistry, groundwater andpollution. Rotterdam, Netherlands, AA Balkema. SegundaEdici{ó}n.

Assima, G.P., Larachi, F., Beaudoin, G., Molson, J., 2012. CO2 sequestration in chrysotile mining residues-implication of watering and passivation under environmental conditions. Ind. Eng. Chem. Res. 51, 8726–8734. doi:10.1021/ie202693q

Assima, G.P., Larachi, F., Molson, J., Beaudoin, G., 2014a. Comparative study of five Québec ultramafic mining residues for use in direct ambient carbon dioxide mineral sequestration. Chem. Eng. J. 245, 56–64. doi:10.1016/j.cej.2014.02.010

Assima, G.P., Larachi, F., Molson, J., Beaudoin, G., 2014b. Impact of temperature and oxygen availability on the dynamics of ambient CO2 mineral sequestration by nickel mining residues. Chem. Eng. J. 240, 394–403. doi:10.1016/j.cej.2013.12.010

Assima, G.P., Larachi, F., Molson, J., Beaudoin, G., 2014c. New tools for stimulating dissolution and carbonation of ultramafic mining residues. Can. J. Chem. Eng. 92, 2029–2038. doi:10.1002/cjce.22066

Assima, G.P., Larachi, F.F., Beaudoin, G., Molson, J., 2013. Dynamics of carbon dioxide uptake in chrysotile mining residues - Effect of mineralogy and liquid saturation. Int. J. Greenh. Gas Control 12, 124–135. doi:10.1016/j.ijggc.2012.10.001

Aubertin, M., Bussiere, B., Chapuis, R.P., 1996. Hydraulic conductivity of homogenized tailings from hard rock mines. Can. Geotech. J. 33, 470–482. doi:10.1139/t96-068

Awoh, A.S., Plante, B., Bussière, B., Mbonimpa, M., 2014. Measurement and prediction of the CO2 effective diffusion coefficient in unsaturated media. Geo Regina.

Bea, S., Wilson, S., Mayer, K.U., Dipple, G.M., Power, I.M., Gamazo, P., 2012. Reactive Transport Modeling of Natural Carbon Sequestration in Ultramafic Mine Tailings. Vadose Zo. J. 11, 0. doi:10.2136/vzj2011.0053

Beaudoin, G., Hébert, R., Constantin, M., Duchesne, J., Cecchi, E., Huot, F., Vigneau, S., Fiola, R., 2008. Spontaneous carbonation of serpentine in milling and mining waste, southern Qué}bec and Italy. Proc. Accel. Carbonation Environ. Mater. Eng. 73À}82.

Beaudoin, G., Nowamooz, A., Assima, G.P., Lechat, K., Gras, A., Entezari, A., Awoh, A.-S., Horswill, M., Turcotte, S., Larachi, F., others, 2017. Passive Mineral Carbonation of Mg-rich Mine Wastes by Atmospheric CO2. Energy Procedia 114, 6083–6086.

Beinlich, A., Austrheim, H., 2012. In situ sequestration of atmospheric CO 2 at low temperature and

surface cracking of serpentinized peridotite in mine shafts. Chem. Geol. 332–333, 32–44. doi:10.1016/j.chemgeo.2012.09.015

Berner, R.A., Kothavala, Z., 2001. Geocarb III: A revised model of atmospheric CO2 over phanerozoic time. Am. J. Sci. 301, 182–204. doi:10.2475/ajs.294.1.56

Bruni, J., Canepa, M., Chiodini, G., Cioni, R., Cipolli, F., Longinelli, A., Marini, L., Ottonello, G., Vetuschi Zuccolini, M., 2002. Irreversible water-rock mass transfer accompanying the generation of the neutral, Mg-HCO3 and high-pH, Ca-OC spring waters of the Genova province, Italy. Appl. Geochemistry 17, 455–474. doi:10.1016/S0883-2927(01)00113-5

Canterford, J.H., Tsambourakis, G., Lambert, B., 1984. Some observations on the properties of dypingite, Mg5 (CO3) 4 (OH) 2{·} 5H2O, and related minerals. Mineral. Mag. 48, 437–442.

Chatterjee, A., Lal, R., Wielopolski, L., Martin, M.Z., Ebinger, M.H., 2009. Evaluation of Different Soil Carbon Determination Methods. CRC. Crit. Rev. Plant Sci. 28, 164–178. doi:10.1080/07352680902776556

Cipolli, F., Gambardella, B., Marini, L., Ottonello, G., Zuccolini, M.V., 2004. Geochemistry of high-pH waters from serpentinites of the Gruppo di Voltri (Genova, Italy) and reaction path modeling of CO2 sequestration in serpentinite aquifers. Appl. Geochemistry 19, 787–802. doi:10.1016/j.apgeochem.2003.10.007

Conyers, M.K., Poile, G.J., Oates, A.A., Waters, D., Chan, K.Y., 2011. Comparison of three carbon determination methods on naturally occurring substrates and the implication for the quantification of "soil carbon." Soil Res. 49, 27–33. doi:10.1071/SR10103

De Vos, B., Lettens, S., Muys, B., Deckers, J.A., 2007. Walkley-Black analysis of forest soil organic carbon: Recovery, limitations and uncertainty. Soil Use Manag. 23, 221–229. doi:10.1111/j.1475-2743.2007.00084.x

Duke, J.M., 1986. Petrology and economic geology of the Dumont sill: an Archean intrusion of komatiitic affinity in northwestern Quebec. Ottawa.

Eckstrand, O.R., 1975. The dumont serpentinite: A model for control of nickel-if erous opaque mineral assemblages by alteration reactions in ultramafic rocks. Econ. Geol. 70, 183–201. doi:10.2113/gsecongeo.70.1.183

Gaillardet, J., Dupré, B., Louvat, P., Allegre, C.J., 1999. Global silicate weathering and CO 2 consumption rates deduced from the chemistry of large rivers. Chem. Geol. 159, 3–30.

Gerdemann, S.J., O'Connor, W.K., Dahlin, D.C., Penner, L.R., Rush, H., 2007. Ex situ aqueous mineral carbonation. Environ. Sci. Technol. 41, 2587–2593. doi:10.1021/es0619253

Gras, A., Beaudoin, G., Molson, J., Plante, B., Bussière, B., Lemieux, J.M., Dupont, P.P., 2017. Isotopic evidence of passive mineral carbonation in mine wastes from the Dumont Nickel Project (Abitibi, Quebec). Int. J. Greenh. Gas Control 60, 10–23. doi:10.1016/j.ijggc.2017.03.002

Harrison, A.L., Dipple, G.M., Power, I.M., Mayer, K.U., 2016. The impact of evolving mineral-

water-gas interfacial areas on mineral-fluid reaction rates in unsaturated porous media. Chem. Geol. 421, 65–80. doi:10.1016/j.chemgeo.2015.12.005

Harrison, A.L., Dipple, G.M., Power, I.M., Mayer, K.U., 2015. Influence of surface passivation and water content on mineral reactions in unsaturated porous media: Implications for brucite carbonation and CO2 sequestration. Geochim. Cosmochim. Acta 148, 477–495. doi:10.1016/j.gca.2014.10.020

Harrison, A.L., Dipple, G.M., Song, W., Power, I.M., Mayer, K.U., Beinlich, A., Sinton, D., 2017. Changes in mineral reactivity driven by pore fluid mobility in partially wetted porous media. Chem. Geol. 463, 1–11. doi:10.1016/j.chemgeo.2017.05.003

Harrison, A.L., Power, I.M., Dipple, G.M., 2013. Accelerated carbonation of brucite in mine tailings for carbon sequestration. Environ. Sci. Technol. 47, 126–134. doi:10.1021/es3012854

Harrison, A.L., Mavromatis, V., Oelkers, E.H., Bénézeth, P., 2019. Solubility of the hydrated Mg-carbonates nesquehonite and dypingite from 5 to 35 °C: Implications for CO2 storage and the relative stability of Mg-carbonates. Chemical Geology, 504: 123-135.

Hitch, M., Dipple, G.M., 2012. Economic feasibility and sensitivity analysis of integrating industrial-scale mineral carbonation into mining operations. Miner. Eng. 39, 268–275. doi:10.1016/j.mineng.2012.07.007

Hopkinson, L., Rutt, K.., Cressey, G., 2008. The transformation of nesquehonite to hydromagnesite in the system CaO-MgO-H2O-CO2: an experimental spectroscopic study. J. Geol. 116, 387–400. doi:10.1086/588834

IPCC, 2014. Climate Change 2014: Synthesis Report. Contribution of Working Groups I, II and III to the Fifth Assessment Report of the Intergovernmental Panel on Climate Change, Core Writing Team, R.K. Pachauri and L.A. Meyer. doi:10.1017/CBO9781107415324

IPCC, 2005. IPCC special report on carbon dioxide capture and storage. Prepared by working group III of the Intergovernmental Panel on Climate Change, in: IPCC Special Report on Carbon Dioxide Capture and Storage. p. 442. doi:10.1002/anie.201000431

Kandji, Plante, B., Bussière, B., Awoh, A.S., Ibrahim Saïb, B.A., Dupont, P.P., 2015. Prediction of drainage water quality from mining waste with carbon sequestration potential. Proc. (IMWA/ICARD), Santiago, Chili, 21-24 avril 2015.

Kandji, Plante, B., Bussière, B., Beaudoin, G., Dupont, P.P., 2017a. Kinetic testing to evaluate the mineral carbonation and metal leaching potential of ultramafic tailings: Case study of the Dumont Nickel Project, Amos, Québec. Appl. Geochemistry 84, 262–276. doi:10.1016/j.apgeochem.2017.07.005

Kandji, Plante, B., Bussière, B., Beaudoin, G., Dupont, P.P., Bussiere, B., Beaudoin, G., Dupont, P.P., Bussière, B., Beaudoin, G., Dupont, P.P., 2017b. Geochemical behavior of ultramafic waste rocks with carbon sequestration potential: a case study of the Dumont Nickel Project, Amos, Québec. Environ. Sci. Pollut. Res. 24, 11734–11751. doi:10.1007/s11356-017-8735-9

Kelemen, P.B., Matter, J.r., 2008. In situ carbonation of peridotite for CO2 storage. Proceedings of

the National Academy of Sciences, 105(45 %U http://www.pnas.org/content/105/45/17295.abstract): 17295-17300.

Lackner, K.S., Wendt, C.H., Butt, D.P., Joyce, E.L., Sharp, D.H., 1995. Carbon dioxide disposal in carbonate minerals. Energy 20, 1153–1170. doi:10.1016/0360-5442(95)00071-N

Langmuir, D., 1965. Stability of Carbonates in the System. J. Geol. 73, 730–754.

Lechat, K., Lemieux, J.M., Molson, J., Beaudoin, G., Hébert, R., 2016. Field evidence of CO2 sequestration by mineral carbonation in ultramafic milling wastes, Thetford Mines, Canada. Int. J. Greenh. Gas Control 47, 110–121. doi:10.1016/j.ijggc.2016.01.036

Lechat, K.D., 2016. Séquestration géologique du CO2 par carbonatation minérale dans les résidus miniers Séquestration géologique du CO2 par carbonatation minérale dans les résidus miniers. Université Laval.

Matter, J.M. et al., 2009. Permanent Carbon Dioxide Storage into Basalt: The CarbFix Pilot Project, Iceland. Energy Procedia, 1(1): 3641-3646.

Marques, J.M., Carreira, P.M., Carvalho, M.R., Matias, M.J., Goff, F.E., Basto, M.J., Graça, R.C., Aires-Barros, L., Rocha, L., 2008. Origins of high pH mineral waters from ultramafic rocks, Central Portugal. Appl. Geochemistry 23, 3278–3289. doi:10.1016/j.apgeochem.2008.06.029

McCutcheon, J., Wilson, S.A., Southam, G., 2016. Microbially Accelerated Carbonate Mineral Precipitation as a Strategy for in Situ Carbon Sequestration and Rehabilitation of Asbestos Mine Sites. Environ. Sci. Technol. 50, 1419–1427. doi:10.1021/acs.est.5b04293

Mills, S.J., Wilson, S.A., Dipple, G.M., Raudsepp, M., 2010. The decomposition of konyaite: importance in CO2 fixation in mine tailings. Mineral. Mag. 74, 903–917. doi:10.1180/minmag.2010.074.5.903

Molson, J., Aubertin, M., Bussière, B., Benzaazoua, M., 2008. Geochemical transport modelling of drainage from experimental mine tailings cells covered by capillary barriers. Appl. Geochemistry 23, 1–24. doi:10.1016/j.apgeochem.2007.08.004

Molson, J.W., Fala, O., Aubertin, M., Bussière, B., 2005. Numerical simulations of pyrite oxidation and acid mine drainage in unsaturated waste rock piles. J. Contam. Hydrol. 78, 343–371. doi:10.1016/j.jconhyd.2005.06.005

Mumpton, F. a., Thompson, C.S., 1966. The Stability of Brucite in the Weathering Zone of the New Idria Serpentinite. Clays Clay Miner. 14, 249–257. doi:10.1346/CCMN.1966.0140122

Nordstrom, D.K., 2011. Hydrogeochemical processes governing the origin, transport and fate of major and trace elements from mine wastes and mineralized rock to surface waters. Appl. Geochemistry 26, 1777–1791. doi:10.1016/j.apgeochem.2011.06.002

Nordstrom, D.K., 2009. Acid rock drainage and climate change. J. Geochemical Explor. 100, 97–104. doi:10.1016/j.gexplo.2008.08.002

Olajire, A.A., 2013. A review of mineral carbonation technology in sequestration of CO2. J. Pet. Sci. Eng. 109, 364–392. doi:10.1016/j.petrol.2013.03.013

O'Neil, J. R.; Barnes, I. C^{13} and O^{18} compositions in some freshwater carbonates associated with ultramafic rocks and serpentinites: Western United States. Geochim. Cosmochim. Acta 1971, 35, 687–697.

Oskierski, H.C., Dlugogorski, B.Z., Oliver, T.K., Jacobsen, G., 2016. Chemical and isotopic signatures of waters associated with the carbonation of ultramafic mine tailings, Woodsreef Asbestos Mine, Australia. Chem. Geol. 436, 11–23. doi:10.1016/j.chemgeo.2016.04.014

Oskierski, Dlugogorski, B.Z., Jacobsen, G., 2013a. Sequestration of atmospheric CO2 in chrysotile mine tailings of the Woodsreef Asbestos Mine, Australia: Quantitative mineralogy, isotopic fingerprinting and carbonation rates. Chem. Geol. 358, 156–169. doi:10.1016/j.chemgeo.2013.09.001

Oskierski, Dlugogorski, B.Z., Jacobsen, G., Oskierski, Dlugogorski, B.Z., Jacobsen, G., 2013b. Sequestration of atmospheric CO2 in a weathering-derived, serpentinite-hosted magnesite deposit: 14C tracing of carbon sources and age constraints for a refined genetic model. Geochim. Cosmochim. Acta 122, 226–246. doi:10.1016/j.gca.2013.08.029

Park, A.H.A., Fan, L.S., 2004. CO2 mineral sequestration: Physically activated dissolution of serpentine and pH swing process. Chem. Eng. Sci. 59, 5241–5247. doi:10.1016/j.ces.2004.09.008

Parkhurst, D.L., Appelo, C.A.J., others, 1999. User's guide to PHREEQC (Version 2): A computer program for speciation, batch-reaction, one-dimensional transport, and inverse geochemical calculations.

Paukert, A.N., Matter, J.M., Kelemen, P.B., Shock, E.L., Havig, J.R., 2012. Reaction path modeling of enhanced in situ CO 2 mineralization for carbon sequestration in the peridotite of the Samail Ophiolite, Sultanate of Oman. Chem. Geol. 330–331, 86–100. doi:10.1016/j.chemgeo.2012.08.013

Peregoedova, A., Aubertin, M., Bussière, B., 2014. Evaluation of the water retention curve of mine waste rock using laboratory tests and predictive models. Geo Regina.

Peregoedova, A., Aubertin, M., Polytechnique, É., 2012. Laboratory measurement and prediction of the saturated hydraulic conductivity of mine waste rock.

Plante, B., Kandji, E.H.B., Bussière, B., Awoh, A.S., Ibrahim-Saib, B.A., Beaudoin, G., Gras, A., Molson, J., Dupont, P.P., 2014. Geochemical behavior of carbon-sequestrating mine wastes: Dumont project Royal Nickel Corporation. Proc. Tailings and mine waste. Proc. Tailings mine waste 2014.

Pokrovsky, O.S., Schott, J., 2000. Kinetics and mechanism of forsterite dissolution at 25 degrees C and pH from 1 to 12. Geochim. Cosmochim. Acta 64, 3313–3325. doi:10.1016/s0016-7037(00)00434-8

Power, I.M., Dipple, G.M., Southam, G., 2010. Bioleaching of ultramafic tailings by

Acidithiobacillus spp. for CO 2 sequestration. Environ. Sci. Technol. 44, 456–462. doi:10.1021/es900986n

Power, I.M., Harrison, A.L., Dipple, G.M., 2016. Accelerating Mineral Carbonation Using Carbonic Anhydrase. Environ. Sci. Technol. 50, 2610–2618. doi:10.1021/acs.est.5b04779

Power, I.M., Wilson, S.A., Thom, J.M., Dipple, G.M., Gabites, J.E., Southam, G., 2009. The hydromagnesite playas of Atlin, British Columbia, Canada: A biogeochemical model for CO2 sequestration. Chem. Geol. 260, 302–316. doi:10.1016/j.chemgeo.2009.01.012

Power, Harrison, A.L., Dipple, G.M., Southam, G., 2013a. Carbon sequestration via carbonic anhydrase facilitated magnesium carbonate precipitation. Int. J. Greenh. Gas Control 16, 145–155. doi:10.1016/j.ijggc.2013.03.011

Power, McCutcheon, J., Harrison, A., Wilson, S., Dipple, G., Kelly, S., Southam, C., Southam, G., 2014. Strategizing Carbon-Neutral Mines: A Case for Pilot Projects. Minerals 4, 399–436. doi:10.3390/min4020399

Power, Wilson, S.A., Dipple, G.M., 2013b. Serpentinite carbonation for CO2 sequestration. Elements 9, 115–121. doi:10.2113/gselements.9.2.115

Pronost, J., Beaudoin, G., Lemieux, J.M., Hébert, R., Constantin, M., Marcouiller, S., Klein, M., Duchesne, J., Molson, J.W., Larachi, F., Maldague, X., 2012. CO2-depleted warm air venting from chrysotile milling waste (Thetford Mines, Canada): Evidence for in-situ carbon capture from the atmosphere. Geology 40, 275–278. doi:10.1130/G32583.1

Pronost, J., Beaudoin, G., Tremblay, J., Larachi, F., Duchesne, J., Hébert, R., Constantin, M., 2011. Carbon sequestration kinetic and storage capacity of ultramafic mining waste. Environ. Sci. Technol. 45, 9413–9420. doi:10.1021/es203063a

Pronost, J., Ph, D., Beaudoin, G., Ph, D., Constantin, M., Ph, D., Duchesne, J., Ph, D., Hébert, R., Ph, D., 2010. Evaluation of the mineral carbonation potential of mining residues produced by Royal Nickel pilot plant , Amos.

Rollo, H.A., Jamieson, H.E., 2006. Interaction of diamond mine waste and surface water in the Canadian Arctic. Appl. Geochemistry 21, 1522–1538. doi:10.1016/j.apgeochem.2006.05.008

Ruiz-Agudo, E., Putnis, C. V., Rodriguez-Navarro, C., Putnis, A., 2012. Mechanism of leached layer formation during chemical weathering of silicate minerals. Geology 40, 947–950. doi:10.1130/G33339.1

Sanna, A., Uibu, M., Caramanna, G., Kuusik, R., Maroto-Valer, M.M., 2014. A review of mineral carbonation technologies to sequester CO2. Chem. Soc. Rev. 43, 8049–8080. doi:10.1039/C4CS00035H

Sciortino, M., Mungall, J.E., Muinonen, J., 2015. Generation of High-Ni sulfide and alloy phases during serpentinization of dunite in the dumont sill, Quebec. Econ. Geol. 110, 733–761. doi:10.2113/econgeo.110.3.733

Seifritz, W., 1990. CO_2 disposal by means of silicates, Nature. doi:10.1038/345486b0

Sipilä, J., Teir, S., Zevenhoven, R., 2008. Carbon dioxide sequestration by mineral carbonation Literature review update 2005 – 2007. Rep. VT 52. doi:10.1080/00908310600628263

Staples, L.P., Bowen, J.M., Bernier, S.B., Warren, D.A., Scott, C.C., Duncan, J.F., Murphy, B.A., Bertrand, V.J., Scott, K.C., Latulippe, S., 2013. Technical Report on the Dumont Ni Project, Launay and Trécesson Townships, Quebec, Canada - 2013 432.

Teir, S., Eloneva, S., Fogelholm, C.J., Zevenhoven, R., 2009. Fixation of carbon dioxide by producing hydromagnesite from serpentinite. Appl. Energy 86, 214–218. doi:10.1016/j.apenergy.2008.03.013

Turvey, C., 2015. Hydrotalcites As a Secondary Carbon Sink in Serpentinites. Fifth Int. Conf. Accel. ed Carbonation Environ. Mater. Eng. New York, 21–24 June 2015. 3208.

Turvey, C.C., Wilson, S.A., Hamilton, J.L., Southam, G., 2017. Field-based accounting of CO2 sequestration in ultramafic mine wastes using portable X-ray diffraction. Am. Mineral. 102, 1302–1310. doi://doi.org/10.2138/am-2017-5953

Ulven, O.I., Beinlich, A., Hövelmann, J., Austrheim, H., Jamtveit, B., 2017. Subarctic physicochemical weathering of serpentinized peridotite. Earth Planet. Sci. Lett. 468, 11–26. doi:10.1016/j.epsl.2017.03.030

Walkley, A., Black, I.A., 1934. An examination of the Degtjareff method for determining soil organic matter, and proposed modification of the chromic acid titration method. Soil Sci. 37, 29–38. doi:10.1097/00010694-193401000-00003

Wilson, S.A., Barker, S.L.L., Dipple, G.M., Atudorei, V., 2010. Isotopic disequilibrium during uptake of atmospheric CO2 into mine process waters: Implications for CO2 sequestration. Environ. Sci. Technol. 44, 9522–9529. doi:10.1021/es1021125

Wilson, S.A., Dipple, G.M., Power, I.M., Barker, S.L.L., Fallon, S.J., Southam, G., 2011. Subarctic weathering of mineral wastes provides a sink for atmospheric CO 2. Environ. Sci. Technol. 45, 7727–7736. doi:10.1021/es202112y

Wilson, S.A., Dipple, G.M., Power, I.M., Thom, J.M., Anderson, R.G., Raudsepp, M., Gabites, J.E., Southam, G., 2009. Carbon dioxide fixation within mine wastes of ultramafic-hosted ore deposits: Examples from the Clinton Creek and Cassiar Chrysotile deposits, Canada. Econ. Geol. 104, 95–112. doi:10.2113/gsecongeo.104.1.95

Wilson, S.A., Harrison, A.L., Dipple, G.M., Power, I.M., Barker, S.L.L., Ulrich Mayer, K., Fallon, S.J., Raudsepp, M., Southam, G., 2014. Offsetting of CO2 emissions by air capture in mine tailings at the Mount Keith Nickel Mine, Western Australia: Rates, controls and prospects for carbon neutral mining. Int. J. Greenh. Gas Control 25, 121–140. doi:10.1016/j.ijggc.2014.04.002

Wilson, S.A., Raudsepp, M., Dipple, G.M., 2006. Verifying and quantifying carbon fixation in minerals from serpertine-rich mine tailings using the Rietveld method with X-ray powder diffraction data. Am. Mineral. 91, 1331–1341. doi:10.2138/am.2006.2058

Zarandi, A., Larachi, F., Beaudoin, G., Plante, B., Sciortino, M., 2017a. Ambient mineral

carbonation of different lithologies of mafic to ultramafic mining wastes/tailings--A comparative study. Int. J. Greenh. Gas Control 63, 392–400.

Zarandi, A., Larachi, F., Beaudoin, G., Plante, B., Sciortino, M., 2017b. Nesquehonite as a carbon sink in ambient mineral carbonation of ultramafic mining wastes. Chem. Eng. J. 314, 160–168. doi:10.1016/j.cej.2017.01.003

Zarandi, A., Larachi, F., Beaudoin, G., Plante, B., Sciortino, M., 2016. Multivariate study of the dynamics of CO2 reaction with brucite-rich ultramafic mine tailings. Int. J. Greenh. Gas Control 52, 110–119. doi:10.1016/j.ijggc.2016.06.022

Figure captions

Figure 1 : a) Site location and b) geological context of the proposed DNP mine site and Dumont sill.

Figure 2 : Textures in the experimental cells EC-1 and EC-2. a) General view of waste-rock cell EC-1 with pluri-centimetric blocks at the surface, b) white crusts coating surfaces and fractures in samples from EC-1, c) surface of a pluri-centimetric block in EC-1 coated with white crusts, d) white crust observed with binocular magnifier, with several phases of precipitation visible, e) general view of the tailings cell EC-2, f) evaporitic structure (cones) observed at the edges of cell EC-2, g) residues cemented and covered with white crust below the wood support beam at the edges of cell EC-2, h) indurated flat crust, sampled at the edge of cell EC-2.

Figure 3 : Evolution of water flux at the bottom of the experimental cells in 2013.

Figure 4 : Water content evolution with depth in EC-2 and rainfall in 2016.

Figure 5 : Evolution of chemical composition of leachate in EC-1 since 2011.

Figure 6 : Evolution of chemical composition of leachate from EC-2 since 2011.

Figure 7 : Evolution of saturation indices of the main carbonate minerals.

Figure 8 : Scanning electron micrographs of surface samples from EC-1 and EC-2. a) Surface of a white crust sampled in cell EC-1; depressions are filled with fissured

carbonates whereas on the top well-crystalized carbonates are visible, b) serpentine grain, from cell EC-1, partially covered with flaky carbonate minerals, c) white crust, from cell EC-1, with well-crystalized hydromagnesite, d) needle of well-crystalized aragonite observed on sample surface from EC-1, e) surface of a flat crust, from EC-2. Carbonate minerals have coated the surface and cemented the tailings grains. f) Serpentine grain, from flat crust in EC-2, partially covered with flaky carbonates overcome by well-crystalized nesquehonite, g) different sizes of nesquehonite crystals observed on a surface sample from EC-2, h) intergrowth of fungi and carbonate minerals observed at the surface of cell EC-2.

Figure 9 : Back-scattered electron micrographs of polished thin sections from cell EC-1 and EPMA chemical compositions reported on ternary diagrams.

Figure 10 : Inorganic* carbon content at the center of cell EC-2

Figure 11 : Cross-section of cell EC-2 in May 2015 and contoured inorganic carbon content.

Figure 1

Click here to download high resolution image

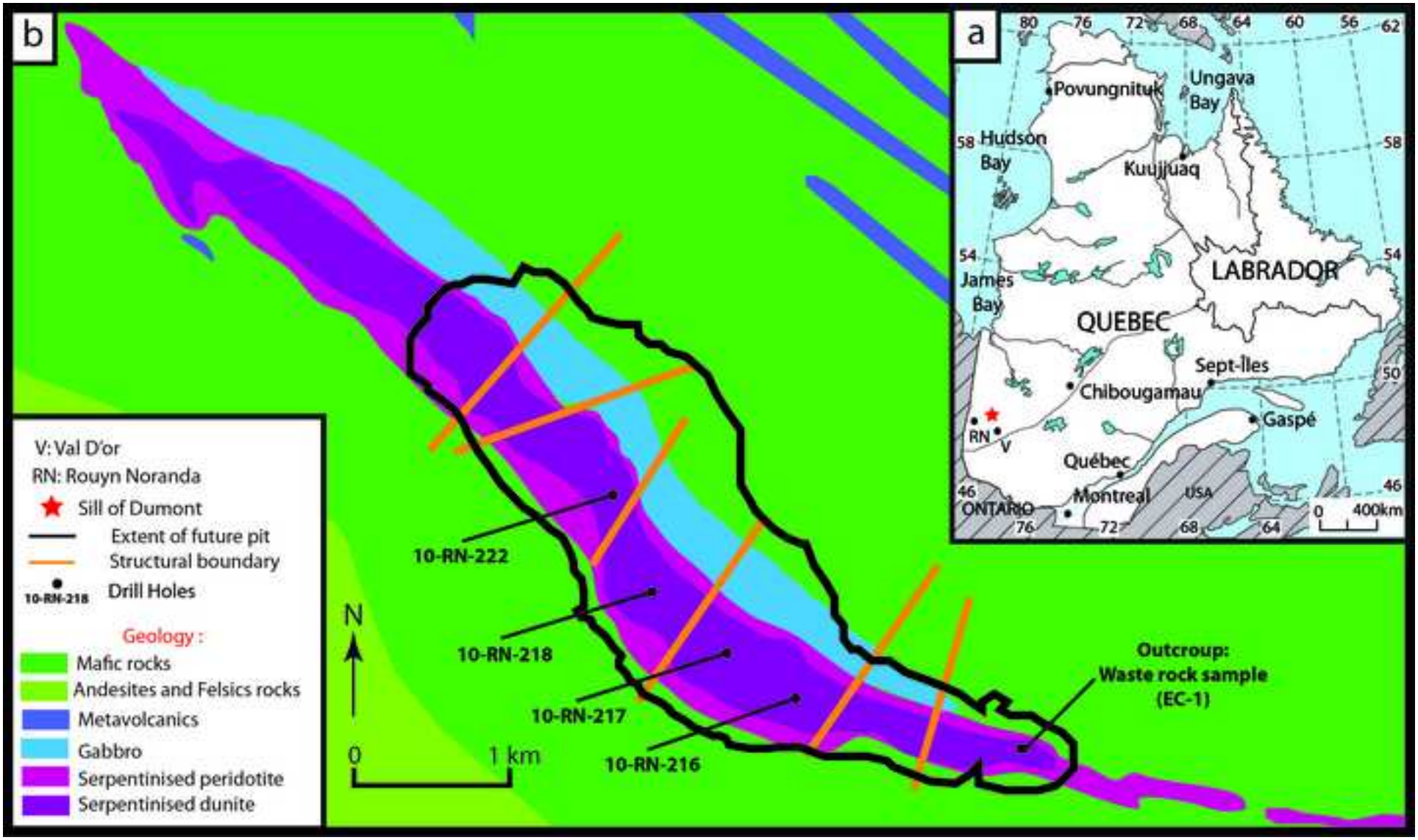

Figure 2

Click here to download high resolution image

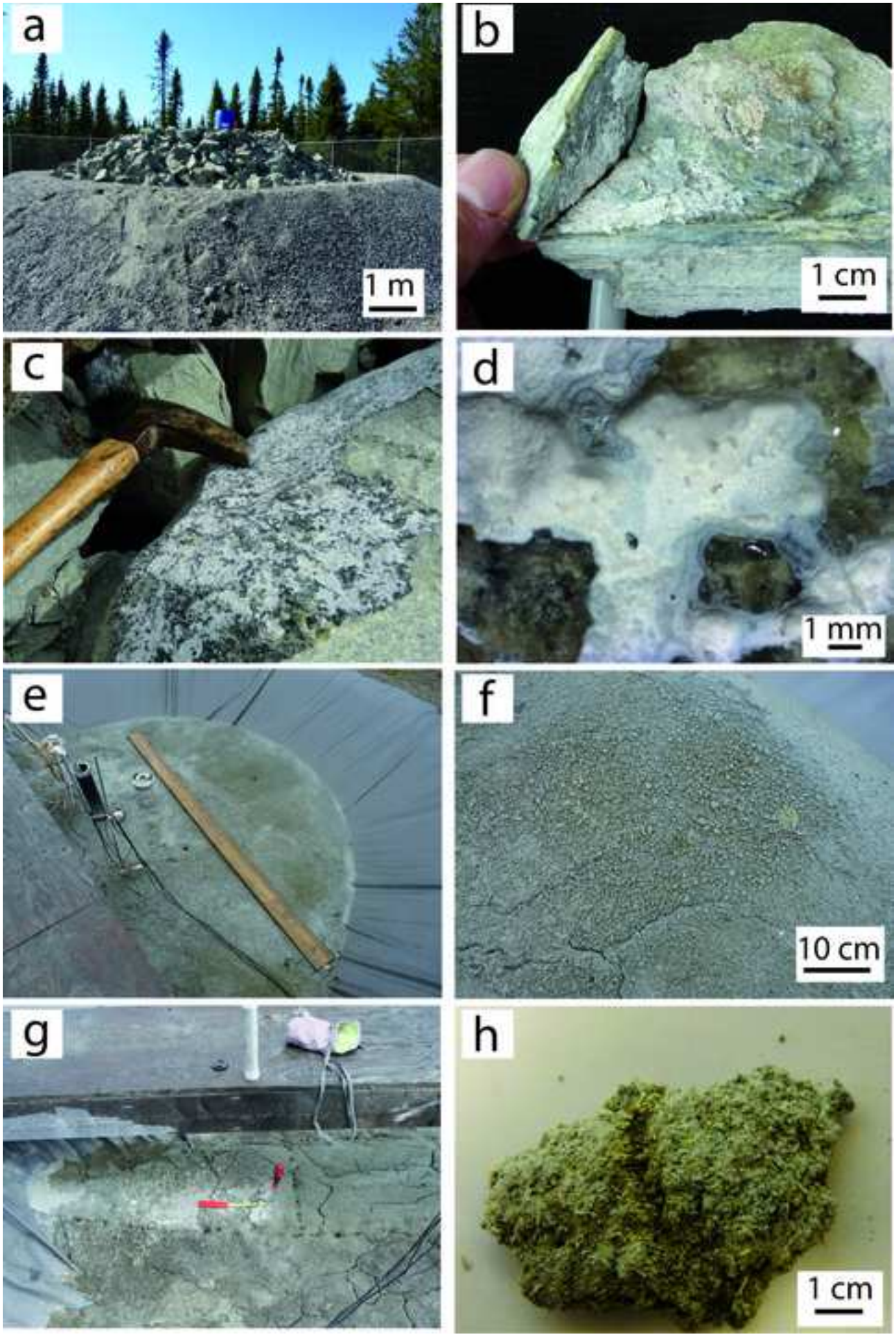

Figure 3

Click here to download high resolution image

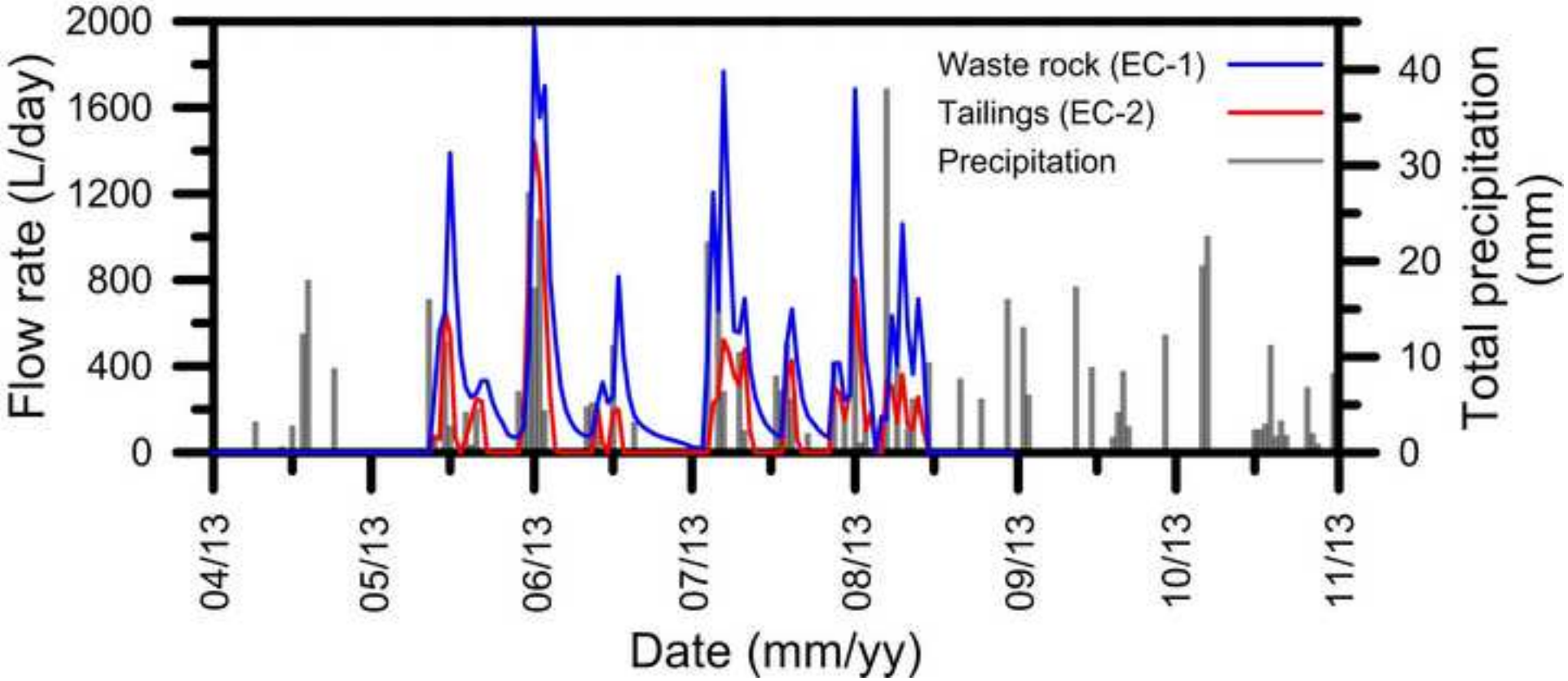

Figure 4

Click here to download high resolution image

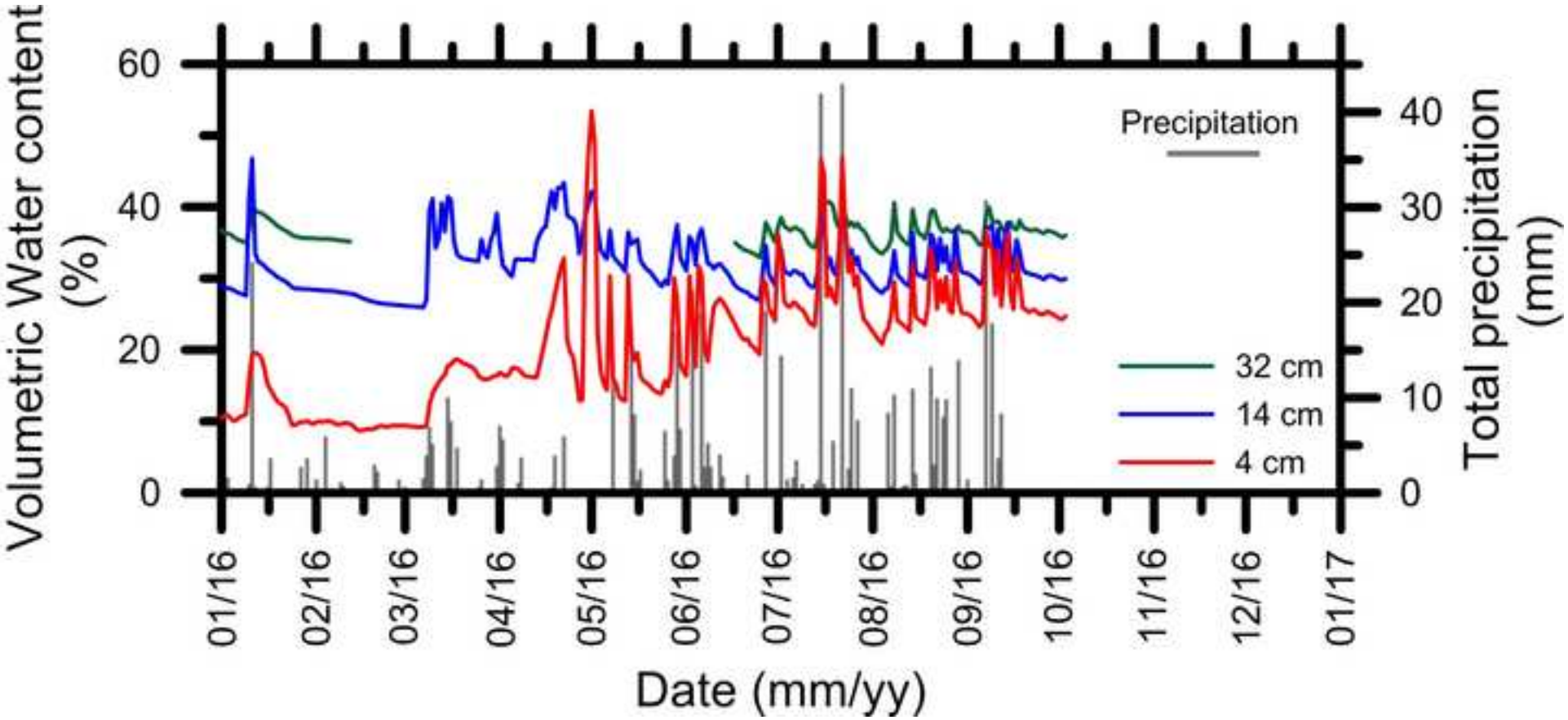

Figure 5

Click here to download high resolution image

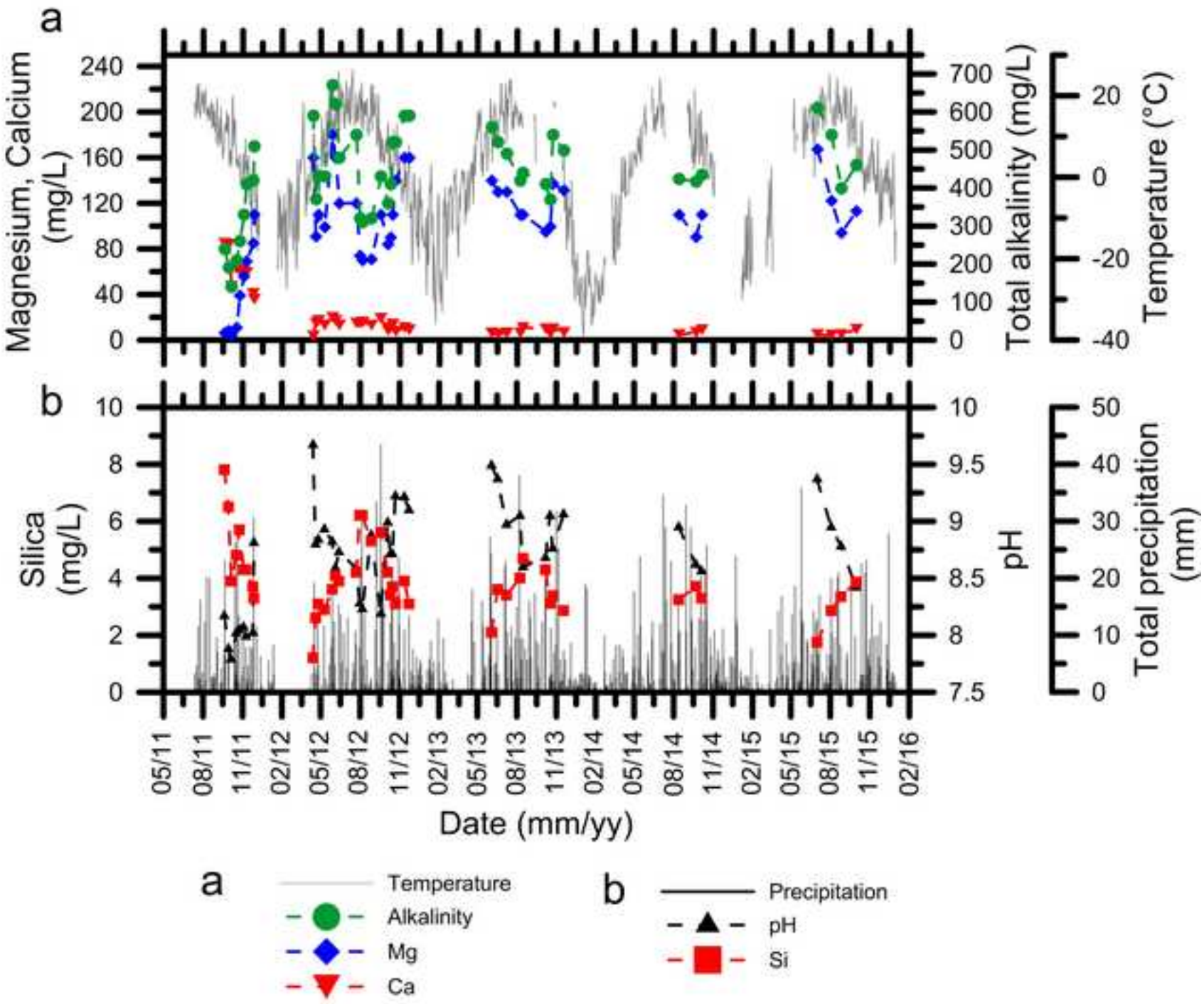

Figure 6

Click here to download high resolution image

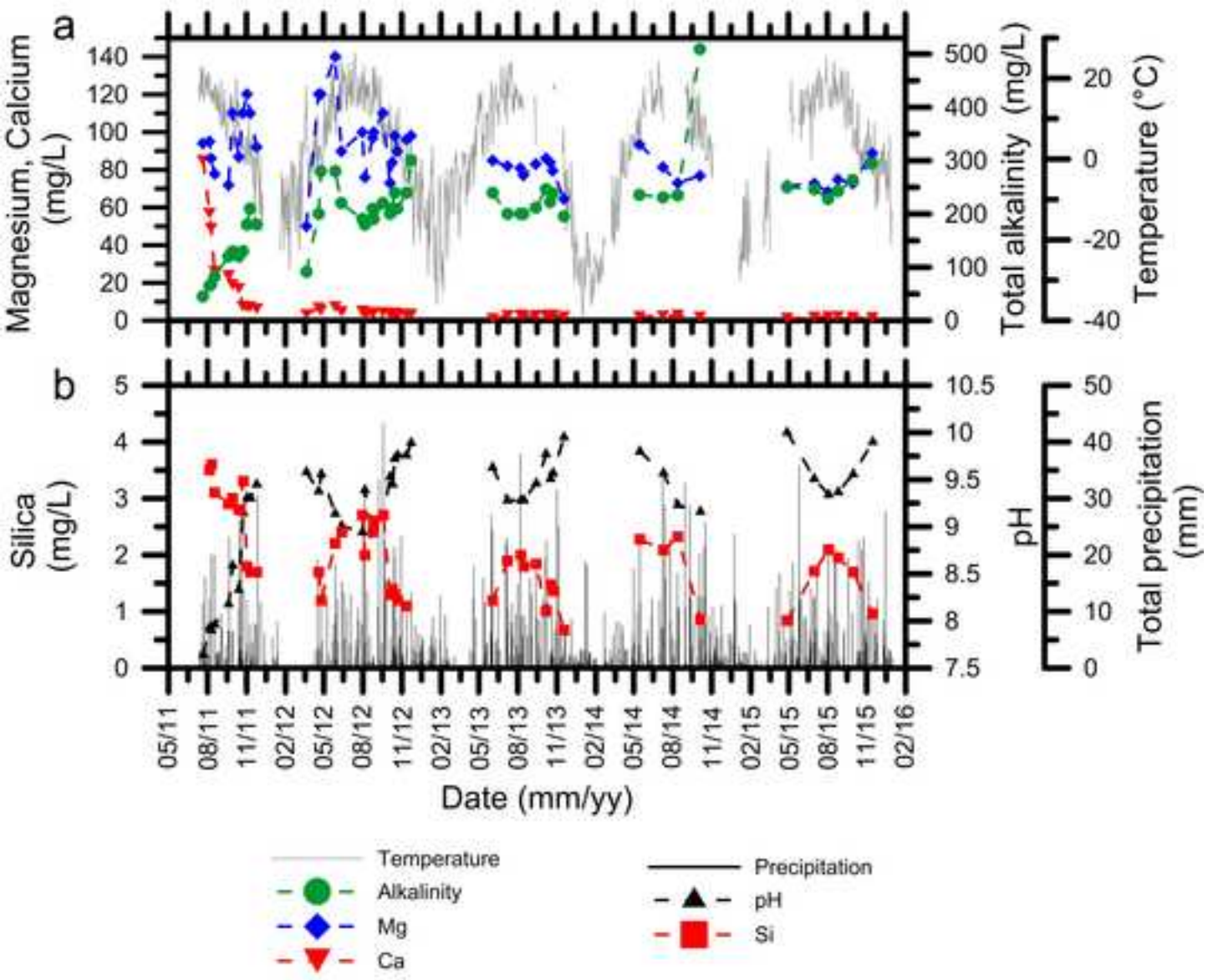

Figure 7

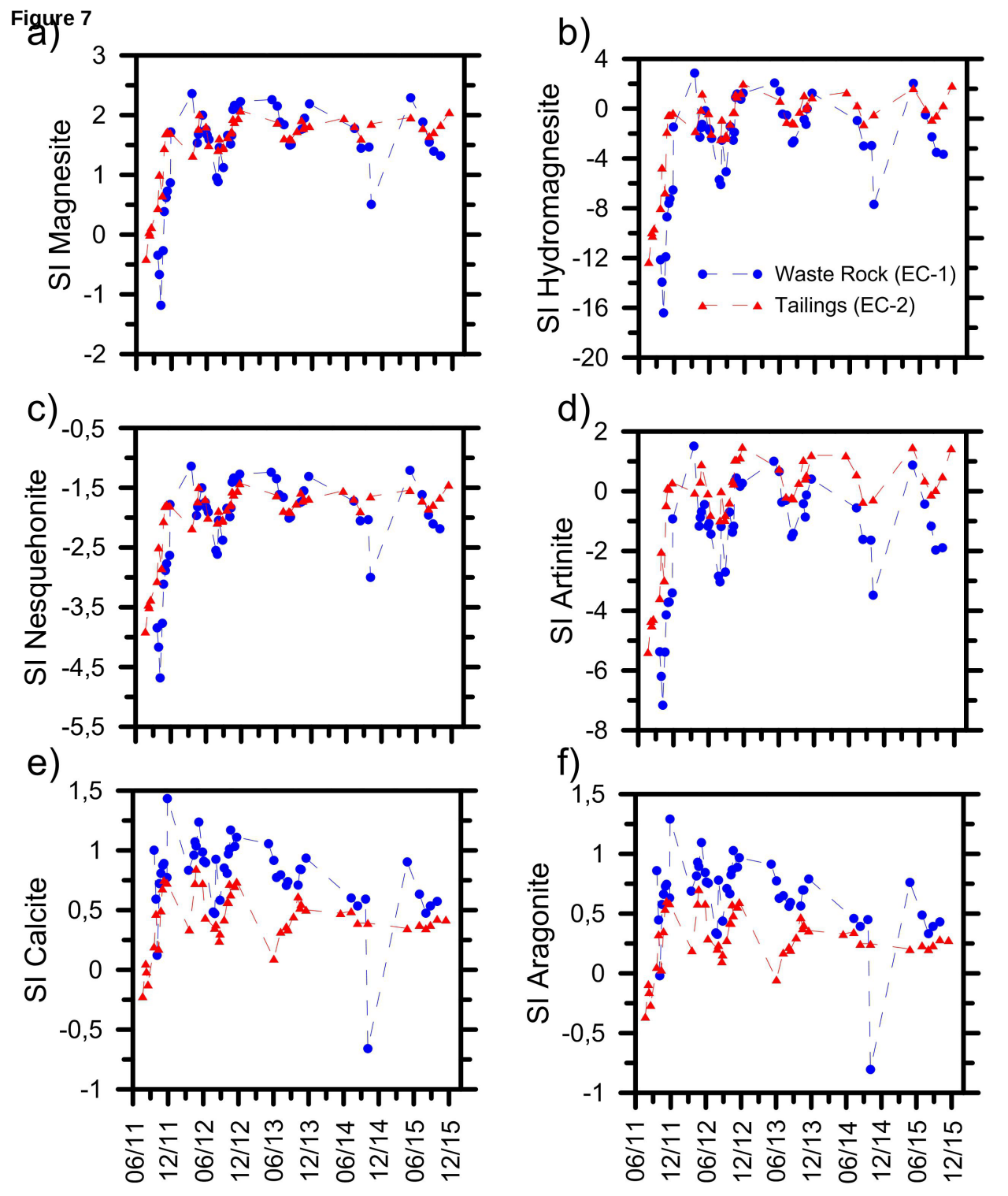
a)
SI Magnesite
b)
SI Hydromagnesite
Waste Rock (EC-1)
Tailings (EC-2)
c)
SI Nesquehonite
d)
SI Artinite
e)
SI Calcite
f)
SI Aragonite
06/11
12/11
06/12
12/12
06/13
12/13
06/14
12/14
06/15
12/15

Figure 8

Click here to download high resolution image

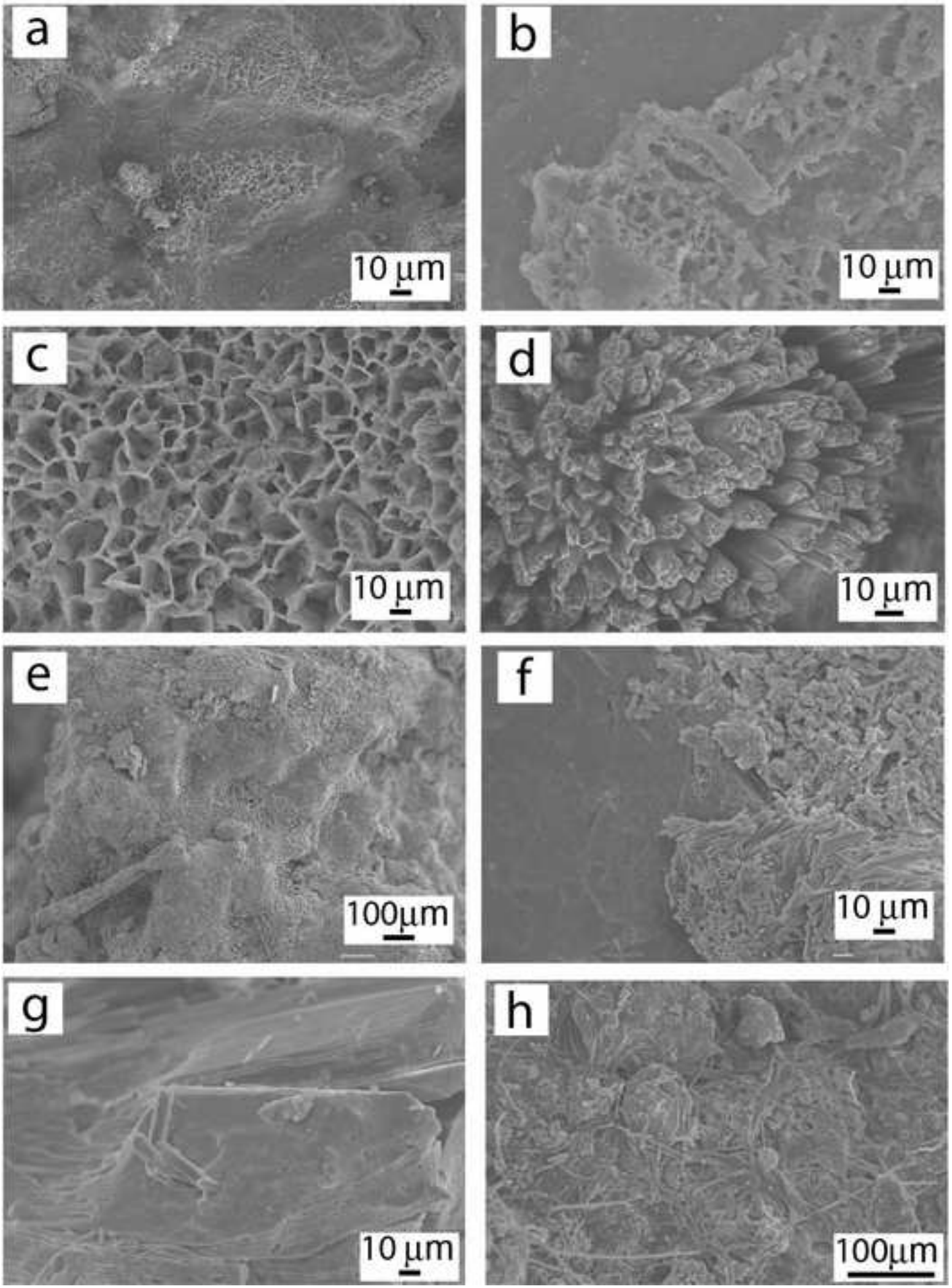

Figure 9

Click here to download high resolution image

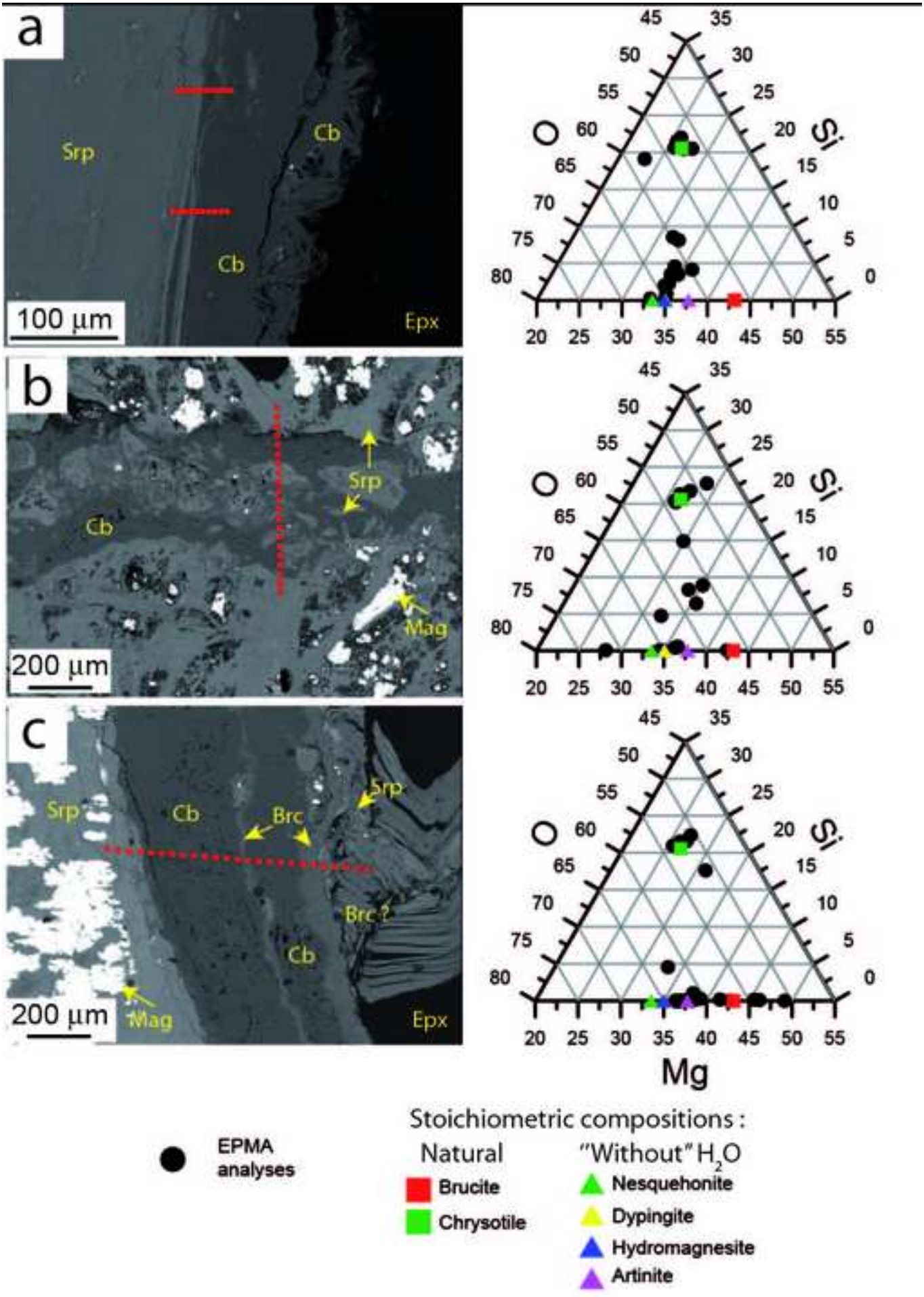

Figure 10

Click here to download high resolution image

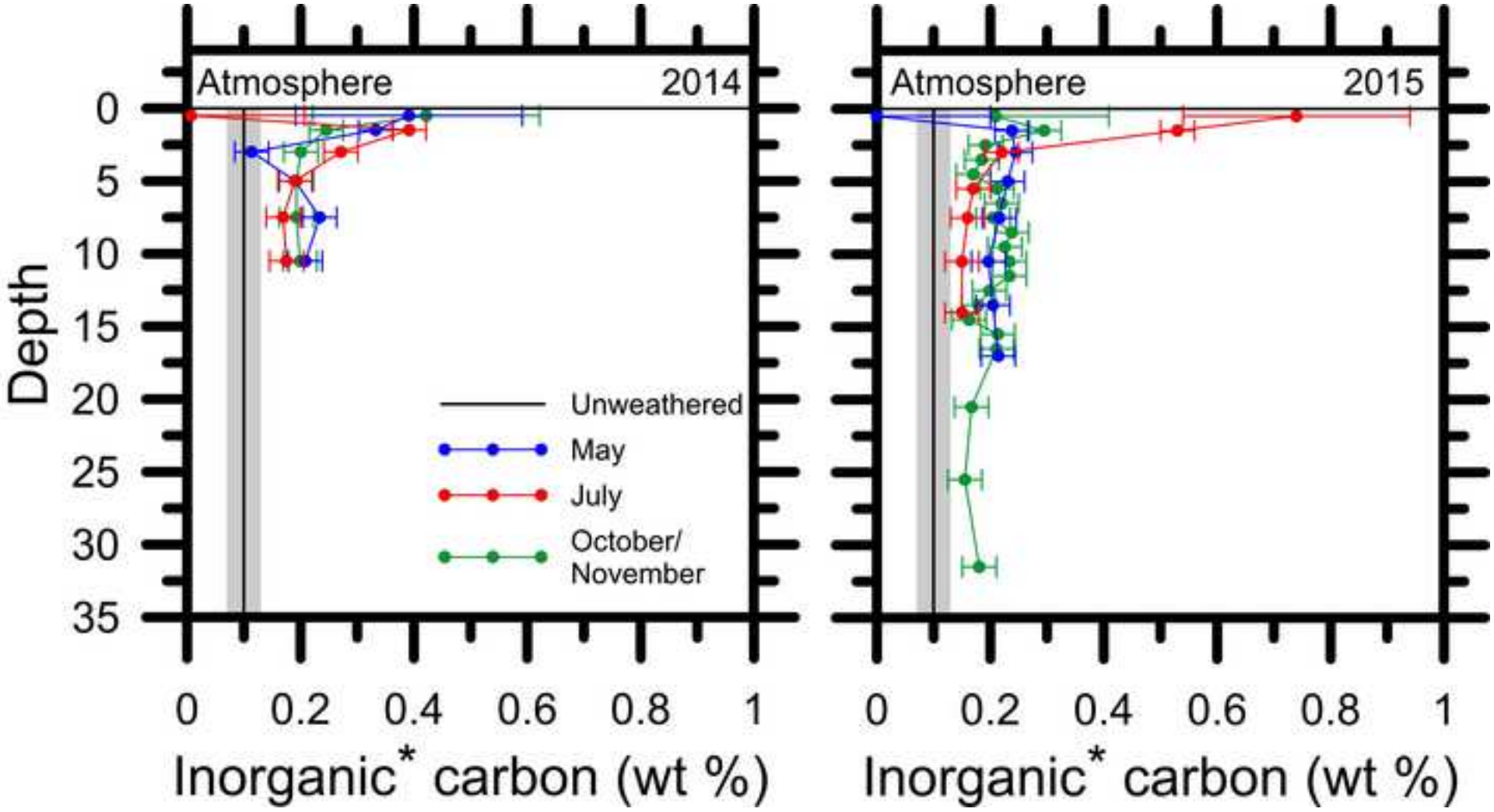

Figure 11

Click here to download high resolution image

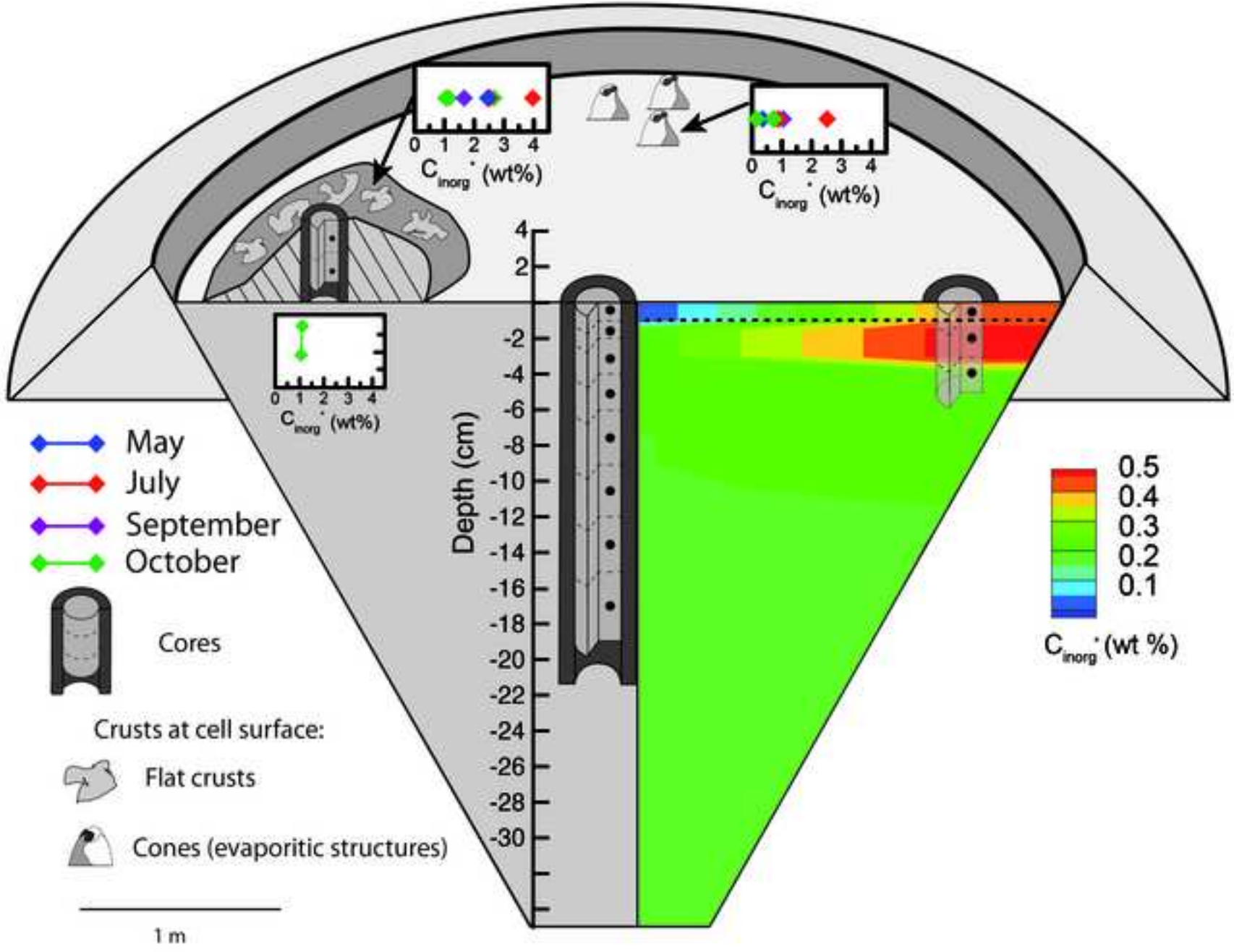

Table

Click here to download Table: Table_1.docx

Month	Temperature (°C)	Solar radiation intensity (W/m^2)	Relative humidity (%)	Total precipitaions (mm)
January	-18	33	87	51
February	-17	68	82	16
March	-7	124	76	15
April	-1	178	69	51
May	10	210	69	90
June	15	231	71	64
July	17	207	79	95
August	16	164	83	103
September	12	114	87	96
October	7	70	78	115
November	-2	47	91	71
December	-11	39	91	66

Table 1: Summary of the meteorological data collected between July 2011 and September 2016.

Supplementary Interactive Plot Data (CSV)

Click here to download Supplementary Interactive Plot Data (CSV): Carbon content and mineralogy.xlsx

Supplementary Interactive Plot Data (CSV)

Click here to download Supplementary Interactive Plot Data (CSV): Leachate water chemistry.xlsx

Declaration of Interest

The authors declare that they have no known competing financial interests or personal relationships that could have appeared to influence the work reported in this paper.